Tectonics®

RESEARCH ARTICLE
10.1029/2024TC008358

Late Jurassic Initial Development of a Salt-Dominated Fold-And-Thrust Belt: The Inverted Passive Margin of the Eastern Alps (Austria)

O. Fernandez[1], H. Ortner[2], W. E. H. Munday[1], M. Moser[1], D. Sanders[2], B. Grasemann[1], and T. Leitner[3]

[1]Department of Geology, University of Vienna, Vienna, Austria, [2]Department of Geology, University of Innsbruck, Innsbruck, Austria, [3]Salinen AG, Altaussee, Austria

Key Points:

- Salt structures controlled the location of initial, Late Jurassic inversion of the salt-bearing Austroalpine margin
- The style of deformation was controlled by supra-salt stratigraphic thickness and the lateral linkage of structures
- Thrusting and squeezing of salt structures exerted a major control on the distribution of Late Jurassic depositional environments

Supporting Information:

Supporting Information may be found in the online version of this article.

Correspondence to:

O. Fernandez,
oscar.fernandez.bellon@univie.ac.at

Citation:

Fernandez, O., Ortner, H., Munday, W. E. H., Moser, M., Sanders, D., Grasemann, B., & Leitner, T. (2025). Late Jurassic initial development of a salt-dominated fold-and-thrust belt: The inverted passive margin of the Eastern Alps (Austria). *Tectonics*, *44*, e2024TC008358. https://doi.org/10.1029/2024TC008358

Received 5 APR 2024
Accepted 17 DEC 2024

Author Contributions:

Conceptualization: O. Fernandez
Data curation: O. Fernandez, H. Ortner, W. E. H. Munday, T. Leitner
Formal analysis: O. Fernandez, H. Ortner, W. E. H. Munday, M. Moser
Funding acquisition: O. Fernandez, B. Grasemann, T. Leitner
Investigation: O. Fernandez, H. Ortner, W. E. H. Munday, M. Moser
Methodology: O. Fernandez
Project administration: O. Fernandez
Supervision: O. Fernandez
Writing – original draft: O. Fernandez, H. Ortner, W. E. H. Munday, M. Moser
Writing – review & editing: B. Grasemann, T. Leitner

Abstract The Northern Calcareous Alps (Eastern Alps, Austria) represent a well-preserved example of the early stages of inversion of a salt-bearing passive margin, which occurred in a fully submarine setting. Late Jurassic shortening led to widespread thrusting and folding that nucleated preferentially, although not exclusively, along salt structures developed during the Triassic passive-margin stage. The presence of a highly effective basal décollement permitted the propagation of deformation without generalized uplift in the area, which was limited to thrusts, folds and squeezed salt structures. The development of individual structures was controlled by the orientation of pre-existing salt structures, the thickness of supra-salt stratigraphy, the lateral propagation of deformation, and, possibly, the redistribution of salt within salt structures prior to contraction and the influence of sub-salt basement faults. Syn-tectonic sediments make it possible to reliably reconstruct the timing of structural inversion. These same sediments were in turn controlled by structural evolution, with depocenters developing roughly parallel to the inverting structures. The structures documented here are evidence for Late Jurassic shortening across the central Eastern Alps, totaling a few to few tens of kilometers. This is the first systematic description of structures of Late Jurassic age in the Eastern Alps and provides a framework within which to understand the abundance of syn-tectonic deposits of this age in the area. Particular attention is paid to the Totengebirge–Trattberg contractional system, an outstandingly long set of structures, whose continuity and significance has gone previously unrecognized.

Plain Language Summary The Eastern Alps (Austria) are a mountain chain with a protracted history. Sedimentary rocks deposited in marine environments in the Northern Calcareous Alps (along the northern Eastern Alps) recorded the initial phases of mountain-building during the Jurassic, at a time that this area lay hundreds of meters below sea level. Multiple instances of submarine landslides preserved in rocks of Late Jurassic age (approximately 150–165 million years old) are the first indication of active faults and relief building in this area. As deformation and uplift progressed, the seafloor reached depths shallow enough for the development of reefs (that need sunlight to grow). This early phase of Alpine history was strongly controlled by the presence of salt diapirs (underground accumulations of rock salt and other evaporitic minerals), which determined what areas experienced the greatest uplift. Although indirect evidence for this phase of Alpine growth evolution has been previously put forward by other authors, this is the first time that specific structures relating to mountain-building are documented, which will require a rewriting of the history of the Alpine mountain chain.

1. Introduction

Evaporite successions (referred here onwards to as *salt*) impact the structural development of contractional systems at all scales, from individual structures (e.g., Callot et al., 2007; Jordan & Noack, 1992; Krzywiec & Vergés, 2007) to entire fold-and-thrust belts (e.g., Bahroudi & Koyi, 2003; Beaumont et al., 2000; Davis & Engelder, 1985; Jourdon et al., 2020). Specific aspects of the relevance of salt in contraction include how pre-existing salt structures localize deformation and control the geometry of shortening structures (e.g., Callot et al., 2012; Célini et al., 2020; Duffy et al., 2018, 2021; Fernández & Kaus, 2014; Flinch & Soto, 2022; Koyi et al., 2008; Letouzey et al., 1995; Rowan & Vendeville, 2006; Santolaria et al., 2021; Soto et al., 2024); how the distribution, geometry and thickness of salt detachments or sedimentary cover condition thrust development (Cotton & Koyi, 2000; Jordan & Noack, 1992; Koyi & Sans, 2006; Letouzey et al., 1995; Muñoz et al., 2024; Santolaria, Harris, et al., 2022; Soto et al., 2024; Storti et al., 2007); how contractional salt structures control the distribution of sedimentary systems

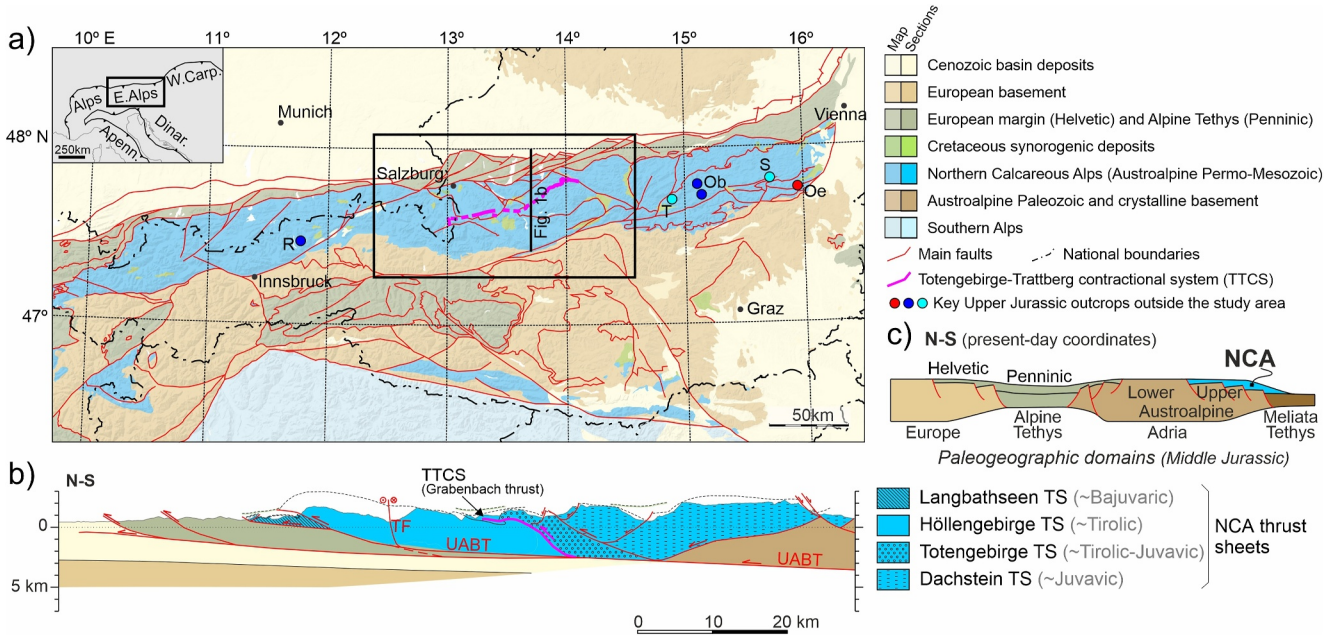

Figure 1. (a) Simplified geological map of the Eastern Alps (updated from Schuster et al., 2013). Localities relevant to Late Jurassic tectonics in the Northern Calcareous Alps (NCA) outside the study area are marked with circles: red for Jurassic thrust; dark blue for Upper Jurassic breccias; light blue for Upper Jurassic reefs (Ob: Obersee; Oe: Oedenhof; R: Rofan; S: Schwarzau; T: Torstein). See inset for location. Abbreviations: Apenn.: Apennines; Dinar.: Dinarides; E. Alps: Eastern Alps; W. Carp.: Western Carpathians. (b) Simplified cross-section through the central NCA showing the structural subdivision of the NCA used in this article (in legend, historic nomenclature equivalence is shown grayed out in brackets). TF: Traunsee fault, UABT: Basal Thrust of the Upper Austroalpine, TS: thrust sheet. (c) Schematic section at Middle Jurassic times showing the paleogeographic domains of the Eastern Alps.

(e.g., Howlett et al., 2020; Kergaravat et al., 2017; Muñoz et al., 2013; Ribes et al., 2018); and the dynamics of salt in inverted rifts or passive margins (e.g., Célini et al., 2020; Ferrer et al., 2023; Granado et al., 2019, 2021; Letouzey et al., 1995; Santolaria, Granado, Wilson, et al., 2022). Significantly, the contractional inversion of pre-existing salt structures often leads to the development of unusual structural relationships, such as subtractive thrust contacts (young-on-old thrusts) or overturned minibasins (e.g., Célini et al., 2020; Graham et al., 2012; Granado et al., 2019; Oravecz et al., 2023; Santolaria, Granado, Wilson, et al., 2022).

All these aspects have also played a key role in the development of the central Northern Calcareous Alps (NCA) of the Eastern Alps (Austria) (Figure 1a). This province presents a unique example in which a high degree of preservation and an outstanding syn-tectonic sedimentary record make it possible to decipher the evolution of the basin. In this contribution we focus on the initial Late Jurassic inversion of salt structures formed in the central NCA during its Triassic passive margin stage, along with the impact on syn-tectonic sedimentation.

Late Jurassic tectonism in the central NCA has been previously discussed (e.g., Mandl, 1982, 2000, 2013; Tollmann, 1987) and linked by some authors to subduction in the Dinarides and Western Carpathians (Gawlick & Missoni, 2019; Plašienka, 2018; Schmid et al., 2008). However, and despite the abundant presence of syn-tectonic sediments (e.g., Gawlick et al., 1999, 2002, 2007, 2009; Gawlick & Frisch, 2003; Gawlick & Missoni, 2015), individual Late Jurassic structures have, to date, only been described in isolation. Here we provide, for the first time, detailed descriptions of structures across the entire central NCA, including a previously unrecognized 80 km long contractional system, and show they are part of a coherent deformation system. We also explore how the dimensions, linkage, and style of the structures developed during Late Jurassic shortening were controlled by the presence of a highly efficient basal salt décollement, the presence of pre-existing salt structures, and variations in the relative thickness of salt and its overburden. Finally, we document the control that shortening exerted on the development of the Late Jurassic NCA sedimentary basin.

2. Geological Setting

The NCA are the Permian to Mesozoic stratigraphic cover of the Upper Austroalpine unit of the Eastern Alps (Adria) (Figures 1a and 1c). The NCA are at present almost entirely decoupled from their basement and

imbricated and thrust northwards over imbricated Penninic ocean (Alpine Tethys) and European margin units (Figure 1b). After an initial Permian to Middle Triassic phase of rifting, the NCA developed into a passive margin facing the Meliata branch of the Neotethys ocean (Mandl, 2000; Strauss et al., 2023). Halokinesis above a thick Permian to Lower Triassic evaporite syn-rift succession was pervasive throughout the Triassic (Leitner & Spötl, 2017; Strauss et al., 2023). After a period of rapid subsidence and basin starvation during the Early to Middle Jurassic, widespread Upper Jurassic breccias and mass-transport complexes in the central NCA are interpreted as the record of contractional or transpressional deformation in the Eastern Alps (Faupl & Wagreich, 2000; Frank & Schlager, 2006; Frisch & Gawlick, 2003; Gawlick et al., 1999, 2009; Schmid et al., 2008). Alpine deformation peaked later, in the Cretaceous to Cenozoic, with internal imbrication in the NCA and its near-complete decoupling from basement during thrusting (Faupl & Wagreich, 2000).

Significant aspects of the geology of the NCA have been the subject of major revision in recent years (e.g., Fernandez et al., 2021, 2024; Granado et al., 2019; Ortner & Kilian, 2022; Strauss et al., 2023). These include a revision of the role of salt tectonics and the structural configuration of the NCA, which will be discussed below.

2.1. Structure

The NCA has been historically subdivided structurally into three main broadly north-directed sets of thrust systems, from structurally lowest to highest: the Bajuvaric, Tirolic and Juvavic thrust systems (Figure 1b) (Hahn, 1913a, 1913b; Mandl, 2000; Schmid et al., 2004; Tollmann, 1976b). Recently, this subdivision has been thrown into question in the western NCA, where thrust sheets from the Tirolic system have been re-classified into the Bajuvaric (Ortner & Kilian, 2022). This debate has also arisen in the central NCA (Frisch & Gawlick, 2003). To avoid confusion, we therefore refer to thrust sheets individually. From structurally lowest to highest these are (Figure 1b): Langbathsee thrust sheet (TS) (historically Bajuvaric), Höllengebirge TS (historically Tirolic), Totengebirge TS (historically Tirolic or Juvavic), and Dachstein TS (historically Juvavic). The Langbathsee TS rides on the Late Cretaceous to Paleogene Langbathsee thrust, which is equivalent to the basal thrust of the NCA (the Upper Austroalpine basal thrust (UABT) or UABT, Figures 1b and 2). The Höllengebirge TS was transported onto the Langbathsee TS by the Early to Late Cretaceous Höllengebirge thrust (Figures 1b and 2). The Totengebirge TS was transported on the Late Jurassic Totengebirge–Trattberg contractional system (TTCS) (Figure 2a), a set of connected or relaying thrusts and folds (discussed as part of this contribution). The TTCS is partially cross-cut and partly overridden by the Early Cretaceous Dachstein thrust (Figures 1b and 2), which transported the Dachstein TS in its hanging wall.

The imbricates of the central NCA were partly offset by younger (Neogene) strike-slip faults and high-angle thrusts (Königssee, Traunssee, Wolfgangsee, and Windischgarsten faults; Figure 2a) (Linzer et al., 1995; Peresson & Decker, 1997) that have not significantly modified the Jurassic to Paleogene structural framework (Fernandez et al., 2024).

2.2. Stratigraphy and Tectonic Evolution of the Central NCA

The stratigraphy in the NCA, from Permian to Cretaceous, is summarized by Tollmann (1976a), Faupl and Wagreich (1992), Gawlick et al. (2009) and Mandl (2000). The terminology used here, which combines both formal and informal stratigraphic terms, corresponds to the accepted nomenclature in the Eastern Alps, as synthesized by Piller et al. (2004). It is illustrated in Figure 3 and described below.

The Permian to Mesozoic evolution of the central NCA is marked by progressive deepening from subaerial conditions in the Permian to bathyal conditions from the Early Jurassic through to the Early Cretaceous, as the province transitioned from post-Variscan rifting to passive margin to the early stages of Alpine orogenesis (Figure 3b). The basin experienced prolonged stages of limited sediment input, with some Triassic and Jurassic intervals being significantly condensed (compare Figure 3a with 3d). Nonetheless, sedimentation was continuous in the central NCA from Permian up to Aptian times (Figure 3a; Piller et al., 2004).

The oldest strata in the central NCA are a succession of Permian coarse continental to shallow marine clastics (Präbichl Fm) that infilled post-Variscan topography and deposited locally in half-grabens (Mostler, 1972; Tollmann, 1976a). This unit unconformably lies on Variscan basement, which crops out along the southern margin of the NCA (Figure 2a).

10.1029/2024TC008358

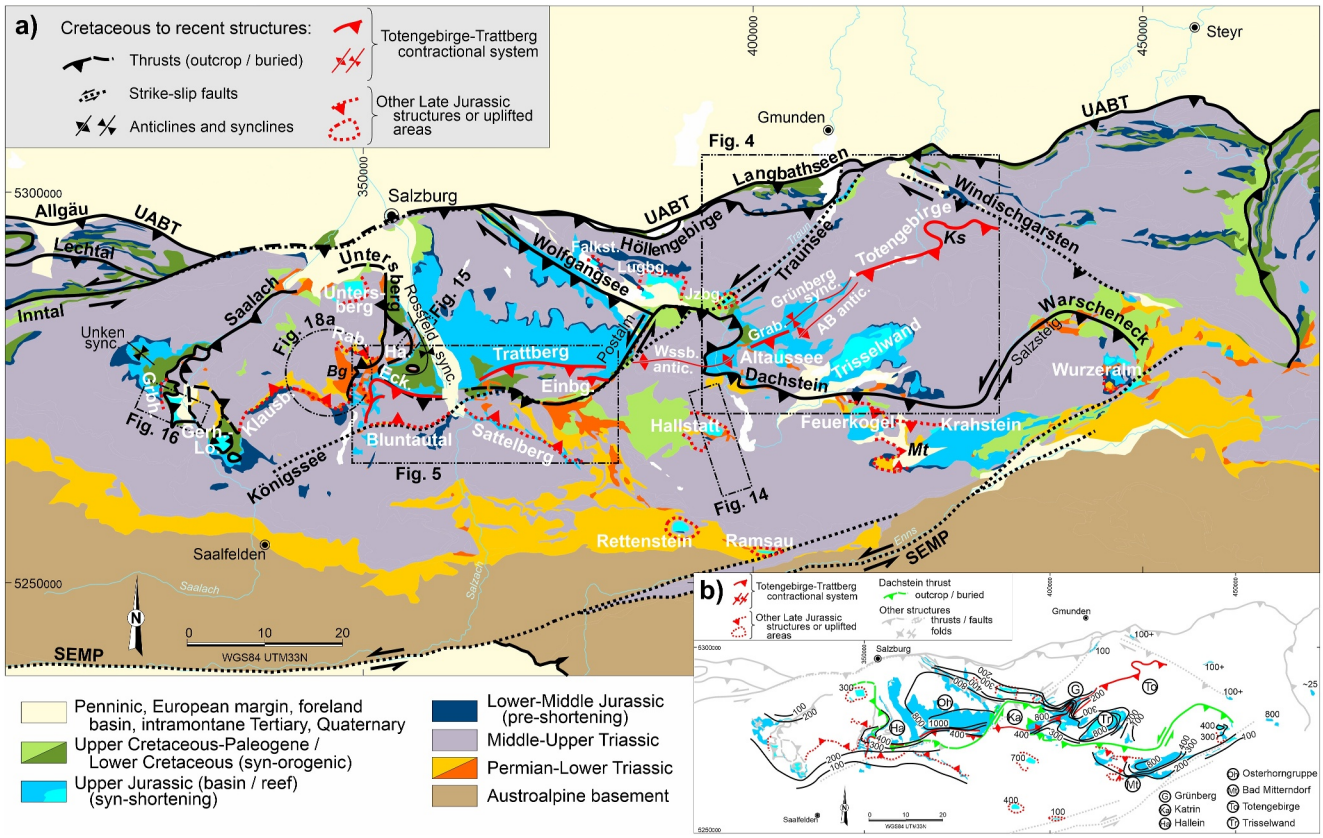

Figure 2. (a) Simplified structural framework of the central Northern Calcareous Alps. Structures with Jurassic tectonic activity are highlighted in red. The map is simplified from Krenmayr (2005) and Krenmayr and Schnabel (2006). Structures are drawn, and partly simplified, from Tollmann (1976b), Braun (1998), Linzer et al. (1995), Ortner and Kilian (2022) and Fernandez et al. (2024). Abbreviations for structures: sync.: syncline; antic.: anticline; AB: Ahornkogel-Brunnkogel; Eck.: Eckersattel; Gerh.-Lo.: Gerhardstein-Lofer; Grab.: Grabenbach; Grbh: Grubhörndl; Ha.: Hallein; Klausb.: Klausbach; Rab.: Rabenstein; SEMP: Salzach-Enns-Mariazell-Puchberg fault system; UABT: Basal thrust of the Upper Austroalpine; Wssb.: Weissenbach. (b) Map of Upper Jurassic stratigraphic thickness (expressed in meters) after Fenninger and Holzer (1970) complemented with thickness measured from 1:50,000 scale geological maps published for the area and the cross-sections of Fernandez et al. (2024). Where only isolated outcrop control points are available, no contours are shown. Although Upper Jurassic sediments covered the entire area, erosion has removed it over large expanses, particularly across the Totengebirge area (label To). The thickness under the Dachstein thrust sheet (TS) in the Katrin area (label Ka) is not shown due to lack of control. However, the depocenter from the Grünberg (label G) was in continuity with that of the Osterhorngruppe (label Oh) before emplacement of the Dachstein TS.

The Präbichl Fm is overlain by evaporites and fine-grained clastics of the Haselgebirge. The Haselgebirge is a mining term that refers to a unit composed of 50%–65% halite and anhydrite, with lesser amounts of mudstone, fine sandstone, and dolostone (Leitner & Mayr, 2017; Leitner et al., 2017). This unit is often internally chaotic or strongly tectonized (Leitner & Spötl, 2017) and has been dated to be Upper Permian to Lower Triassic (Klaus, 1965; Pak & Schauberger, 1981). The Haselgebirge is a syn-rift unit, with variable original thickness (Leitner & Spötl, 2017; Strauss et al., 2023). Its depositional water depth varied between few meters to tens of meters (Leitner et al., 2017) (Figure 3b). The Werfen beds, a unit composed of shallow marine (Krystyn, 1975) fine-grained sandstones, mudstones and carbonates, are dated to be coeval with the Haselgebirge, but are generally found to overlie it (Tollmann, 1976a). During the Triassic, the Haselgebirge cored widespread salt structures, and during later inversion it acted as the main décollement in the central NCA.

The Lower Triassic is directly overlain by Anisian limestones and dolomites (Gutenstein and Steinalm Fms; referred to onwards as Anisian "carbonates") often under 200 m thick, but locally absent or hundreds of meters thick. These units were deposited in shallow marine to neritic water depths (Nittel, 2006; Tollmann, 1976a) (Figure 3b). Rapid thickness changes and pinch-outs observed across the NCA (Cornelius & Plöchinger, 1952; Mandl et al., 2014) are interpreted to relate to the onset of salt tectonism (Fernandez et al., 2024; Granado et al., 2019; Leitner & Spötl, 2017; Strauss et al., 2021, 2023).

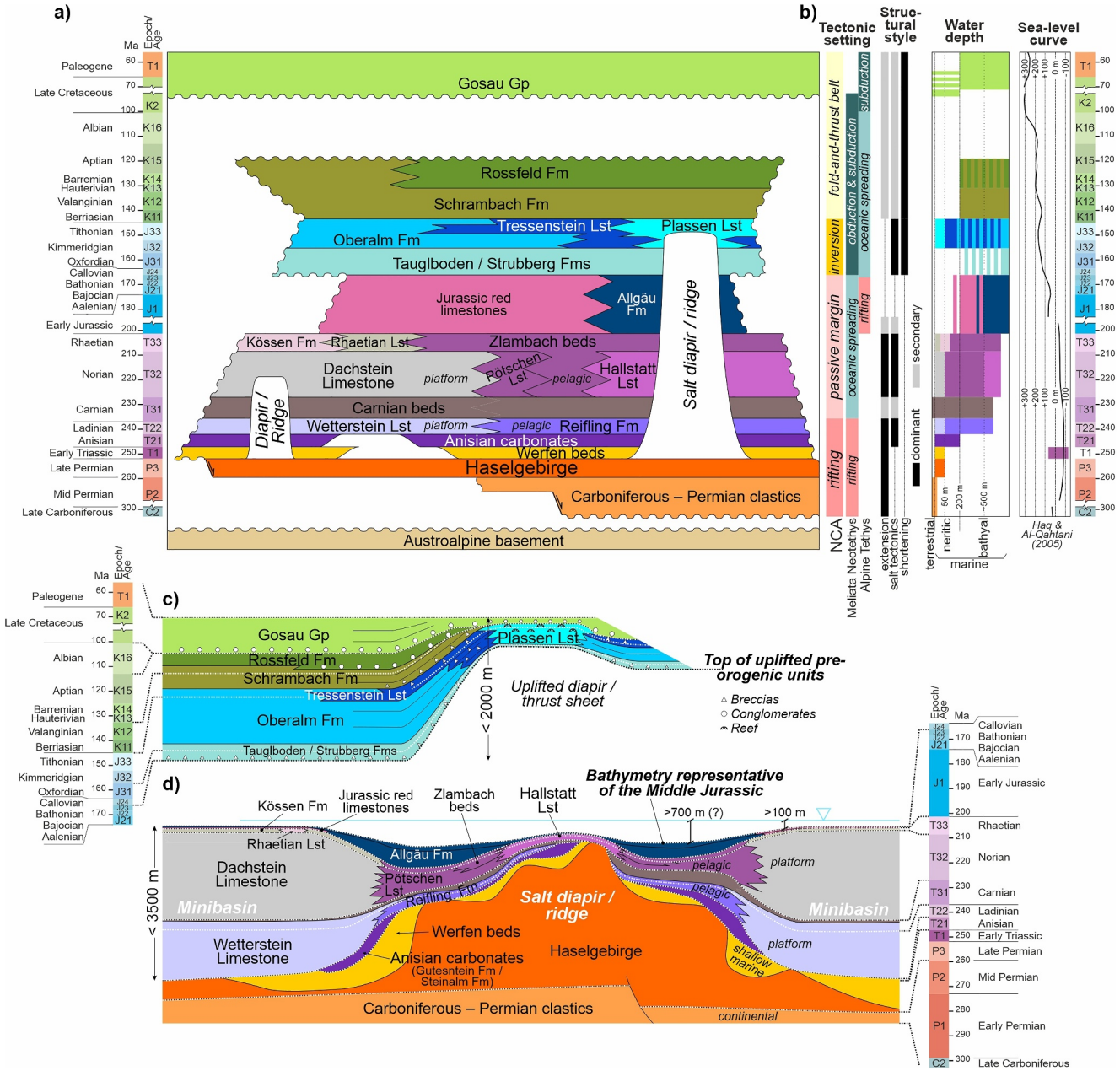

Figure 3. (a) Chornostratigraphic chart for the central Northern Calcareous Alps (NCA) Permo-Mesozoic stratigraphy. A variety of condensed red limestones of Early to Middle Jurassic age are grouped informally under "Jurassic red limestones." Informal units are termed "beds" (from the German *Schichten*), Lst (limestone) or with a simple name (e.g., Haselgebirge, Carnian). Modified from Piller et al. (2004). The time scale of Walker and Geissman (2022) has been used for absolute ages. (b) Columns representing (from left to right): main tectonic phases experienced by the central NCA and its surrounding oceanic domains (Meliata Neotethys and Alpine Tethys); structural style of deformation and intensity; ranges of depositional water depths; and global eustatic curve (from Haq & Al-Qahtani, 2005). (c), (d) Synthetic structural-stratigraphic sketch of central NCA stratigraphy showing the relative thickness and geometric relationships of units during Jurassic–Cretaceous shortening (c) and prior to Jurassic shortening (d). Dashed white lines represent isochrons tied to the time scales on either side. The geometry in panel (d) shows the configuration after cessation of Triassic salt tectonics, with minibasins accumulating thick platform successions and intervening inflated salt bodies roofed by condensed pelagic facies. Modified from Fernandez et al. (2024) and Mandl (2000).

By Ladinian times, halokinesis was fully established (Granado et al., 2019; Strauss et al., 2021, 2023) and led to the development of minibasins and intervening bodies of inflated salt (diapirs and ridges). Ongoing rift-related extension exceeded the rate of salt migration in the diapirs, and thus prevented the growing diapirs from rising to shallow depths (Fernandez et al., 2024; Strauss et al., 2023; Vendeville & Jackson, 1992). The result was a configuration where the tops of diapirs remained at bathyal depths, while thick carbonate platforms aggraded in

the flanking minibasins (illustrated in Figure 3d). Thick lagoonal carbonates of the Wetterstein Lst (up to 2,000 m thick) deposited in water depths of few meters (Nittel, 2006) and infilled the minibasins. The relatively condensed pelagic marls and limestones of the Reifling Fm, under 400 m thick, accumulated above intervening inflated salt bodies (Strauss et al., 2021). In contrast to the shallow water Wetterstein Lst, the Reifling Fm accumulated at water depths of up to 400 m or more (as measured from clinoform height; Kilian & Ortner, 2019) (Figure 3b).

Clastic influx during the Carnian pluvial event lead to the extinction of the Wetterstein Lst platforms (Schlager & Schöllnberger, 1974). The Carnian marked the cessation of rifting in the NCA, although continental break-up progressed to its south (Strauss et al., 2023). Sediments deposited during this time infilled the post-Ladinian bathymetry (Mandl, 2000; Strauss et al., 2023) and are relatively thin (mostly under 200 m thick, often absent). The Carnian of the NCA includes shallow marine to bathyal clastics, shallow water carbonates, and evaporites.

Carbonate platform development restarted in the late Carnian to Norian, leading to the deposition of the thick Dachstein Lst lagoonal and reefal carbonates (up to 2,000 m thick) (Fischer, 1964) and its deep-water equivalents: allodapic slope limestones and turbidites (Pötschen Lst and Zlambach beds) and pelagic marls, limestones, and marly limestones (Hallstatt Lst) (under 400 m thick). The lagoonal Dachstein Lst and its pelagic equivalents replicated the shallow-minibasin and subsiding-diapir configuration of the Ladinian (Figure 3d). In this case, down-slope gliding on the newly formed passive margin led to ongoing extension of the supra-salt sedimentary succession (Strauss et al., 2023). In contrast to the shallow water deposition of the Dachstein Lst, the Hallstatt Lst deposited in water depths of 500 m or greater (Kenter & Schalger, 2009) (Figure 3b).

Deposition in the photic to neritic water domain (water depths up to 80 m) during the Rhaetian was replaced by reefal limestones (Rhaetian Lst) and marls and marly limestones of the Kössen Fm. The Zlambach beds continued to accumulate in deeper waters (Tollmann, 1976a) (Figure 3b). Although some Kössen Fm basins have been documented to have developed above collapsing diapirs, halokinesis reduced significantly, or ceased altogether, as the minibasins containing the thick Ladinian and Norian platforms became welded (Granado et al., 2019; Santolaria, Granado, Wilson, et al., 2022).

Rapid and generalized subsidence across the NCA, starting in the Early Jurassic and likely related to the opening of the Alpine Tethys (Froitzheim & Manatschal, 1996), resulted in the drowning of the Triassic platforms. Subsidence was accompanied by localized extensional faulting in the central NCA (Böhm et al., 1995; Krainer et al., 1994). Extension was limited, and fault scarps exposed only the uppermost Triassic, if at all (Böhm, 1992). The Early to Middle Jurassic are otherwise considered a prolonged period (~35 Ma) of relative tectonic quiescence dominated by pelagic sedimentation (Mandl, 2000; Schlager & Schöllnberger, 1974). The pelagic Zlambach beds graded upwards into the Lower to Middle Jurassic pelagic siliceous marls of the Allgäu Fm, which deposited in waters at least 500 m deep (Krainer et al., 1994; Mandl et al., 2012) (Figure 3b). The Triassic platforms, in turn, were capped by condensed red pelagic limestones deposited below 100–200 m water, and possibly much deeper but above the aragonite compensation depth (ACD) (Krystyn, 1971). Water depth in the NCA is interpreted to have peaked at the end of the Middle Jurassic, but no precise depth has been established but depths of around 1,000 m or greater have been proposed (Channell et al., 1992; Garrison & Fischer, 1969; Kurz et al., 2023). The Lower to Middle Jurassic is a few meters to few hundreds of meters thick, with a regional northward thickening trend (Böhm, 1992; Daurer & Schäffer, 1983; Weber, 1958).

A major change occurred in the late Middle Jurassic, with the deposition of bathyal siliceous Mn-bearing marls (Strubberg Fm; Callovian-Oxfordian) and bathyal siliceous limestones and marls (Tauglboden Fm; Oxfordian-Kimmeridgian) (Gawlick et al., 1999, 2007, 2009; Mandl, 2013). Both units contain abundant breccias and MTDs (mass-transport deposits) containing re-worked Triassic lithologies (Gawlick & Missoni, 2015; Gawlick et al., 1999, 2007; Mandl, 2013). The breccias and MTDs of the Strubberg and Tauglboden Fms indicate a major shift in the history of the NCA basin after the prolonged stability experienced during the Early and Middle Jurassic. This shift is considered to record the onset of Alpine orogenesis in the central NCA (Gawlick & Frisch, 2003; Gawlick et al., 1999; Mandl, 2000).

The Tauglboden Fm grades upwards into or is unconformably overlain by the Kimmeridgian-Berriasian Oberalm Fm, a succession of calciturbidites, pelagic marls and limestones, containing also thick banks of re-sedimented carbonates (Garrison, 1967; Gawlick et al., 2005, 2007; Mandl, 2013; Mandl et al., 2012; Ortner et al., 2008;

Steiger, 1981). The Oberalm Fm was deposited in bathyal depths, and in general below the ACD (Garrison, 1967) (Figure 3b). Coeval to the Oberalm Fm, reefs of the Plassen Lst developed above local bathymetric highs (as illustrated in Figure 3c) (Kurz et al., 2023; Mandl, 2000; Tollmann, 1987). Within and to the top of the Oberalm Fm, reef slope deposits and breccias of reworked Triassic limestones accumulated in thick, relief-forming banks grouped under the term Tressenstein Lst (Mandl, 2013; Schäffer, 1982). The entire Middle to Upper Jurassic succession varies in the area from being absent to being around 1,000 m thick, with the thickest accumulations occurring in E–W to WSW–ENE trending depocenters (Figure 2b).

Due to the generalized bathyal depth reigning over the central NCA during the Late Jurassic, it is commonly accepted that uplift of the seafloor was tectonically driven (Gawlick & Missoni, 2019; Mandl, 2000; Tollmann, 1987). Ophiolitic detrita (clasts and Cr-spinel grains) found in the Oberalm Fm and Plassen Lst (Drvoderic et al., 2023; Missoni & Gawlick, 2011; Steiner et al., 2021) have been associated to the initial obduction along the Neotethyan margin (Gawlick & Missoni, 2019; Plašienka, 2018).

Deposition of the Plassen Lst and Oberalm Fm was gradually replaced by the bathyal, marl-dominated Berriasian to Hauterivian Schrambach Fm (Decker et al., 1987; Faupl & Wagreich, 1992; Rasser et al., 2003). This unit is overlain by and partly laterally grades into the Rossfeld Fm, a succession of turbiditic sandstones, polymictic breccias and shales whose deposition lasted into the Aptian (Decker et al., 1987; Faupl & Wagreich, 1992; Krische et al., 2014). The Schrambach and Rossfeld Fms and their temporal equivalents, with a combined thickness of under 500 m, deposited during the imbrication of the Dachstein, Höllengebirge and Langbathsee thrust sheets (Levi, 2023; Mandl, 2000). A gradual increase in the abundance of ophiolitic detrita in the Lower Cretaceous is interpreted to indicate progressing mountain building to the south of the NCA (Decker et al., 1987; Krische et al., 2014).

A sedimentary hiatus in the Aptian to Albian (Figure 3a) was the result of tectonically driven uplift. Internal imbrication in the NCA is partly sealed by strata of the Upper Cretaceous to Paleogene Gosau Gp, a thick assemblage of continental to deep marine sediments that infilled pre-existing topography (Sanders, 1998; Wagreich & Faupl, 1994). The Gosau Gp itself deposited synchronous to further, although limited, internal deformation of the NCA (Ortner, 2001; Ortner et al., 2016; Wagreich & Decker, 2001; Wagreich & Faupl, 1994). Thickness of the Gosau Gp is highly variable, but can locally exceed 1,000 m.

Syn-thrusting extensional faulting, coeval with the Schrambach and Rossfeld Fms and the Gosau Gp has been documented throughout the central NCA (Fernandez et al., 2024; Wagreich & Decker, 2001). The origin of this extensional deformation is interpreted to be internal to the NCA (Wagreich & Decker, 2001), possibly relating to the extensional collapse of salt structures (Fernandez et al., 2022, 2024) and subsidiary to the generalized contractional regime.

There is a very limited sedimentary record of the final stages of Alpine deformation (Neogene) in the central NCA.

2.3. Late Jurassic Tectonics and Structures in the Central NCA

Although the earliest record of widespread subduction-related metamorphism in the Eastern Alps is of Late Cretaceous age (e.g., Miladinova et al., 2022), Late Jurassic tectonics have been documented in the central NCA by previous authors in various sectors, mostly from indirect indications (Table 1). Likewise, kilometer-sized blocks of Triassic (with or without accompanying Haselgebirge) are frequently found lying on top of Middle to Upper Jurassic sediments (Table 2). These blocks, accepted to have emplaced in the Late Jurassic, have been diversely interpreted as olistrostromes emplaced due to tectonic uplift (e.g., Tollmann, 1987) or as part of an accretionary prism (Gawlick & Missoni, 2019). More recently, Fernandez et al. (2024) have argued in favor of these units (particularly the Sattelberg thrust, Figures 2a, Tables 1 and 2) being salt-sourced thrust sheets, as will be further elaborated here.

Jurassic thrust emplacement has been documented locally in the easternmost NCA (Oedenhof (Mandl, 1996; Strauss et al., 2023) ("Oe" in Figure 1a) and a Late Jurassic stratigraphy similar to that of the central NCA is present along the entire NCA, with the presence of Upper Jurassic breccias of age equivalent to the Tauglboden and Strubberg Fms (Rofan and Obersee breccias; Gawlick et al., 2011; Lein et al., 2009) ("R" and "Ob" in Figure 1a), Oberalm Fm deposits, and isolated Plassen Lst reef development (Schwarzau, Torstein; Birkenmajer, 1996; Moser, 2003) ("S" and "T" in Figure 1a). Although these are isolated observations, and have not

Tectonics

10.1029/2024TC008358

Table 1
Areas in the Central Northern Calcareous Alps Interpreted to Have Middle to Late Jurassic Tectonism by Previous Authors (Lacking the Description of Specific Structures)

	Sector of observation	Elements described to date	Authors
Localities with description of Late Jurassic tectonism without specific structural interpretation (from west to east)	Grubhörndl	Block of Dachstein Lst overlying Oberalm Fm	Ortner et al. (2008)
	Eckersattel	Uplift and erosion of the Dachstein Lst with onlap of the Oberalm Fm and overturned Dachstein Lst overlying the Oberalm Fm along strike	Braun (1998)
	Hallein	Resedimented fragments of Haselgebirge within Oberalm Fm in the vicinity of Hallein	Plöchinger (1984)
	Trattberg (sector)	Trattberg "Rise" (E–W uplift along the Trattberg) defines a boundary between the Tauglboden Fm to its N and the Strubberg Fm to its S	Frisch and& Gawlick (2003)
	Sattelberg (sector)	Multiple blocks of Triassic carbonates (from metric to map-scale) overlying or embedded within the Strubberg Fm	Gawlick and& Missoni (2015, 2019); Plöchinger (1979); Tollmann (1975)
	Rettenstein	Isolated Plassen Lst reef directly overlying Werfen beds (omitted or extremely condensed Triassic stratigraphy)	Tollmann (1987); Auer et al., 2008, 2009)
	Hallstatt	Isolated Plassen Lst reef overlying Triassic pelagic carbonates and Haselgebirge. Haselgebirge locally overlies Callovian radiolarites	Mandl et al. (2012); Suzuki and& Gawlick (2009); Tollmann (1987)
	Altaussee	Mass-transport deposits in the Strubberg, Tauglboden and Oberalm Fms and osolated Plassen Lst reef on top of Triassic pelagic carbonates and Haselgebirge	Mandl (1982, 2013); Gawlick et al. (2007); Tollmann (1987)
	Bad Mitterndorf	Isolated Plassen Lst reef overlying Triassic pelagic carbonates and Haselgebirge	Tollmann (1987)
	Wurzeralm	Haselgebirge overlies Oxfordian radiolarites	Lein (1987)

Note. Recent re-interpretations of some of these areas are included in Table 2. Refer to Figure 2a for locations.

Tectonics

10.1029/2024TC008358

Table 2
Specific Structures in the Central Northern Calcareous Alps Identified as Late Jurassic by Previous Authors

	Structure described	Type of structure	Elements described to date	Authors	Estimated shortening	Shown in figure(s)
Localities with description of Late Jurassic structures with age constraints (from west to east)	Grubhörndl olistolith (?)	W-directed low-angle contact	Rhaetian Lst and Dachstein Lst block overlying Oxfordian breccia, originally interpreted as an olistolith	Ortner et al. (2008)	Undetermined	Figure 2a (revised interpretation in Figure 16)
	Trattberg thrust	N-directed high-angle thrust	Growth strata in the Oberalm Fm in the footwall of the Trattberg thrust. Uplifted hanging wall was mass-wasted and fed megabreccias in the Oberalm Fm in the footwall	Ortner (2017)	2–3 km to N (refer to text)	Figures 2a, 5, 12
	Sattelberg thrust	S-directed low-angle thrust	Backthrust placing Triassic pelagic carbonates on the Strubberg Fm. Olistoliths (metric to decametric) of the hanging wall incorporated in the Strubberg Fm	Fernandez et al. (2024)	>2 km to S, 5 km according to Fernandez et al. (2024)	Figures 2a, 5, 17
	Hallstatt diapir	Diapir	Hallstatt diapir squeezed during the Late Jurassic, leading to allochthony on Callovian radiolarites and Plassen Lst reef growth atop	Fernandez et al. (2021)	Revised here (see text)	Figures 2a and 14
	Altaussee diapir	Diapir	Triassic pelagic carbonates above squeezed and thrusted diapir capped by Plassen Lst	Fernandez et al. (2024)	Revised here (see Grabenbach thrust Table 4)	Figures 2a, 4, 6
	Bad Mitterndorf sector	N- & S-directed low-angle salt-fed thrusts	Doubly-vergent thrusts, with hanging wall overlain by Plassen Lst	Fernandez et al. (2024)	10 km according to Fernandez et al. (2024)	Figure 2a
	Wurzeralm salt allochthon	S-directed salt tongue	Allochthonous salt sheet of Haselgebirge emplaced southwards onto Middle Jurassic radiolarites. Plassen Lst reef developed above the squeezed salt feeder	Kurz et al. (2023)	1–2 km according to Kurz et al. (2023)	Figure 2a

Note. Refer to Figure 2a for location.

been previously associated to salt structures, their presence supports the fact that Late Jurassic tectonics in the central NCA was part of a larger scale process.

Despite the number of localities indicative of Late Jurassic tectonism in the central NCA, most have been described without referring to any specific structures (Table 1; Figure 2a). Only few discrete Late Jurassic structures have been described to date (Table 2; Figure 2a). The analysis presented here is targeted at identifying further structures that relate to Late Jurassic deformation in the central NCA, and the control exerted by Permo-Triassic evaporites.

3. Methodology

The analysis presented in this contribution is based on the review of published data and geological maps, complemented with field data and observations acquired by the authors (Fernandez, 2024; Fernandez & Eggerth, 2024). Geological mapping of the study area at 1:50,000 scale (Egger, 1996; Egger & van Husen, 2007; Griesmeier & Hornung, 2023; Moser, 2014; Moser & Moshammer, 2018; Moser & Pavlik, 2013; Pavlik, 2006, 2007; Plöchinger, 1982, 1987; Schäffer, 1982) has been revised during field mapping and used to generate updated maps (Figures 4 and 5). Structural data (bedding dip and dip direction) and observations on tectono-sedimentary relationships and contacts between different stratigraphic units have been collected during mapping. These have been interpreted in stereographic projections and through the analysis of mapped contacts (e.g., Platt, 1998). All data have and maps discussed here are in WGS84 UTM33N coordinates (other than Figure 1).

Cross-sections across key structures have been constructed following conventional methods of down-plunge projection and interpolation (De Paor, 1988; Groshong, 2006; Lopez-Mir, 2019; Wojtal, 1988). Due to the significant topographic variations within the study area, field observations projected down-plunge constrain the cross-sections to within 500–1000 m above and below topography (e.g., Figures 6a and 6b). At depth, cross-sections have been interpreted using the following constraints:

1. Borehole and mine gallery data (referenced in the figure captions) has been incorporated where available.
2. The NCA are underlain by a gently dipping basal thrust (the UABT, Figure 1b) (Geutebrück et al., 1984; Kramer & Kröll, 1979; Linzer et al., 1995, 2002), whose depth is constrained by the regional cross-sections of Fernandez et al. (2024).
3. The stratigraphic thickness of units follows the relative trends discussed above and shown in Figures 3b and 3c. The transition between thick Triassic platforms and thinner pelagic equivalents is estimated to occur over a distance of at least 2–3 km (Kenter & Schalger, 2009).
4. Pelagic Triassic facies are interpreted to have originally deposited above inflated salt (Fernandez et al., 2024; Mandl, 2000; Strauss et al., 2021).
5. The present-day geometry has been contrasted with the restored geometry for consistency. Restoration has been performed by unfolding fault blocks preserving bed thickness and lngth, allowing for area differences to be accommodated by the Haselgebirge (Griffiths et al., 2002; Rowan & Ratliff, 2012).

A final critical aspect in this contribution is the determination of ages of deformation. The following criteria have been used:

1. Growth strata or progressive unconformities indicate the timing and kinematics of growth on individual structures (e.g., Ortner, 2001; Riba, 1976; Vergés et al., 2002).
2. Undeformed strata overlying folded or faulted units, if present, have been considered to seal deformation and provide a minimum age.
3. The central NCA is characterized by continuous sedimentation from Jurassic to the end of Early Cretaceous (Figure 3a; Piller et al., 2004). Therefore, the youngest units in the footwalls of thrusts or in the core of isoclinal synclines (i.e., in which younger units could not have been eroded) are interpreted to give the age of the structure, as the absence of sediments of a certain age reliably indicates that the structure already existed at that time (e.g., Ortner, 2003; Ortner & Kilian, 2022). This is reinforced by the fact that for thrust sheets resting on Upper Jurassic, the Jurassic units in the footwall contain abundant re-worked clasts of Permian and Triassic rocks from the hanging wall (e.g., Gawlick & Missoni, 2015; Ortner, 2017), indicating that thrusts were emergent at the seafloor (or near to emergent) and that the Upper Jurassic sediments are syn-thrusting.

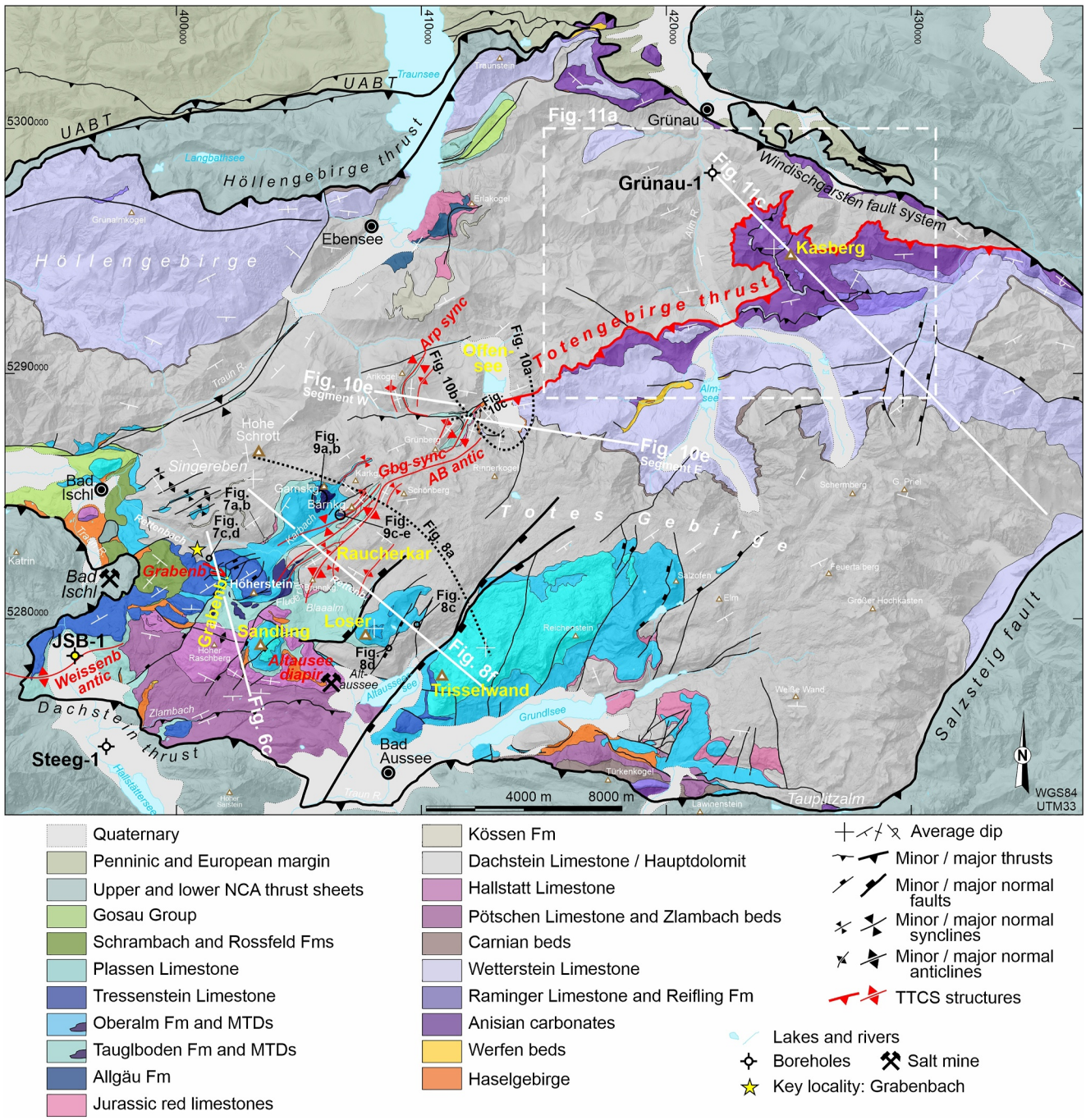

Figure 4. Map of the eastern segment of the Totengebirge–Trattberg contractional system (TTCS) and surrounding areas. AB antic: Ahornkogel–Brunnkogel anticline; Alt. diapir: Altaussee diapir; Arp sync: Ariplan syncline; Gbg sync: Grünberg syncline; Grabenb.: Grabenbach; Fludergr.: Fludergraben; Rettenb.: Rettenbach; UABT: Upper Austroalpine basal thrust. Peak names with ending *kg.: *kogel; R.: River; sys.: system. This map is based on fieldwork by the authors and previously published 1:50,000 scale geological mapping (Egger, 1996; Egger & van Husen, 2007; Griesmeier & Hornung, 2023; Moser & Moshammer, 2018; Plöchinger, 1982; Schäffer, 1982).

4. Erosion or mass-wasting are interpreted to relate to uplift of an area, and the deposition of re-sedimented units (breccias, mass-transport deposits or olistoliths) are interpreted to result from the development of structural relief in the vicinity. Eustatic variations played a subsidiary role as their magnitude is smaller than the changes in bathymetry (Figure 3b).

10.1029/2024TC008358

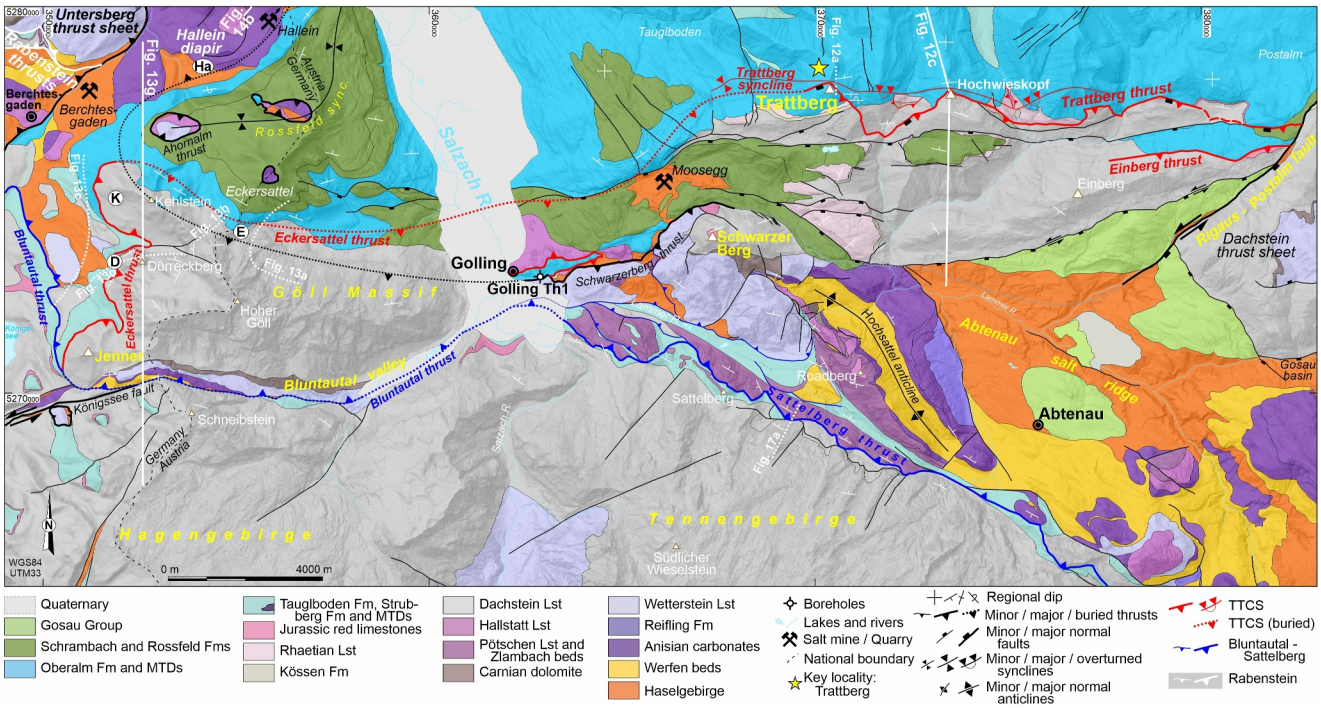

Figure 5. Map of the western segment of the TTCS. This map is based on fieldwork by the authors and previously published 1:50,000 scale geological mapping (Pavlik, 2007; Plöchinger, 1982, 1987).

5. Upper Jurassic reefs have been used as an indication of Late Jurassic uplift of the seafloor from bathyal depths (Kurz et al., 2023; Tollmann, 1987). This is particularly relevant where the Plassen Lst was deposited directly on Triassic pelagic facies (Hallstatt Lst or Reifling Fm), which required uplift in the order of many hundreds of meters.

4. Middle to Late Jurassic Deformation in the Central NCA

The analysis of literature, published geological maps and fieldwork has allowed us to identify a number of features in the central NCA as potential Late Jurassic structures (Table 3; Figure 2a). These features are the target of this contribution.

When plotted on the map, the Jurassic-age elements in Table 3 are seen to spread across the entire central NCA, over more than 100 km in an E–W direction, and up to 40 km in a N–S direction (features with white labels and red traces in Figure 2a). Prominently, a set of thrusts and folds (Eckersattel thrust, Trattberg thrust, Einberg thrust, Weissenbach anticline, Garbenbach thrust, Grünberg syncline, and Totengebirge thrust) are seen to align in a roughly WSW–ENE trend for over 80 km along strike (Figure 2a). Evidence for Jurassic tectonic activity along this corridor has been previously identified by multiple authors (Table 1), but only as isolated observations.

We propose here that this corridor of relaying thrusts, folds, and squeezed salt structures developed as a structurally linked system, and refer to it as the Totengebirge–Trattberg contractional system (TTCS). Below, we describe the TTCS, its relationship to pre-existing salt structures, and its syn-tectonic sedimentary record. We also describe the other Late Jurassic structures in the area.

4.1. The Totengebirge–Trattberg Contractional System (TTCS)

The TTCS runs roughly parallel to, and south of, an E–W trending depocenter of Middle to Upper Jurassic syntectonic Tauglboden and Oberalm Fms (Figures 2a, 4, and 5), whose infill recorded growth of the TTCS, as discussed below. The TTCS is thrust over, in its central segment, by the Dachstein TS (Figure 2a), a unit emplaced in the Early Cretaceous (Fernandez et al., 2024; Levi, 2023). This Dachstein thrust is used here to subdivide the TTCS into and eastern segment (from the Windischgarsten fault system to the Weissenbach anticline; Figures 2a

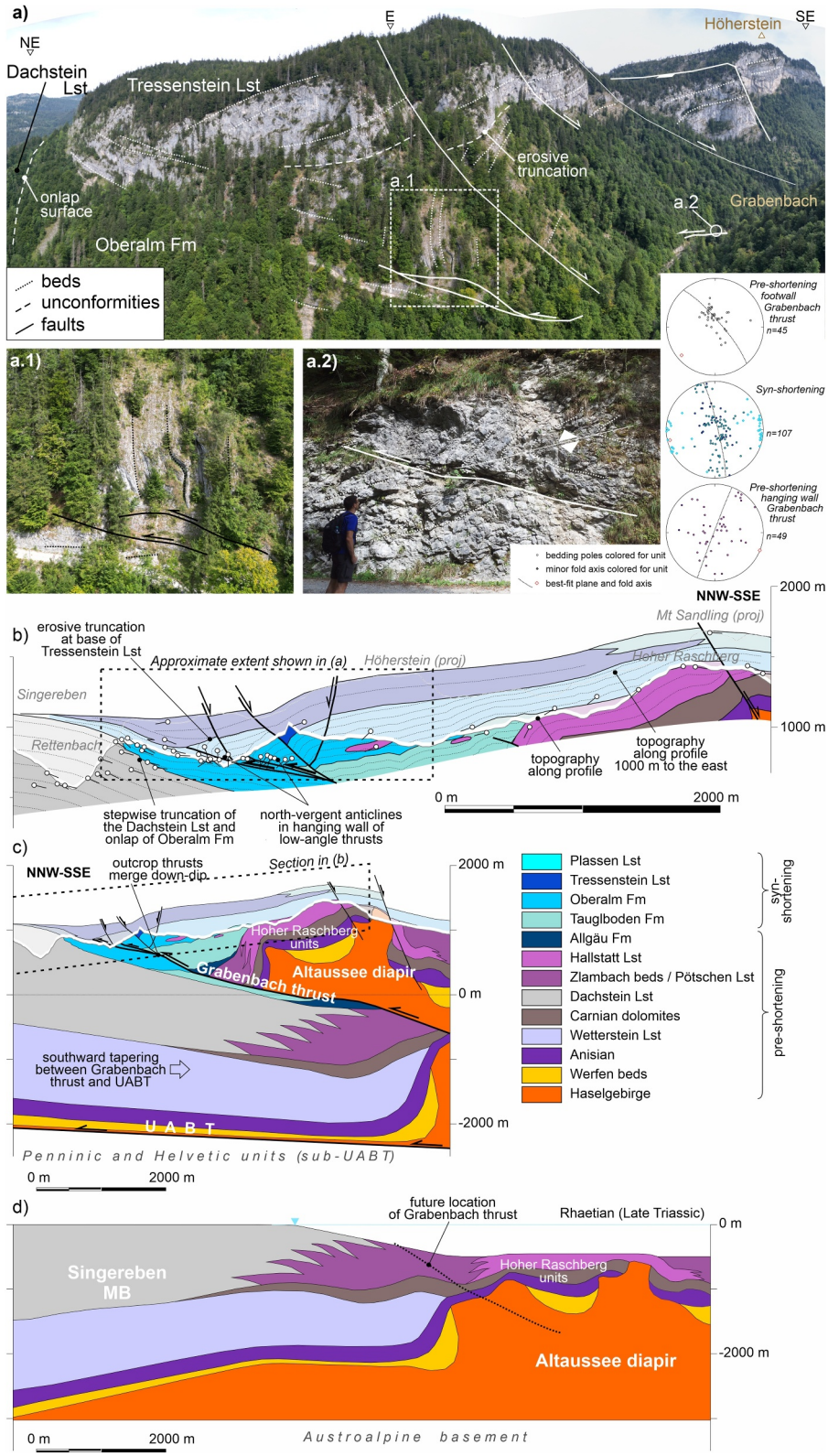

Figure 6.

and 4) and a western segment (from the Einberg and Trattberg thrusts to the Eckersattel thrust; Figures 2a and 5). Two localities, the Grabenbach in the east (star in Figure 4) and the Trattberg in the west (star in Figure 5), exhibit the best sedimentary record to establish the age of the TTCS. The description below hinges on these two localities to describe both segments of the TTCS.

4.1.1. Structure of the Eastern TTCS

Along the Grabenbach valley (star in Figure 4), the Oberalm Fm is observed to be folded and thrusted northwards on at least two low-angle thrusts (Figures 6a and 6b). In the hanging wall of both thrusts, beds of the Oberalm Fm are folded into north-vergent anticlines whose vertical frontal limbs are truncated erosively and sealed by the Tressenstein Lst. The Tressenstein Lst dips gently (~10°) north and is offset by normal faults (Figures 6a and 6b) that extend regionally with a NE–SW trend (Figure 4). The normal faults and the low-angle thrusts are roughly parallel in strike, possibly indicating that the normal faults detach into the thrusts. However, observations on smaller scale structures are also compatible with a cross-cutting relationship (e.g., Figure 7c).

Below the thrusts, the Oberalm dips 20–30° to the south. The Dachstein Lst below the Oberalm Fm is erosively truncated in a stair-step geometry (Figure 6b), with the Oberalm Fm and the Tauglboden Fm onlapping the erosive surface (Figures 7c and 7d). Map-scale olistoliths of Hallstatt Lst are observed within the Tauglboden and Oberalm Fms (Mandl, 1982, 2013). In the Grabenbach area, the Tauglboden and Oberalm Fms reach a maximum thickness of roughly 1000 m (Gawlick et al., 2007). To the south, they taper out and only roughly 100 m of Oberalm Fm lie between the Plassen Lst (above), and Hallstatt Lst (below) (Figure 6b). The Hallstatt Lst and underlying Carnian and Anisian carbonates rest on a body of inflated salt, the Altausee diapir (Leitner & Neubauer, 2011; Mandl et al., 2012). The Altaussee diapir is also cross-cut by NE–SW trending normal faults, that are interpreted to detach within the salt (Figures 4 and 6c).

At depth, the structure of the Grabenbach is interpreted to correspond to a thrusted diapir (Figure 6c). The low-angle thrusts that crop out (Figures 6a and 6b) are interpreted to be minor splays of a single thrust, named here the Grabenbach thrust, that dips southwards and extends into the Altaussee diapir (Figure 6c). Below the Oberalm Fm and the Grabenbach thrust, the Dachstein Lst is also interpreted to extend southward at relatively constant dip. Given the low dip of the UABT, the Triassic succession must also thin in that direction. This is interpreted to correspond to a transition of the Triassic platform toward a domain of thin pelagic facies that is the footwall equivalent of the Hallstatt Lst roof of the Altaussee diapir (Figure 6c). The precise location of the footwall ramp of the Grabenbach thrust is uncertain. The geometry proposed here results in 4 km of interpreted shortening between the initial (Figure 6d) and deformed states (Figure 6c), a magnitude compatible to that observed in the transect of Figure 8 (see below).

To the east of the Grabenbach, in the transect in Figure 8, the Grabenbach thrust disappears and is replaced by a train of NE–SW trending folds (TTCS label in Figure 8a). The two major folds in the fold train are the Grünberg syncline and the Ahornkogel–Brunnkogel anticline (or AB anticline for short), both previously described by Ganss (1937), Mandl et al. (2012), Mandl (2013), and Tollmann (1985). Two smaller isoclinal folds (the Bärnkogel and Sattelkogel anticlines) run between the Grünberg syncline and the AB anticline (Figure 8a). Based on their isoclinal geometry and half-wavelengths of under 500 m in the Dachstein Lst (Figure 7c), we interpret that the Dachstein Lst at this location is only around 200 m thick, and that units older than the Dachstein Lst are not involved in the folds.

Figure 6. (a) Aerial panorama of the Grabenbach valley, roughly parallel to the profile in panel (b). Vertical beds of the Oberalm Fm in the hanging wall of a N-directed low angle thrust (a.1) are unconformably overlain by the Tressenstein Lst. The Tressenstein Lst seals thrust-related deformation. A second low angle thrust is visible in outcrop with folded and steeply dipping beds of the Oberalm Fm (a.2). The structure is overprinted by extensional faults, which have been interpreted to root into the thrusts (see text for details). Photograph taken from: 401531E 5282008N 815 m. Stereonets show orientation of bedding of pre-orogenic Dachstein Lst in the footwall of the Grabenbach thrust and their best-fit fold-axis (10/229); bedding, best-fit fold-axis (06/257), and minor fold-axes of syn-orogenic Oberalm Fm; and bedding of pre-orogenic Hallstatt Lst and best-fit fold-axis (01/110) in the hanging wall of the Grabenbach thrust. All data are from within 1 km of the section in panel (b). (b) Detailed surface cross-section of the leading edge of the Grabenbach thrust, along the Grabenbach creek (see Figure 4 for location). The topography of the Höherstein and Mt Sandling (immediately east of the profile location) have been projected for reference. (c) Cross-section corresponding to (b) extended south and to depth. Note that the contrast in facies in the Upper Triassic between the hanging wall and footwall (pelagic vs. platform carbonates) requires the presence of a lateral transition at depth. (d) Cross-section in panel (b) restored to Late Triassic times.

Table 3

Structures Having Been Documented or Identified as Potential Late Jurassic Age in the Central Northern Calcareous Alps

Structure described	Evidence for Late Jurassic age (and object of revision)	Age constraints	Shown in figure(s)
Grubhörndl thrust	See Table 2. Possible interpretation as a thrust explored here.	Structure sealed by Oxfordian breccias (Ortner et al., 2008)	Figures 2a and 16
Gerhardstein–Lofer	Hallstatt Limestone capped by Plassen Lst (Mosna, 2010)	Kimmeridgian reef (Mosna, 2010)	
Klausbach thrust	Contact previously mapped (In Pavlik, 2007) but uninterpreted. Youngest rocks in the footwall are Strubberg Fm that also contains re-worked reefal Dachstein Lst (potentially sourced from its hanging wall) (Gawlick, Janauscheck, et al., 2003)	Youngest sediments in footwall are Callovian-Oxfordian (Gawlick, Janauscheck, et al., 2003)	Figures 2a and 18
Rabenstein thrust	Contact previously mapped (Risch, 1993) but uninterpreted. Youngest rocks in the footwall are Allgäu Fm (Risch, 1993) and Strubberg Fm	Youngest sediments in the footwall are Callovian-Oxfordian (Figure 5)	Figures 2, 5, and 18a
Untersberg	Plassen Lst reef lying on Dachstein Lst (Fenninger & Holzer, 1970)	Kimmeridgian reef (Fenninger & Holzer, 1970)	Figure 2a
Bluntautal thrust	Contact previously mapped (Braun, 1998; Pavlik, 2007) but uninterpreted or assumed to be purely strike-slip (Decker et al., 1994). Youngest rocks in the footwall are Strubberg Fm that contains re-worked reefal Dachstein Lst (potentially sourced from its hanging wall) (Gawlick, Janauscheck, et al., 2003)	Youngest sediments in the footwall are Callovian-Oxfordian (Gawlick, Janauscheck, et al., 2003)	Figures 2a, 5, 13, and 18a
Eckersattel thrust	Erosion surface sealed by the Oberalm Fm in its hanging wall (Braun, 1998), and faults across the Oberalm Fm sealed by Schrambach Fm (Fernandez et al., 2024)	Uplift sealed by Tithonian-Berriasian (Braun, 1998)	Figures 2a, 5, and 13f
Hallein diapir	Haselgebirge encountered overlying the Oberalm Fm sediments and covered unconformably by younger Oberalm Fm (Medwenitsch, 1960)	Salt sheet covered by Tithonian-Berriasian sediments (Medwenitsch, 1960)	Figures 2a, 5, and 15
Trattberg thrust	See Table 2. Relationship with salt tectonics explored here.	Oxfordian breccias and Tithonian-Berriasian growth wedges (Ortner, 2017)	Figures 2a, 5, and 12
Einberg thrust	Previously unnamed; mapped by Plöchinger (1982). Late Jurassic age by correlation with the Trattberg thrust and presence of thicker Oberalm Fm in its footwall	N/A	Figures 2a and 5
Falkenstein, Lugberg, Jainzenberg	Three Plassen Lst reefs (Falkenstein, Lugberg, Jainzenberg) along a NW–SE trend (Kügler et al., 2003; Schlagintweit & Gawlick, 2008; Steiner et al., 2021)	Oxfordian breccias and Kimmeridgian reef (Kügler et al., 2003; Schlagintweit & Gawlick, 2008; Steiner et al., 2021)	Figure 2a
Rettenstein diapir (?)	Highly condensed Middle-Upper Triassic stratigraphy in pelagic facies, capped by Callovian breccias and isolated Plassen Lst reef (Auer et al., 2008, 2009)	Oxfordian-Kimmeridgian reef (Auer et al., 2008, 2009)	Figure 2a, Figure S2 in Supporting Information S1
Ramsau diapir (?)	Isolated Plassen Lst reef directly overlying Werfen beds or condensed Triassic stratigraphy (Mandl et al., 2014) at its top	Kimmeridgian reef (Mandl et al., 2014)	Figure 2a, Figure S3 in Supporting Information S1
Hallstatt diapir	See Table 2. Revised mapping shows presence of Oberalm Fm in the area (Figure 14)	Youngest sediments below extrusive salt are Callovian (Suzuki & Gawlick, 2009) and Kimmeridgian-Berriasian reef (Gawlick & Schlagintweit, 2006)	Figures 2a and 14
Weissenbach anticline	Anticline previously dated as Cretaceous (Levi, 2023) but variable thickness in Upper Jurassic observed on crest and limbs	Anticline folds the Dachstein thrust, that is of Early Cretaceous age (Mandl, 2000). Late Jurassic age proposed in this contribution based on thickness changes in the Upper Jurassic.	Figures 2a and 4

Table 3
Continued

Structure described	Evidence for Late Jurassic age (and object of revision)	Age constraints	Shown in figure(s)
Grabenbach thrust	Feature newly identified in the field: vertical beds of the Oberalm Fm truncated by nearly flat-lying Tressenstein Lst (Gawlick et al., 2007)	Thrusting and folding presented here, sealed by Tithonian sediments (Gawlick et al., 2007). Oxfordian breccias in footwall of thrust (Gawlick et al., 2007)	Figures 2a, 4, and 6
Altaussee diapir	See Tables 1 and 2. Revised interpretation in association to Grabenbach thrust.	Callovian breccias on flank of diapir and Tithonian reef on top (Gawlick et al., 2007)	Figures 2a, 4, and 6
Grünberg syncline & Ahornkogel-Brunnkogel (AB) anticline	Tauglboden Fm are the youngest sediments in the Grünberg syncline in the north, Oberalm Fm are the youngest sediments in the syncline in the south (Schäffer, 1982)	Youngest sediments in syncline are Oxfordian-Kimmeridgian in northern Grünberg syncline, Tithonian in southern Grünberg syncline (Schäffer, 1982)	Figures 2a, 4, 8, and 10
Ariplan syncline	Tauglboden Fm are the youngest sediments in the isoclinal Ariplan syncline (Schäffer, 1982)	Youngest sediments in syncline are Oxfordian-Kimmeridgian (Schäffer, 1982)	Figures 2a, 4, and 10
Loser	Newly identified erosion surfaces. Upper Triassic (Dachstein Lst) is tilted and eroded, with erosions surface sealed by the Oberalm Fm	Erosional unconformity onlapped by Kimmeridgian-Tithonian (Schäffer, 1982)	Figures 2a, 8, and 9
Trisselwand	Areally extensive Plassen Lst reef	Kimmeridgian reef (Schlagintweit & Ebli, 1999)	Figures 2a and 4
Totengebirge thrust	Previously mapped by Egger & van Husen (2007) and Moser and Moshammer (2018) and interpreted by Linzer et al. (1995) as a low angle thrust of Cretaceous age. Correlation with the Grünberg syncline and AB anticline by Tollmann (1985) and Mandl (2013) indicates Late Jurassic age	Youngest sediments in footwall are Upper Triassic (Moser & Moshammer, 2018)	Figures 2a, 4, and 11
Feuerkogel, Krahstein (Bad Mitterndorf)	See Table 2. Plassen Lst reefs of the Krahstein and Feuerkogel cap pelagic Triassic (Hallstatt Lst and Reifling Fm) (Gawlick, Schlagintweit, et al., 2003)	Kimmeridgian reefs (Gawlick, Schlagintweit, et al., 2003)	Figure 2a
Wurzeralm	See Table 2.	Callovian breccias, Haselgebirge emplaced on Oxfordian rocks, and Kimmeridgian reef (Ottner, 1990)	Figure 2a

To the northwest of the Grünberg syncline, the Dachstein Lst dips to the south, in a geometry equivalent to that of the footwall of the Grabenbach thrust along strike (Figures 4 and 8a). The Dachstein Lst at this location is overlain unconformably by red pelagic Jurassic limestones (Figure 7a). Both are folded along E–W trending folds that are onlapped by beds of the Tauglboden Fm (Figure 7b). The Tauglboden Fm grades upwards into the Oberalm Fm, which forms the main unit cropping out in the core of the Grünberg syncline (Figure 8a). Dachstein Lst is found re-sedimented as clasts, boulders or decametric-sized olistoliths interbedded within the Oberalm Fm in the Grünberg syncline (Figure 9). Tilting, uplift and erosion of the Dachstein Lst is particularly visible on the southern flank of Mt Loser (right end of Figure 8a), where Oberalm beds unconformably lie above truncated and tilted Dachstein Fm (Figure 8c).

Besides tilting of the Dachstein Lst, the southeastern end of the transect in Figures 8a and 8f is characterized by the presence of numerous NE–SW trending normal faults. Some are of Triassic age, as indicated by facies changes in the Upper Triassic across them (Figure 8d). However, two major normal faults, that bound the block of Mt Loser to the north and south (Figure 8a; bold faults in Figure 8f), exhibit thickening of the Upper Jurassic across them and are interpreted to be at least partly Late Jurassic in age.

Along Figure 8 transect, outcrop constraints above, and the geometry of the UABT below, indicate that the Triassic varies in thickness along the transect. The Triassic is the thinnest across the TTCS (where only Dachstein Lst is present), and thicker on either side, where the Dachstei Lst is thicker and the Wetterstein Lst is interpreted to be present at depth (Figure 8f). The present-day configuration is interpreted to be the result of the TTCS folds

10.1029/2024TC008358

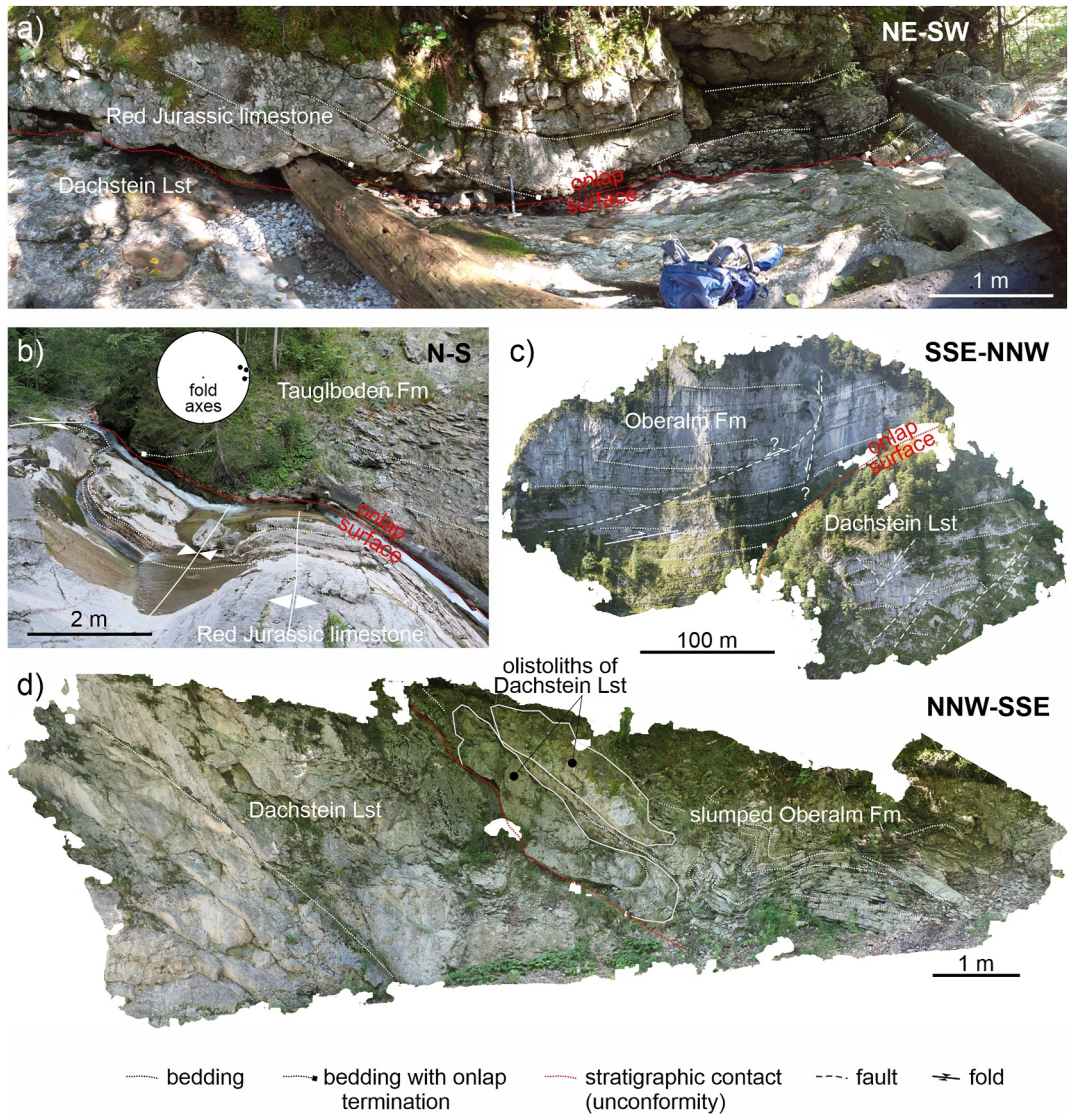

Figure 7. (a) Unconformable contact between red Jurassic limestone (of Lower to Middle Jurassic age) on the underlying Triassic Dachstein Fm. Outcrop location: 403930E 5283470N (see Figure 4). (b) The limestone in panel (a) is folded into gentle E–W trending anticlines that are onlapped by Middle to Upper Jurassic Tauglboden Fm beds. (a) and (b) are under 300 m apart. Outcrop location: 403730E 5283235N (see Figure 4). (c, d) Unconformable contact of the Upper Jurassic Oberalm Fm on the Triassic Dachstein Lst. Note that beds of both the Dachstein Lst and Oberalm Fm are oblique to the contact and both the Lower Jurassic and parts of the Dachstein Lst have been eroded. Reworked blocks of Dachstein Lst are sometimes contained in the Oberalm Fm (d). Both images are orthophotos generated with photogrammetry out of handheld and airborne photographs. Both outcrops are approximately 100 m apart across a valley (note opposing orientations) and 2,500 m west of the outcrop in panel (a). Outcrop (c) is located at 401355E 5282365N and (d) is located at 401400E 5282100N (see Figure 4).

forming by the buckling of the thin Dachstein Lst roof a previously inflated salt body (Figure 8g). Shortening estimated for Figure 8 transect based is of roughly 4 km. Significantly less shortening (~2 km) would result if the thrust interpreted cutting the Grünberg syncline were absent. This feature is unconstrained and its absence would also be compatible with field observations.

The Grünberg syncline and AB anticline extend NE from Figure 8 transect into the area of the Offensee, 10 km to the northeast (Figure 4). The minor Bärnkogel and Sattelkogel anticlines die out in this direction and the Grünberg becomes an upright isoclinal syncline. The Grünberg syncline here folds the Dachstein, that is under 200 m thick

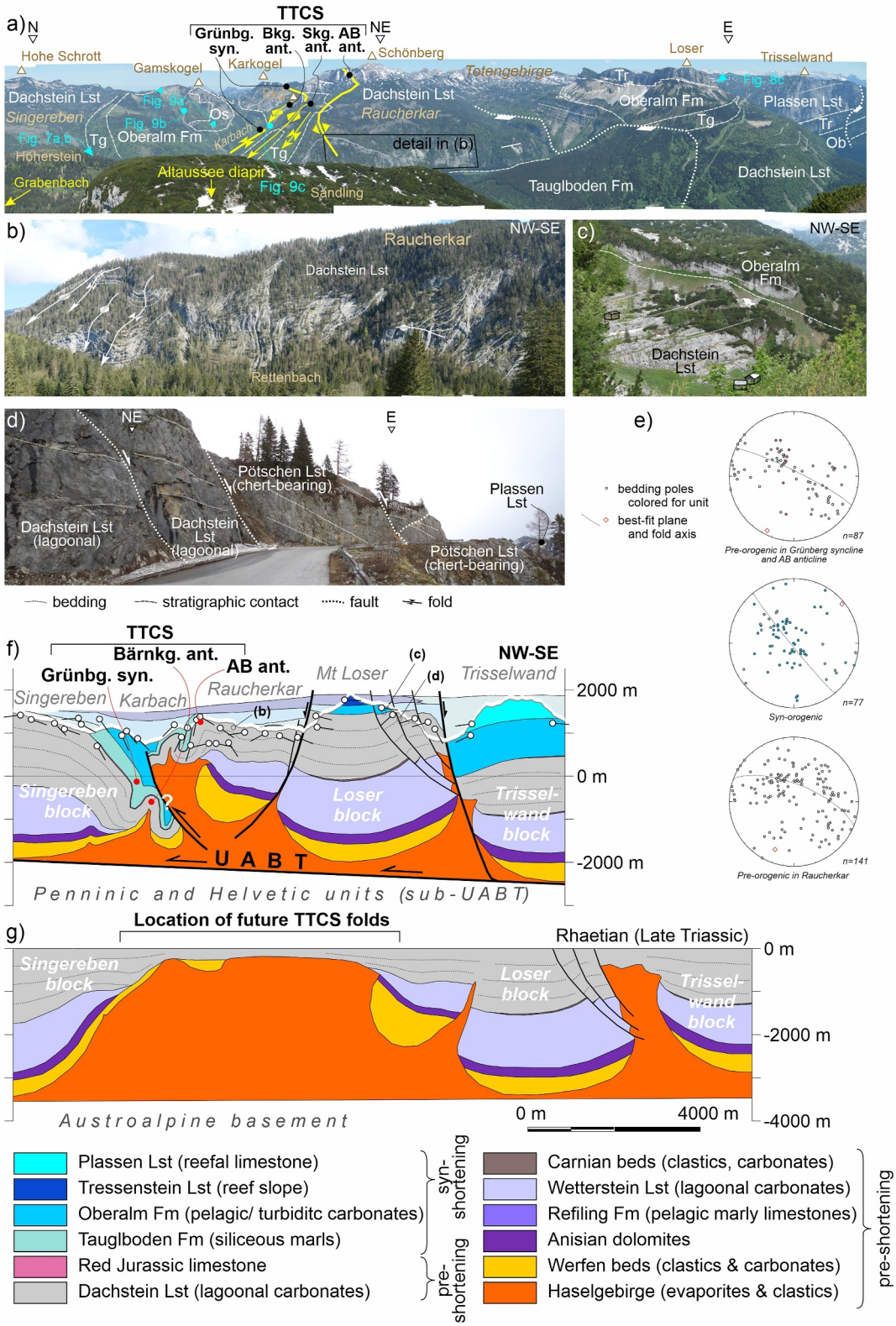

Figure 8.

(Figures 10a and 10c), and has Jurassic red limestone and Tauglboden Fm (but no Oberalm Fm) in its core (Figure 10c).

East of the Grünberg syncline, the Dachstein Lst is folded by the AB anticline into near horizontal beds, that expand stratigraphically rapidly toward the east (Figure 10b). The top of the Dachstein Lst remains gently dipping across the area whereas its base is folded into a tight overturned anticline formed exclusively by Dachstein Lst (Figure 10a). An internal unconformity separates the upper, gently-dipping interval of the Dachstein Lst from its basal, folded and overturned interval (Figures 10a and 10b). This geometry, already recognized by Spengler (1924), is interpreted to be a salt-related extensional rollover (as defined by Brun & Mauduit, 2008; Rowan et al., 2022; and analogous to the geometry of the Cotiella basin and Reduno anticline in Figures 4 and 6 of López-Mir et al., 2015) and therefore a geometry resulting from Triassic salt tectonics.

To the west of Grünberg syncline, the upright isoclinal Ariplan syncline runs SSW-NNE for about 3 km, with Tauglboden Fm as the youngest unit in its core (Figure 4). The Ariplan syncline has a very reduced half-wavelength (∼1 km). On either side of the syncline, the Dachstein Lst dips gently and is at least 1,000 m thick (as measured from valley bottoms to mountain tops). It is therefore interpreted that the Dachstein Lst thins into the Ariplan syncline, analogous to what happens in the Grünberg syncline (Figures 8f and 10e).

The Tauglboden Fm also crops out between the southern tip of the Ariplan and northern tip of the Grünberg synclines (Figures 4 and 10b). Outcrop is limited, but this outcrop possibly represents the linkage of the Ariplan syncline to the Grünberg syncline. Faulting at this location (Figures 4 and 10b) masks the precise relationship between both synclines. Nonetheless, due to similarity in the structure and orientation, the Ariplan syncline is grouped with the Grünberg syncline and the AB anticline into the TTCS at this location (Figure 10e). Faulting at their intersection, although not resolved in detail, might be due space problems related to the non-cylindrical geometry.

In both the Ariplan and Grünberg synclines the reduced thickness of the Dachstein Lst is interpreted to be primary, and to have resulted from it having deposited above inflated salt bodies (Figure 10f). Away from the Offensee area, it is interpreted that the Triassic succession is up to 3500 m thick (Singereben and Totengebirge minibasins on both ends of Figures 10e and 10f).

Shortening across the TTCS at the Offensee is estimated at roughly 5 km.

Mandl (2013) and Tollmann (1985) already observed that the Grünberg syncline and AB anticline terminate at the Offensee (Figure 4) and proposed that shortening is relayed onto the Totengebirge thrust (Figure 10a). The Totengebirge thrust at the Offensee places the Haselgebirge and Wetterstein Lst of its hanging wall on the Dachstein Lst in its footwall (Figure 10a). This configuration requires at least 1–2 km of vertical offset, which is the thickness of the Wetterstein Lst in the hanging wall of the Totengebirge thrust.

The Totengebirge thrust extends eastwards from the Offensee and is best exposed at the location of the transect in Figure 11. Here, the thrust is subhorizontal (Figure 11a) and a hanging wall flat of Anisian limestones lies directly on a footwall flat of Dachstein Lst (Figure 4) (Fernandez et al., 2024; Linzer et al., 1995; Moser & Moshammer, 2018). Above the Anisian limestones, the Ladinian Wetterstein Lst transitions northwards into the pelagic Reifling Fm (Figure 4). No Norian or younger rocks have been preserved in this area.

In the footwall of the Totengebirge thrust, the Grünau borehole (Figure 4) encountered a thick Norian Dachstein Lst (in total >2,000 km thick) and barely over 50 m of pelagic Reifling Fm (as shown on Figure 11c) (Hamilton, 1989). South of the Kasberg, geological mapping indicates an almost inverted situation, with a nearly 2,000 m

Figure 8. (a) Panorama photograph from Mt Sandling spanning the transect in panel (f), showing the train of folds that forms the TTCS north of the Raucherkar (see Figure 4). Photograph taken from Mt Sandling: 403450E 5278950N. (b) Panorama looking due NE coinciding partially with that in panel (a). The Dachstein Fm dips steeply down into the valley. Photograph taken from: 406820E 5280900N. (c) Photograph of the Oberalm Fm unconformably overlying the tilted Dachstein Lst on the Mt Loser. Photograph taken from: 409410E 5279530N (see Figure 4). (d) Facies change in Upper Triassic rocks from lagoonal Dachstein Fm to (pelagic) chert-bearing Pötschen Fm related to syn-depositional (Triassic age) faulting on the south flank of Mt Loser. Photograph taken from: x408560 y5278750 (see Figure 4). (e) Stereonets of bedding of pre-orogenic (Upper Triassic to Lower Jurassic) rocks in the Grünberg syncline and AB anticline and best-fit fold-axis (07/206); bedding of syn-orogenic (Upper Jurassic) rocks and best-fit fold-axis (03/052); bedding of pre-orogenic (Upper Triassic) rocks in the Raucherkar area and best-fit fold-axis (22/202). All dip data are within 1 km of the section in panel (f). (f) Cross-section of the TTCS in the Raucherkar area. The TTCS is dominated by a train of isoclinal folds, potentially thrusted. Grünbg. syn.: Grünberg syncline; Bärnkg./Bkg. ant.: Bärnkogel anticline; AB ant.: Ahornkogel-Brunnkogel anticline. See Figure 4 for location. The approximate location of photos in panels (b), (c), and (d) are shown. (g) Restoration of the section in panel (f) to Late Triassic times.

10.1029/2024TC008358

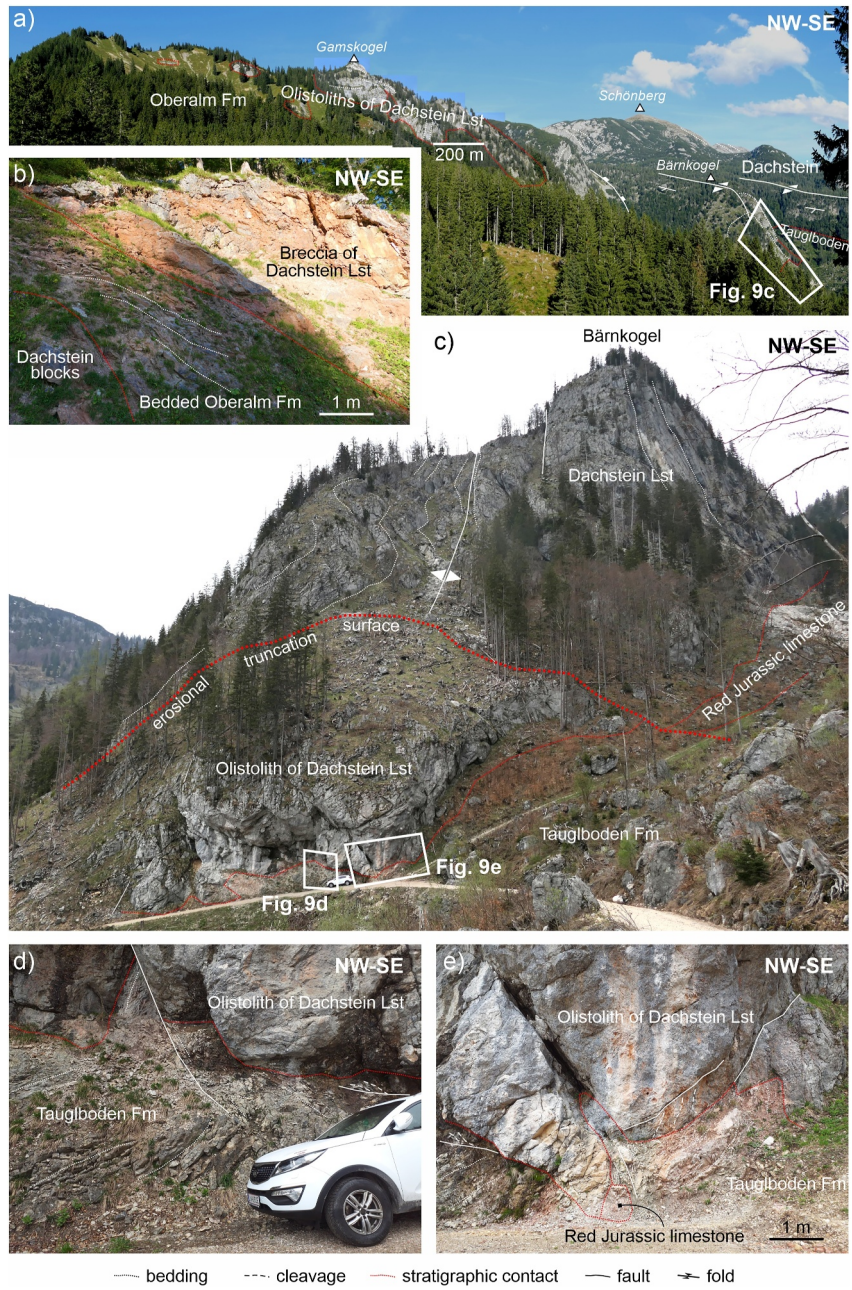

Figure 9. (a) Panorama showing olistoliths of Dachstein Lst within the Oberalm Fm on the flank of the Gamskogel mountain (see Figure 4). An approximate scale bar is provided for the main body of olistoliths. Photos taken from 404915E 5284585N. (b) Detail of breccias of Dachstein Lst with interbedded Oberalm Fm. Outcrop location: 405615E 5285000N (see Figure 4). (c) Erosional truncation of a tight anticline in the Dachstein Lst (Bärnkogel anticline) overlain by an olistolith of Dachstein Lst. The car in the photo is roughly 5 m long. (d, e) Detailed pictures of the contact between the Dachstein Lst olistolith and the underlying Tauglboden Fm. Note strong folding and development of foliation in the Tauglboden Fm. The car in panels (c, d) was parked in front of the outcrop by a third party and does not obstruct any key structures. Outcrop location: 406720E 5284215N (see Figure 4).

thick Wetterstein Lst platform and 1,000 m of Dachstein Lst platform. We interpret that this configuration is the result of lateral migration of subsidence of Triassic platforms into the Haselgebirge unit (Figures 11d and 11e) (cf. Figure 4 in Granado et al., 2019).

10.1029/2024TC008358

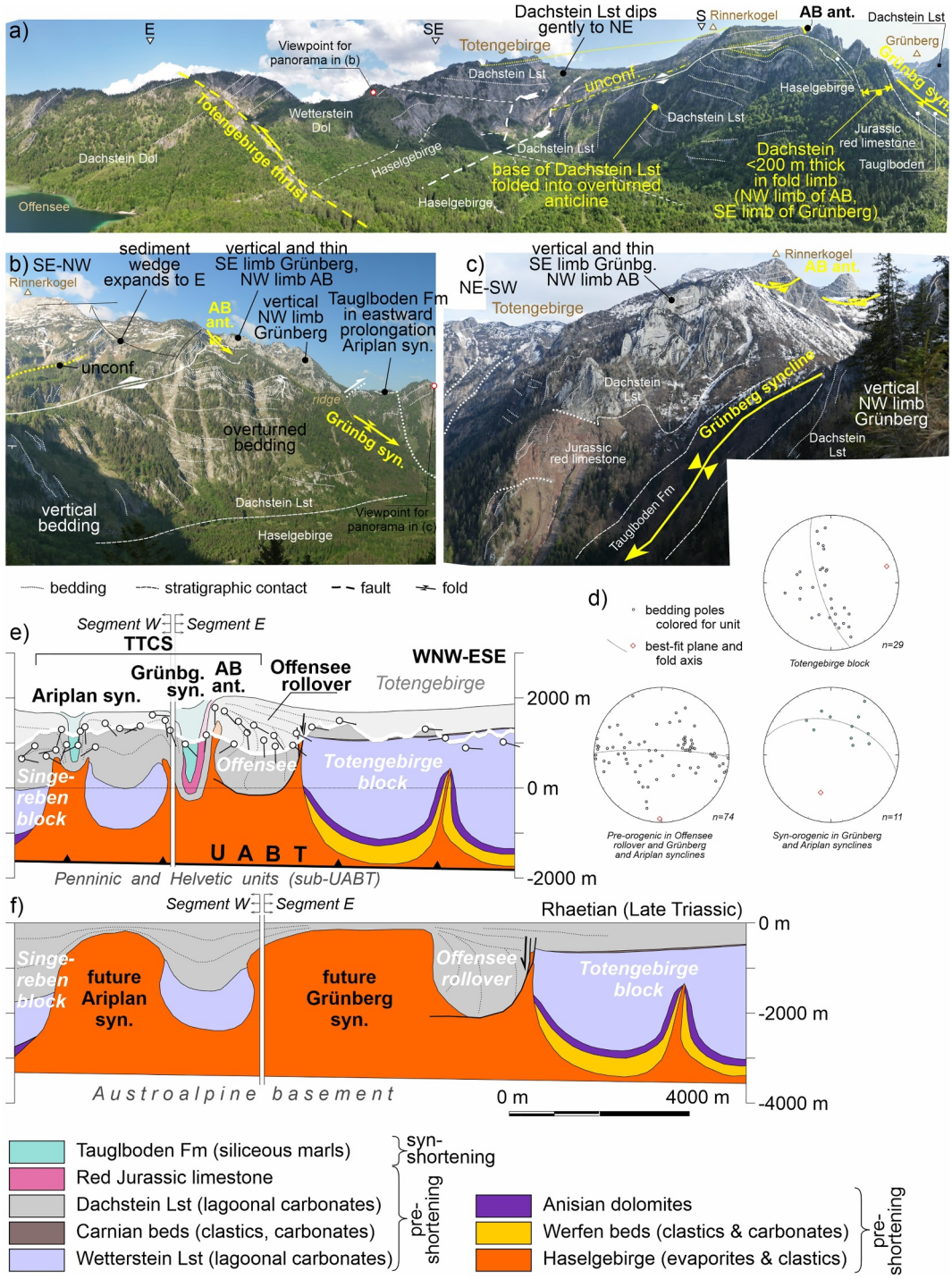

Figure 10. (a) Aerial panorama of the TTCS at the Offensee (see Figure 4). From left to right in the panorama, note the ramp-on-ramp configuration of the Totengebirge thrust, the overturned rollover anticline in Dachstein Lst, the Ahornkogel-Brunnkogel anticline (AB ant.) and the upright isoclinal Grünberg syncline (Grünbg. syn.) at the right end of the panorama. Photograph taken from: 412944E 5289025N 740 m. (b) Photograph of the overturned rollover anticline in panel (a) taken from the NE. See (a) for panorama point: 414290E 5288330N. (c) Photograph of the eastern limb of the Grünberg syncline. See (b) for panorama point: 411400E 5288970N. (d) Stereonets of bedding in the Totengebirge block and best-fit fold axis (15/073); bedding of pre-orogenic (Triassic) rocks in the Offensee rollover, Grünberg and Ariplan synclines and best-fit fold-axis (05/181); bedding of syn-orogenic (Upper Jurassic) rocks in the Grünberg and Ariplan synclines and best-fit fold-axis (42/195). (e) Cross-section of the TTCS in the area of the Offensee. The TTCS here is dominated by two isoclinal synclines involving the Dachstein Lst and Jurassic units: the Ariplan and Grünberg synclines. In contrast to the highly reduced thickness of the Dachstein Lst in the synclines, the eastern flank of the AB anticline presents a major stratigraphic expansion of the Dachstein Lst associated to an extensional roll-over. The cross-section has been built in two segments to avoid local structural complexity in the area when representing the regional–scale relationship between the Ariplan and Grünberg synclines. See Figure 4 for location. (f) Restoration of the section in (e) to Late Triassic times.

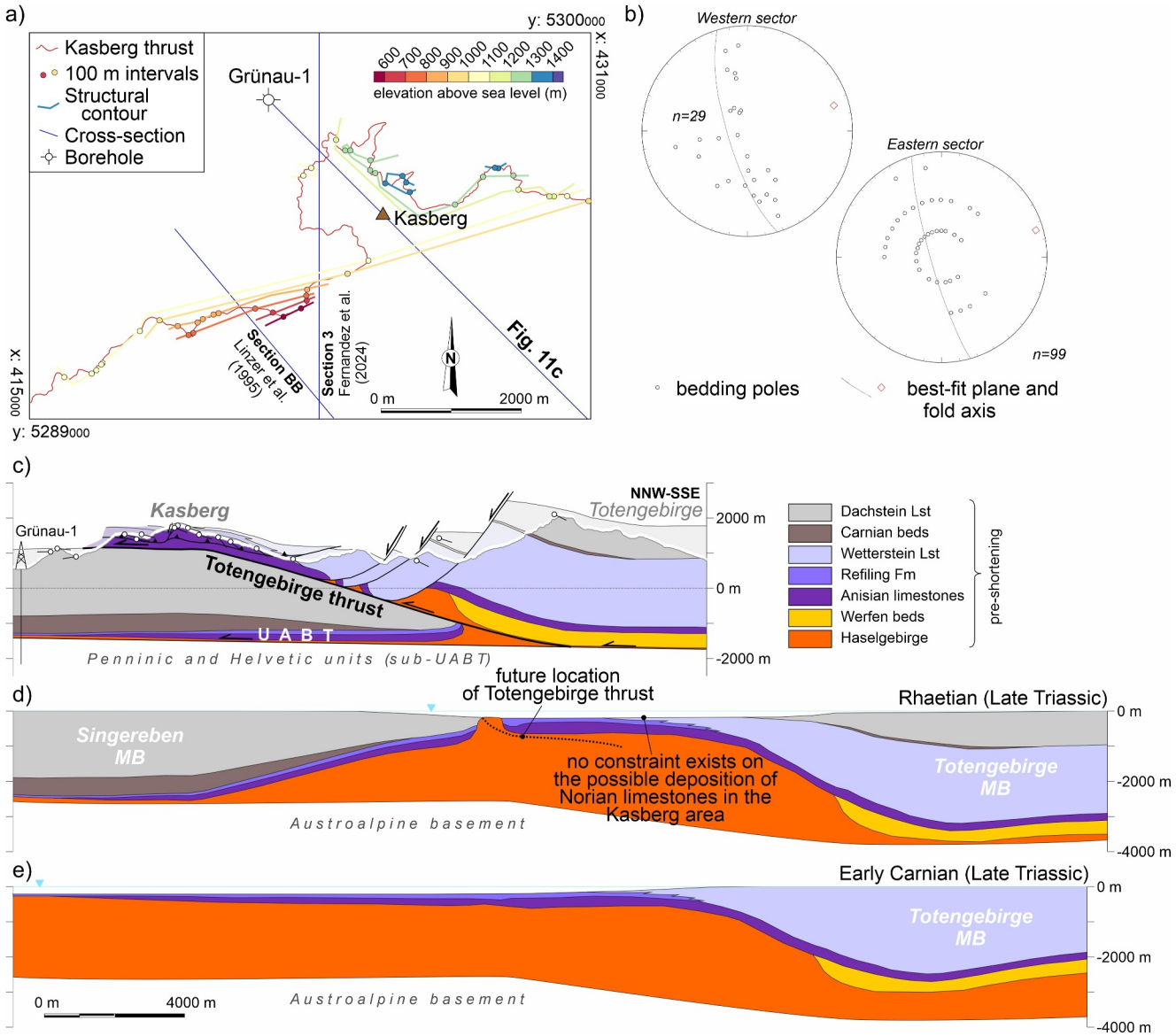

Figure 11. (a) Structural contour map of the Totengebirge (Kasberg) thrust between the Offensee and the Windischgarsten fault system (see Figure 4 for location). The colored dots along the trace of the thrust represent 100 m elevation intervals. The bold colored lines are contour lines for the thrust surface drawn based on the elevation of the trace. Note that the contours between 600 and 1,100 m above sea level have a roughly WSW–ENE strike. The shallowest contours (>1,100 m) reveal that the surface climbs to the NE in its northeastern corner, with a possible culmination to the ENE of Mt Kasberg. (b) Stereonets with bedding from the hanging wall of the Totengebirge thrust by the Offensee, and best-fit fold (15/073); and bedding from the hanging wall of the Totengebirge thrust within the map area in panel (a) from Egger and van Husen (2007) and Moser and Moshammer (2018). The blocky nature of the dip measurements is due to standards in rounding of the Austrian Geological Survey. The best-fit fold axis plunges 08/074. (c) Cross-section of the Totengebirge thrust at the Kasberg. See Figure 4 for location. (d) Restoration of the section in panel (c) to Late Triassic times. (e) Restoration of the section in panel (c) to early Late Triassic times.

Southwest of the Kasberg peak, the Totengebirge thrust surface is observed to dip to the SSE (Figure 11a). Although this geometry is equivalent to that of a footwall ramp, we interpret that it is partly the result of southward dip (and thinning) of the footwall block (Figure 11c), similar to the footwall of the Grabenbach thrust (Figure 6c). Northeast of the Kasberg peak, the thrust presents an inflection and strikes NW–SE (Figure 11a). This direction is parallel to the NW-directed kinematic indicators documented by Linzer et al. (1995) on the thrust surface, and therefore likely represents an oblique ramp.

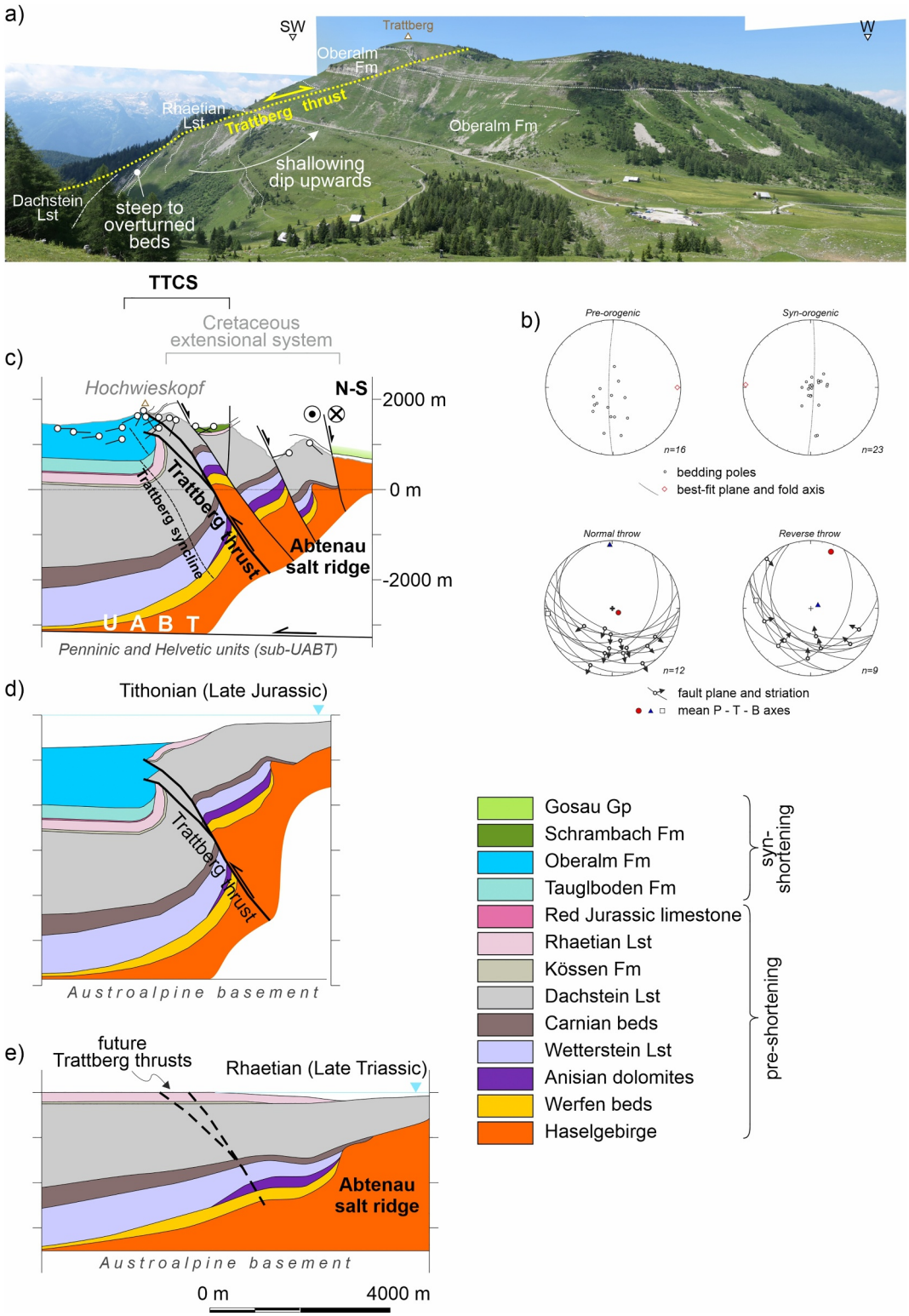

Figure 12.

The hanging wall ramp of the Totengebirge thrust has not been preserved and therefore, thrusting estimates are minimum values. Linzer et al. (1995) estimated a minimum 8 km displacement (assuming layer-cake stratigraphy). The cross-section presented here (Figures 11c and 11d) implies a shortening of roughly 11 km.

The Totengebirge thrust extends east into the Windischgarsten fault system (Figures 2 and 4), a system of faults most recently active in the Miocene (Linzer et al., 2002) but which was originally an area of inflated salt during the Triassic (Eggerth, 2023). An equivalent thrust has not been documented east of this fault system.

4.1.2. Structure of the Western TTCS

West of the Grabenbach (star in Figure 4), the TTCS is represented by the Weissenbach anticline, an E–W trending structure that also folds the Dachstein thrust (Levi, 2023). In the footwall of the Dachstein thrust, the Jodschwefelbad borehole (JSB-1 in Figure 4; Mandl et al., 2012) drilled the crest of the Weissenbach anticline. Borehole and field data indicate that the Upper Jurassic is significantly thinner on the crest and backlimb (southern limb) of the Weissenbach anticline (Figure 2b). This is interpreted to indicate that growth on the Weissenbach anticline is in part Late Jurassic, and coeval with the TTCS. Folding on this anticline was long-lived and continued after it had been overthrust by the Dachstein TS (Levi, 2023).

Thanks to post-Jurassic folding, the Weissenbach anticline can be traced across the Dachstein TS (Figure 2a) and ends along strike of the Trattberg thrust (Figure 2a), slightly north of the Einberg thrust (Figure 2a). This correlation is further supported by the trend of Upper Jurassic depocenters. The E–W Upper Jurassic depocenter that runs along and north of the Grünberg syncline and the Grabenbach thrust (label G in Figure 2b) extends west under the Dachstein TS into to the depocenter that runs north of the Trattberg thrust (Osterhorngruppe depocenter; label Oh in Figure 2b) (Gawlick et al., 2007).

The Trattberg thrust (star in Figure 5), which defines the southern margin of the Osterhorngruppe depocenter, is a prominent thrust that can be mapped for 10 km along its roughly E–W strike (Figure 5; Ortner, 2017). The thrust is a high-angle reverse fault that juxtaposes Dachstein Lst in its hanging wall against the Oberalm Fm in its footwall (Figure 12a). At outcrop, the surface of the Trattberg thrust displays kinematic indicators that indicate reverse-throw overprinted by normal-throw (Figure 12b). In the footwall of the thrust, bedding is steep to overturned at the elevation of the Dachstein and Rhaetian Lsts. The oldest beds of the Oberalm Fm are also vertical to overturned, but dip in the Oberalm Fm decreases stratigraphically upwards, defining a growth syncline geometry (Figures 12a and 12c; Ortner, 2017). Both the pre-shortening and syn-shortening units in the footwall form a roughly E–W trending syncline, the Trattberg syncline (Figure 12b).

Thickness of the pre-shortening Middle-Upper Triassic succession is interpreted to be over 3000 m thick north of the Trattberg thrust (Vordersee-1 borehole; Fernandez et al., 2024; Geutebrück et al., 1984) and to thin southwards to under 1000 m at the Schwarzer Berg, some 3 km to the south (Figures 5 and 12c). Extensive outcrops of Haselgebirge to the SE of the Trattberg, around the locality of Abtenau (Figure 5), are interpreted to be the remnants of a large Triassic body of inflated salt (Abtenau salt ridge). This body is interpreted to extend northwards under the hanging wall of the Trattberg thrust (Figure 12c).

In the immediate footwall of the Trattberg thrust, the Oberalm Fm lies directly on the Dachstein Lst, without any intervening Rhaetian Lst. This is the result of mass wasting during uplift prior t thrusting (Ortner, 2017) (Figure 12d). Whereas the Oberalm Fm reaches a thickness of up to 1,000 m in the footwall of the Trattberg thrust (Figure 2b) (Fernandez et al., 2024; Ortner, 2017) it is mostly absent to its south (Figure 5; Frisch & Gawlick, 2003), implying broad uplift of the hanging wall of the Trattberg thrust. Plöchinger (1953) and Frisch and

Figure 12. (a) Photograph of the Trattberg at Mt Trattberg (see Figure 5 for location). Note the reverse throw on the fault (juxtaposition of Rhaetian Lst on Upper Jurassic Oberalm Fm) and vertical to overturned dips in the footwall (to the left). Fault reactivation in extension is indicated by S-C fabrics seen in outcrop. The topographic drop to the S of Mt Trattberg is also related to post-Jurassic extensional faults (Fernandez et al., 2024). Photograph taken from: 371500E 5278730N. (b) Above, stereonets of bedding of pre-orogenic (Upper Triassic) rocks in the footwall and hanging wall of the Trattberg thrust and best-fit fold-axis (06/091); bedding of syn-orogenic (Upper Jurassic) rocks in the footwall and hanging wall of the Trattberg thrust, and best-fit fold-axis (04/273). Data within 1 km from the section in panel (c). Below, fault dips and striations indicating normal and reverse throw measured along the Trattberg thrust. The average of individually calculated P-T and B axes are shown. (c) Cross-section of the TTCS immediately west of the Trattberg. Thrusting of Jurassic age along the Trattberg thrust is partly inverted in extension along a set of Cretaceous extensional faults. See Figure 5 for location. (d) Restoration of the section in panel (c) to Late Jurassic times. Uplift during the Late Jurassic was accompanied by erosion, as evidenced by the local absence of the uppermost Triassic (Rhaetian reefal limestone) under the Upper Jurassic Oberalm Fm in the footwall of the Trattberg thrust. (e) Restoration of the section in (c) to Late Triassic times.

Gawlick (2003) have already identified the Trattberg as a major paleogeographic barrier within the central NCA in the Late Jurassic.

The hanging wall of the Trattberg thrust is cross-cut by E–W trending extensional faults (Figure 5) that have been interpreted to relate to Cretaceous extension within the NCA thrust stack (Fernandez et al., 2024; Ortner, 2017; Plöchinger, 1953). Removing the effect of Cretaceous extension (Figures 12d and 12e) it is estimated folding and thrusting along the Trattberg accommodated roughly 2 km of shortening.

To the east, the Trattberg thrust disappears under the western lateral ramp of the Dachstein TS (the Rigaus–Postalm fault, Figure 5) where it is interpreted to link with the Weissenbach anticline, as discussed above. In this area, the Trattberg thrust overlaps with the Einberg thrust (Figure 5), a high-angle thrust of Late Jurassic age (Table 3) that also disappears under the Dachstein TS, and is also interpreted to be part of the TTCS.

Toward the west, the Trattberg thrust is buried by the syn-shortening Oberalm Fm and overprinted by E–W Cretaceous extensional faults (immediately west of the Trattberg peak, Figure 5). West of the Salzach River valley, and along strike of the Trattberg thrust, Braun (1998) documented that the Dachstein Lst along the northern Göll Massif is truncated by an erosional unconformity that is onlapped by the Oberalm Fm (label E in Figures 5, 13a, and 13b). Likewise, Braun (1998) described a thrust contact along the western margin of the Göll Massif, between vertically dipping Dachstein Lst and Tauglboden Fm below (label D in Figures 5 and 13c). This thrust contact (the Eckersattel thrust) can be traced along the entire western margin of the Göll Massif, where it progressively ramps up in the footwall into the Oberalm Fm (label K in Figures 5 and 13c). To the east the thrust becomes buried (sealed) by the onlapping Oberalm Fm beds described by Braun (1998) (label E, Figure 5). The linkage between the Eckersattel and the Trattberg thrusts is buried by the Oberalm Fm, and could be either a hard thrust link or an intervening Late Jurassic age anticline.

Similar to what is observed north of the Trattberg, the Upper Jurassic expands stratigraphically to the north of the Göll Massif (toward label Ha in Figures 2b and 5). Along with the Late Jurassic erosion and onlap outlined above (label E in Figure 13a) these observations are interpreted to indicate Late Jurassic uplift of the Göll Massif. Nonetheless, folding in the Rossfeld and Schrambach Fms in this area (Rossfeld syncline, Figure 5) indicates that deformation continued into the Early Cretaceous (discussed with the Hallein diapir in Section 4.1.2), overprinting and accentuating Jurassic deformation.

Along the western Göll Massif, the Eckersattel thrust transports extensional faults in its hanging wall (bright blue in Figure 13c) that offset the top of the Dachstein Lst by almost 1,000 m (label D in the hanging wall and K in the footwall; Figures 13c, 13e, and 13f). More regionally, however, the Dachstein Lst in the Göll Massif (hanging wall of the Eckersattel) forms a single N-dipping panel (Figure 13a). To the north of the Göll Massif, the structure at depth becomes uncertain, but significant volumes of Haselgebirge are known to be present in the subsurface related to the Hallein diapir (Kellerbauer, 1996; Medwenitsch, 1960; Schauberger, 1972) (Figure 13f). To the south, the Göll Massif is backthrust on the Bluntautal thrust onto the north-dipping Hagengebirge unit (details discussed below).

West of the Göll Massif there are no further north-directed shortening structures that could represent a continuation of the TTCS. In total, the TTCS extends over more than 80 km in a WSW–ENE direction.

4.2. Other Jurassic Contractional Structures in the Central NCA

Although the TTCS represents the most continuous and best constrained system of contractional structures in the central NCA, other Late Jurassic contractional features exist in the area. These include both features, that at present appear in isolation, as well as thrusts that potentially form a second linked system.

4.2.1. Isolated Late Jurassic Shortening Features

Some isolated shortening structures have been identified in the central NCA that are associated with Triassic age diapirs. The Wurzeralm salt allochthon (Kurz et al., 2023) (eastern end of the study area, Figure 2a), for instance, resulted from extrusion driven by squeezing of a diapiric stock (in the order of 1–2 km of shortening based on Kurz et al., 2023). The extruding salt modified the Late Jurassic seabed locally, generating a local high above the squeezed salt stock, where a Plassen Lst reef developed (Kurz et al., 2023).

10.1029/2024TC008358

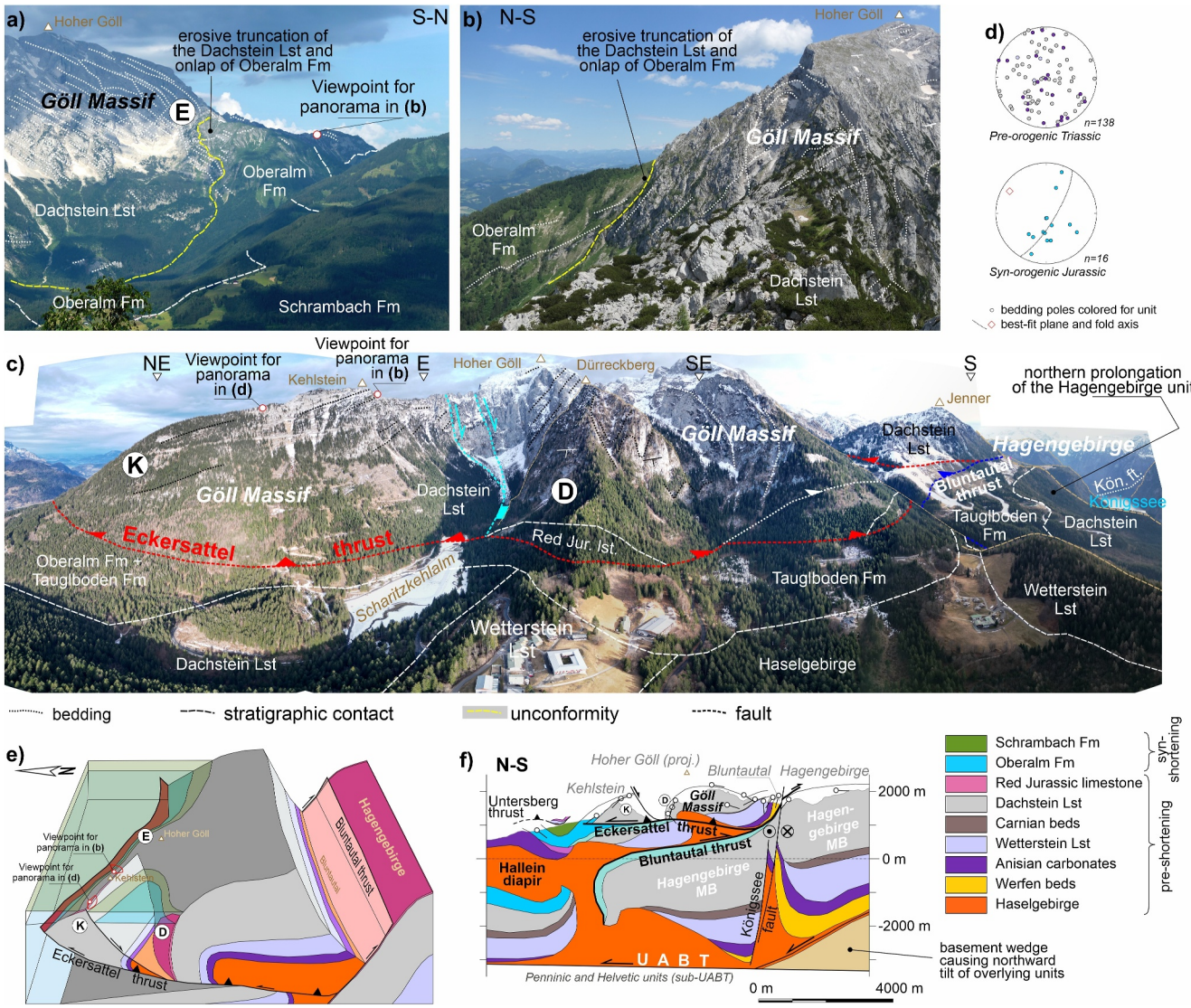

Figure 13. (a) Photograph of the Göll Massif from the east (see Figure 5 for location). Note the truncation of the Dachstein Lst along the northern slope of the Göll Massif and its onlap by Jurassic Oberalm Fm and Lower Cretaceous Schrambach Fm. Photograph taken from: 364580E 5276050N. (b) Panorama of the unconformity of Oberalm Fm on Dachstein Lst from the west (see Figure 5 for location). Photograph taken from: 353170E 5274740N. (c) Aerial panorama of the western side of the Göll Massif (see Figure 5 for location). The Eckersattel thrust (yellow in the figure) carries the Dachstein Lst of the Hoher Göll (HG) in its hanging wall with Jurassic and Permo-Triassic units in its footwall. The Bluntautal thrust is shown in magenta. This panorama is at 180° from that in Figure 18. Photograph taken from 351129E 5273938N 1,515 m. (d) Stereonet of bedding of pre-orogenic (Middle-Upper Triassic) rocks; and bedding of syn-orogenic Upper Jurassic and best-fit fold-axis (18/301). Data from within 1 km of the section in panel (f). Bedding of pre-orogenic strata are scattered due to the non-cylindricity of the structure of the HG. (e) 3D block diagram (not to scale) of the Göll Massif depicting the structure of the area at Cretaceous times (prior to strike-slip faulting on the Königssee fault). The block diagram represents a view direction like that in panel (c) from a higher position. (f) Cross-section of the Göll Massif area with the Eckersattel and Bluntautal thrusts. The Eckersattel thrust places the Göll Massif onto the margin of the Hallein diapir and the Bluntautal backthrust places it onto the Hagengebirge block. The Bluntautal thrust is cross-cut by the Neogene sinistral Königssee fault. The base of the Hallein diapir is known to lie below sea level based on data from exploratory boreholes in the Hallein and Berchtesgaden salt mines (Kellerbauer, 1996; Medwenitsch, 1960; Schauberger, 1972) but is otherwise unconstrained. See Figure 5 for location.

Fernandez et al. (2021) also proposed a process of Late Jurassic salt allochthony to explain the juxtaposition of Haselgebirge on Middle Jurassic radiolarites in the Hallstatt diapir (in the center of the study area, Figure 2a). A revised map of the Hallstatt diapir (Figure 14a), with the recognition of previously undocumented Oberalm Fm above the diapir, has been used to construct an updated restoration for the cross-section of Fernandez et al. (2021) (Figures 14b–14d). Restoration yields a shortening of roughly 4 km in a NW–SE direction (Figure 14). As with the Wurzeralm, a Plassen Lst reef grew atop the Hallstatt diapir during Late Jurassic contraction.

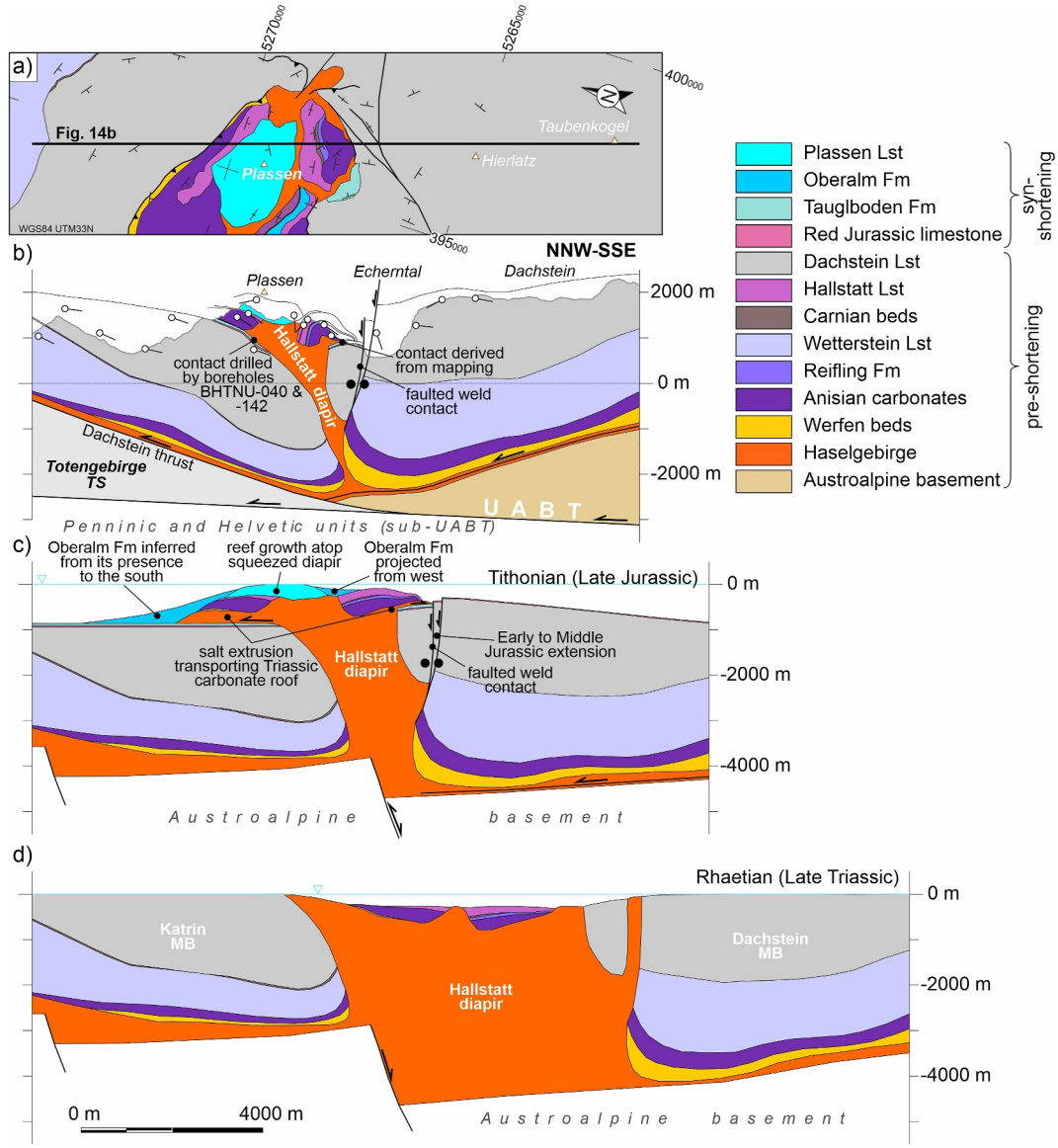

Figure 14. (a) Geological map along a transect crossing the Hallstatt diapir. Map based on mapping by the authors and Schäffer (1982). See Figure 2a for location. (b) Cross-section of the Hallstatt diapir, updated from Fernandez et al. (2021). (c) Restoration of the section in panel (b) to Late Jurassic times. This interpretation contrasts with that in Fernandez et al. (2021) because of the revised dating and structural analysis of the southern flank of the Hallstatt diapir presented by Fernandez et al. (2022). (d) Restoration of the section in panel (b) to Late Triassic times.

Besides these localities of isolated reef buildup, other areas of Plassen reef growth appear to align along NW–SE trends:

1. The Krahstein and Feuerkogel reefs in the Bad Mitterndorf area (Figure 2a; Gawlick, Schlagintweit, et al., 2003).
2. The Rettenstein and Ramsau reefs (south-central study area, Figure 2a) (Auer et al., 2009; Mandl & Matura, 1995; Mandl et al., 2014; Neubauer & Moser, 2022) (preliminary cross-sections are presented in the Figures S1, S2, and S3 in Supporting Information S1).
3. The Gerhardstein-Lofer area (western study area, "Gerh.Lo." in Figures 2a and 16) (Mosna, 2010; Ortner et al., 2008; Pavlik, 2006; Sanders et al., 2007).

4. The Falkenstein, Lugberg and Jainzenberg reefs (north-central study area, Figure 2a; Kügler et al., 2003; Schlagintweit & Gawlick, 2008; Steiner et al., 2021). The Altaussee diapir and its overlying Plassen reef define the southeastern end of the NW–SE trend of the Falkenstein–Lugberg–Jianzenberg reefs.

In contrast to these areally limited reef buildups and their NW–SE trend, the Trisselwand covers an area tens of square kilometers with a rough NE–SW elongation (Figures 2a and 4; SE end of the section in Figure 8f) (Schlagintweit & Ebli, 1999). It developed as the culmination of a shallowing-up Upper Jurassic succession that rests above the Dachstein Lst (Figure 8f). In spite representing the shallowest Upper Jurassic facies, at present it lies deeper than the slope units immediately to its north (see Figure 8f). This is interpreted to result from post-Jurassic subsidence (possibly akin to that described south of the Trattberg). The greater thickness of the Upper Jurassic succession in the Trisselwand block, compared to its neighboring Loser block (Figure 4; depicted on the section in Figure 8f) indicates subsidence of the Trisselwand block must have also been in part Upper Jurassic, possibly due to salt evacuation from under the Trisselwand depocenter driven by the overburden.

Further to these areas of Late Jurassic reefal growth, three other localities in the west of the study area present evidence of Late Jurassic shortening, namely:

1. The Hallein diapir ("Ha." in Figures 2a and 5, northern end of Figure 13f), where Haselgebirge has been documented by mine galleries and boreholes to be sandwiched between strata of Oberalm Fm (Plöchinger, 1977, 1984, 1990; Schauberger, 1972) (Figure 15). This is interpreted to represent a Late Jurassic allochthonous salt sheet extruded onto the seafloor (where it was partially reworked into the Oberalm Fm; Plöchinger, 1974) before being blanketed by younger Oberalm Fm strata. The Hallein salt tongue tips out to the east. A potential candidate for a feeder diapir is the salt stock of Berchtesgaden (NW corner of Figure 5) (Kellerbauer, 1996). A link to the Plassen Lst reef of the Untersberg to its NW (Figure 2a) has not been established but is likewise not ruled out.
2. The Rabenstein backthrust (top NW corner of Figure 5; Figure 18) is a relatively short (~5 km long) S-directed thrust, that places Middle-Upper Triassic on the Allgäu and Strubberg Fms (Risch, 1993).
3. the Grubhörndl thrust, a structure that places Dachstein Lst on Upper Jurassic breccias (Figures 2a and 16). The Dachstein Lst block, previously interpreted as an olistolith derived from the footwall of a major extensional fault (Ortner et al., 2008), is interpreted here as a thrust-block (an option already discussed by Ortner et al., 2008). The geometry of this structure is best understood in its interpreted Cretaceous geometry (Figure 16c). The entire structure of the Grubhörndl is unconformably overlain by Lower Cretaceous clastics and overthrust by the Lofer–Gerhardstein units (Figure 16c).

4.2.2. The Klausbach–Bluntautal–Sattelberg Thrusts

A set of thrusts with individual length exceeding 10 km completes the picture of Late Jurassic contractional structures in the central NCA. These are the Klausbach, the Bluntautal and the Sattelberg thrusts (Figure 2a). The Sattelberg thrust (Figures 2a, 5, and 17) has been previously described by Fernandez et al. (2024) as a NW–SE trending backthrust (south directed) roughly 20 km long. This thrust carries in its hanging wall a thin succession (<200 m) of pelagic Middle to Upper Triassic carbonates and local interfingering of shallow water carbonates (Gawlick, 1998; Gawlick & Missoni, 2015) that dip parallel to the thrust (Figure 17a). Given the consistency in thickness of the hanging wall succession along strike, it is interpreted that it is close to the primary, non-eroded thickness of the pelagic Triassic carbonates. The hanging wall of the Sattelberg thrust has been previously interpreted as olistostromes (Gawlick & Missoni, 2015, 2019). Although its dimensions could be compatible with such an origin (Woodcock, 1979), the along-strike continuity for over 10 km with stratigraphically upright bedding, and the consistent indications for south-directed emplacement (Cornelius & Plöchinger, 1952; Fernandez et al., 2024; Häusler, 1979; Tollmann, 1975) are taken as strong indicators for the thrust nature of this feature.

In the footwall of the Sattelberg thrust is the Strubberg Fm (with abundant metric-to decametric-sized olistoliths) that paraconformably overlies the Upper Triassic (Figure 17a). The footwall Triassic succession displays a north-directed transition of Dachstein Lst into pelagic facies and is at least 1,000 m thick. As per criteria in Section 3, this would require the hanging wall of the thrust to have originally been 2–3 km farther north of its present-day location (at least). Heave on the Sattelberg thrust was estimated at about 5 km by Fernandez et al. (2024).

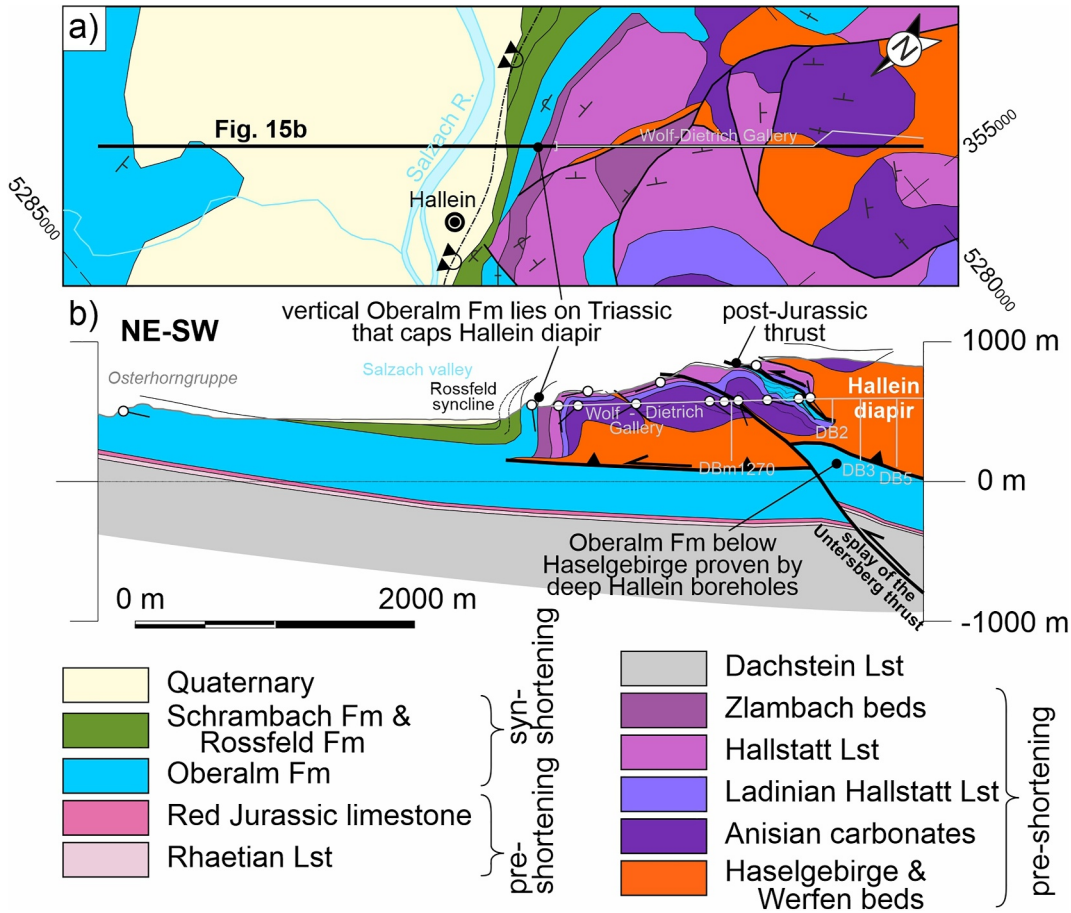

Figure 15. (a) Geological map along a transect crossing the eastern portion of the Hallein diapir. Map based on mapping by Plöchinger (1987) and Pavlik (2007). See Figure 2a for location. (b) Cross-section of the Hallein diapir along the Wolf-Dietrich Gallery of the Hallein salt mine. Four deep boreholes constrain the interpretation at depth (Medwenitsch, 1960; Schauberger, 1972). Biostratigraphy along the Wolf-Dietrich Gallery is based on the work of Gawlick and Lein (1997).

The eastern termination of the Sattelberg thrust has not yet been documented, but the thrust remains in a flat-on-flat configuration all the way to its easternmost mapped location (cf. Figure 15 of Fernandez et al., 2024). Beyond its mapped eastern extent lies an area with north-directed thrusts and north-vergent folds (Mostler & Roßner, 1977; Neubauer & Genser, 2018; Roßner, 1972). It is unclear if backthrusting on the Sattelberg thrust is relayed into these structures or dies out in this direction. In total, the Klausbach–Bluntautal–Sattelberg thrusts extend over 40 km in an E–W direction.

To the west, the Sattelberg thrust is covered by Quaternary sediments of the Salzach River valley (Figure 5). On the opposite side of the valley, the north-dipping Göll Massif (Figure 13a) is juxtaposed on the Dachstein Lst and Strubberg Fm of the Hagengebirge Massif across the E–W Bluntautal valley (Figures 5 and 13e,f). The contact between both units has previously been interpreted as being a strike-slip contact (Königssee fault of Decker et al., 1994). However, the fact that this contact places the entire Triassic of the northern block (Göll Massif) onto the Upper Jurassic of the southern block (Hagengebirge) consistently along strike is interpreted to indicate that south-directed thrusting on the Bluntautal thrust is a key component of this contact (Figures 13e and 13f). The Bluntautal thrust can be mapped extending to the west (Figure 18) and merges with the Klausbach thrust (Figures 2a and 18a), a SW-NE trending thrust. The Klausbach extends westwards for a further 15 km (Figure 2a). A westward extension of the Klausbach thrust has not been documented.

A feature common to the Bluntautal and Sattelberg backthrusts is the local presence of high-angle faults that cross-cut the backthrusts (Kuchlberg thrust in Figure 17a; Schönau thrust in Figure 18b). These faults cut

10.1029/2024TC008358

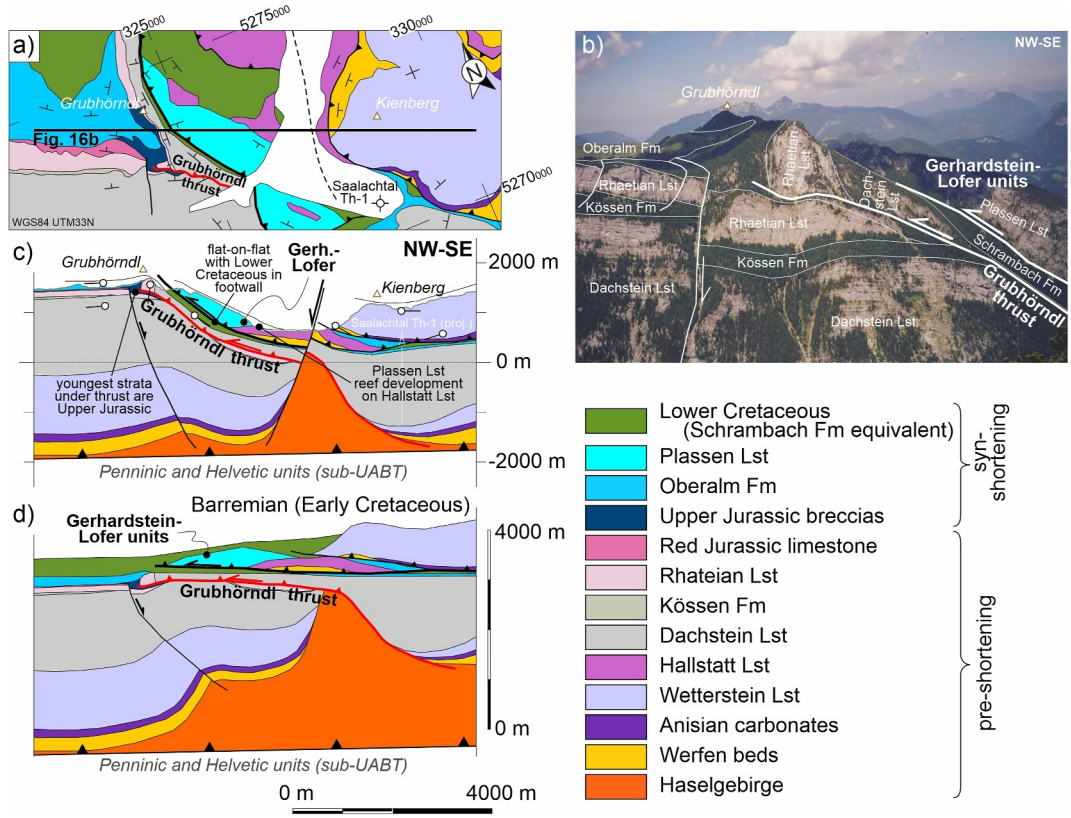

Figure 16. (a) Geological map along a transect crossing the Grubhörndl thrust. Map based on mapping by Ortner et al. (2008) and Pavlik (2006). See Figure 2a for location. (b) Photograph of the Grubhörndl from Ortner et al. (2008) with revised interpretation of the structural configuration. (c) Cross-section of the Grubhörndl thrust. The Grubhörndl thrust is sealed by Jurassic breccias in its leading edge and is overthrust by thrust sheets of the Gerhardstein-Lofer system (Early Cretaceous in age). The entire area experienced Cretaceous extensional collapse. The wellbore Saalachtal Th-1 drilled a 1,600 m thick Dachstein Lst with 35–40° dips (Elster et al., 2016). (d) Restoration of the section in panel (c) to Early Cretaceous times. Thrusting in the area is interpreted to be dominantly out of the section plane and therefore no balance is expected. Jurassic and Cretaceous age thrusting are further expected to have variable transport directions.

relatively thick platform blocks, and it is possible that they represent inverted Triassic extensional faults (Figure 17c), although an alternative interpretation as Jurassic extensional faults is also possible (Figure 17b).

5. Pre-Shortening Configuration of the Central NCA

The map distribution of salt structures in the central NCA prior to inversion can be inferred from the distribution of salt and of pelagic Middle-Upper Triassic carbonates. In general, the central NCA can be subdivided into three types of domains: (a) domains of thick (>2,000 m) Middle-Upper Triassic in platform facies ("platform blocks" of Fernandez et al., 2024); (b) elongate domains of thinner (<500 m) Middle–Upper Triassic in pelagic facies ("Hallstatt zones") (Figure 19e); and (c) domains of highly reduced thickness (<200 m) in Upper Triassic platforms (e.g., in the Grünberg syncline; Figures 6, 8, and 10). Jurassic and younger structures in the central NCA have developed, almost exclusively, along the domains of thin Triassic stratigraphy, and therefore define the boundaries of the platform blocks (Figure 19e) (Fernandez et al., 2024).

The platform blocks are interpreted to have developed as minibasins, rapidly subsiding into the Haselgebirge (salt) (Figure 20a) (Fernandez et al., 2024). Salt accumulated in elongate inflated salt bodies (salt ridges) between the platform blocks. Depending on the amount of extension they experienced, these ridges were either subsiding and covered by pelagic facies or remained at, or near sea level and were covered by thin platform sediments (Figure 20a). Salt ridge subsidence was driven by extension (Fernandez et al., 2024) and preferentially affected NW–SE trending ridges. Non-subsiding ridges predominantly trend NE–SW. The origin of this pattern relates to the evolution of the system during the Triassic and is not further explored here.

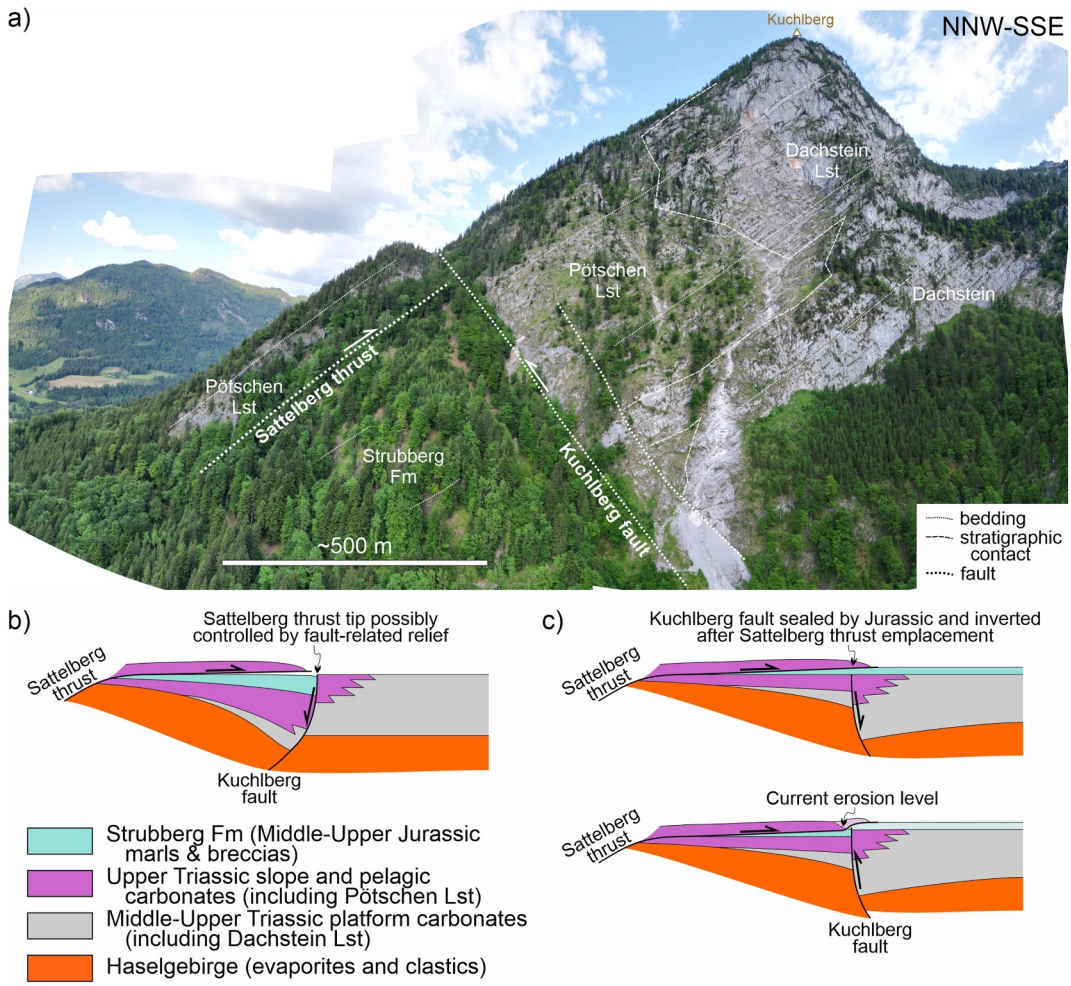

Figure 17. (a) Aerial photograph of the south-directed Sattelberg thrust (backthrust) that places Pötschen Lst in its hanging wall on the Strubberg Fm in the footwall (see Figure 5 for location). South-directed thrusting is confirmed by deformation fabric in the Strubberg Fm (Tollmann, 1975). The Sattelberg thrust is cross-cut at a high angle (nearly 90°) by a fault (here the Kuchlberg fault). The Kuchlberg fault carries in its hanging wall Dachstein Lst and Pötschen Lst, that are thicker than the equivalent stratigraphy in the hanging wall of the Sattelberg thrust. Note the change in physiographic aspect of the flank of Mt Kuchlberg, related to a transition between well-bedded lagoonal Dachstein Lst (to the south) and marly and chert-bearing pelagic Pötschen Lst (to the north). Photograph taken from: 368707E 5269560N 830 m. (b, c) Illustration of possible origins for the Kuchlberg fault as an extensional fault of either Jurassic (b) or Triassic (c) age. Jurassic extension on the Kuchlberg fault (b) could explain the lack of Strubberg Fm outcrops south of this fault, and the fault tip might have acted as a back-stop for southward emplacement of the Sattelberg thrust. Triassic extension on the Kuchlberg fault (c) would have been related to fault-controlled subsidence of a minibasin margin and would have led to uplift and erosion of the leading edge of the Sattelberg thrust and underlying Strubberg Fm during inversion. The option displayed in panel (c) is equivalent to the structure of the Bluntautal thrust west of the Königssee, where it is offset by the Schönau fault (Figure 18b). Triassic-age extensional faults in the Dachstein Lst that could give rise to such inverted structures are shown in Figure 8d.

Qualitatively a ratio between the thickness of supra-salt overburden carbonates and that of the salt (OB/S) can be defined for the different domains (Figure 20a): OB/S >> 1 in areas of platform development, OBS < 0.1 in domains of thin platform roofs, and 0.1 < OB/S < 1 in domains of pelagic Triassic facies. Minibasins tapered out in the direction of inflated salt bodies (Figures 19a and 19e), such that the changes in the OB/S are gradual and occur over distances of 2–5 km (Fernandez et al., 2024; Kenter & Schalger, 2009).

To understand the role of pre-existing salt structures on Jurassic shortening, a restoration of the platform blocks (minibasins) and the intervening domains of inflated salt (Hallstatt zones and thin platform domains) to Late Triassic times is presented (Figure 19a). The restoration is based on sequentially removing displacement between minibasins according to the shortening on Jurassic structures calculated in this contribution (Tables 2 and 3) and

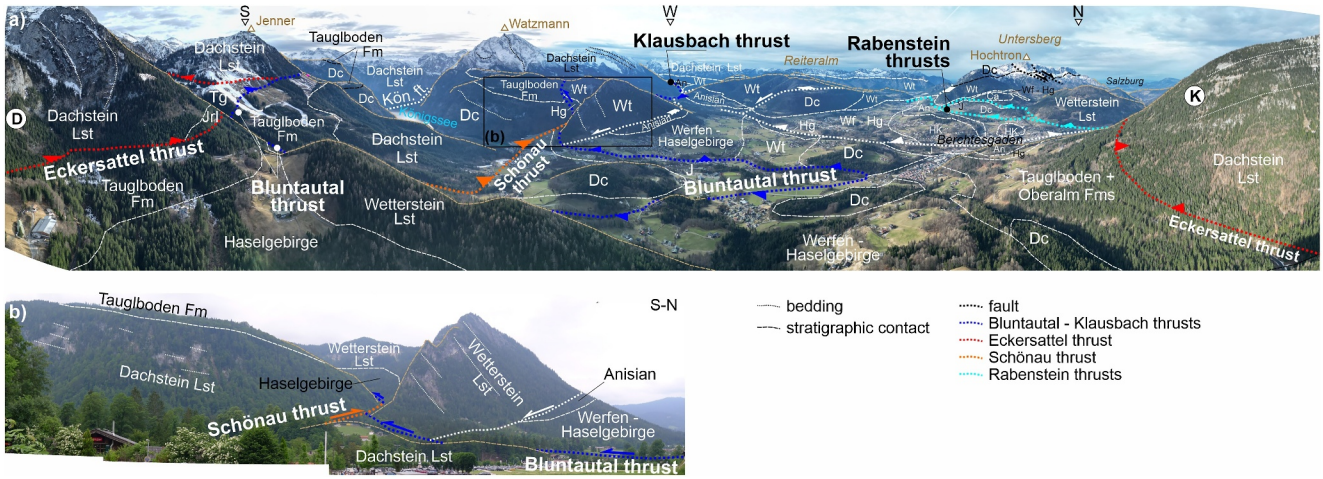

Figure 18. (a) Aerial photo of the western segment of the Klausbach–Bluntautal–Sattelberg system and the Berchtesgaden area (west of the Göll Massif; see Figure 2a for location). The roughly E–W trending Bluntautal backthrust (S-directed thrust) cuts across the entire area an extends to the Klausbach thrust (background). The Bluntautal backthrust is partly offset by a north-directed thrust (here, the Schönau thrust). This panorama is at 180° to that in Figure 13c. Photograph taken from 351128E 5274062N 1,515 m. (b) Detail of the relationship between the Bluntautal thrust and the Schönau thrust at the northern end of the Königssee Lake. Approximate extent of the photo is shown by the black rectangle in panel (a). Photograph taken from 346810E 5272815N.

those for younger structures discussed by Fernandez et al. (2024; cf. Table 1) (for details please refer to the Figure S4 in Supporting Information S1). Where overlaps between minibasins appeared, minibasins were allowed to rotate by under 10° to remove overlaps. This magnitude is compatible with the work of Pueyo et al. (2007), who determined differential vertical-axis rotation between platform blocks to be under 30° in the center of the study area.

6. Discussion

6.1. Early Inversion of a Salt-Bearing Rifted Margin

Jurassic shortening structures conform a complex system of thrusts, folds, and squeezed salt ridges, that span the entire central NCA (Figure 19b). Thrusts and folds occur both as hard-linked systems (the TTCS and the Klausbach–Bluntautal–Sattelberg thrusts) and as more isolated features. All Jurassic structures developed along pre-existing salt structures (diapirs and walls) (OB/S < 1), except for the Eckersattel, Trattberg and Einberg thrusts, which cut across the relatively thick (>1 km, OB/S ∼ 1) margins of Triassic minibasins.

The structures that developed during the Late Jurassic (Figures 19b and 20c) can be grouped into 4 main types:

1. Salt overthrusts (*sensu* Jackson & Hudec, 2017), where salt ridges and their roofs were shortened and thrust over multiple kilometers, both north- and southwards (Totengebirge, Grabenbach, Sattelberg, Bad Mitterndorf, and Grubhörndl thrusts; Figures 6, 11, 16, and 17). These preferentially developed in areas of 0.1 < OB/S < 1.
2. High-angle thrusts that cut through platform domains (OBS >1) (Trattberg thrust, Schönau thrust, Kuchlberg fault; Figures 12, 13, 17, and 18). These are potentially inverted extensional faults.
3. Trains of synclines and anticlines developed in areas of originally inflated salt with thin platform roofs (OBS < 0.1) (Grünberg and Ariplan synclines; Bärnkogel, Sattelkogel and AB anticlines; Figures 8 and 10). The dominant geometry is that of a syncline subsiding into the salt, rather than uplift.
4. Relatively isolated, plug-fed thrusts (*sensu* Jackson & Hudec, 2017), where salt extruded from diapirs transporting their roofs passively (Hallstatt, Hallein, Wurzeralm; Figures 14 and 18; Kurz et al., 2023).

Besides thrusting and folding, Upper Jurassic reefs are interpreted to indicate areas that experienced uplift due to the squeezing of Triassic diapirs (Figure 19b). Reefs grew directly on platform carbonates (on the tapered margins of minibasins) or above domains of Triassic pelagic sedimentation immediately adjacent to platform domains (Figure 19b). Interestingly, most thrusts did not provide sufficient uplift on their own for the development of reefs on their hanging walls. Thrusts on whose hanging walls reefs did develop (Grabenbach, Bad Mitterndorf;

10.1029/2024TC008358

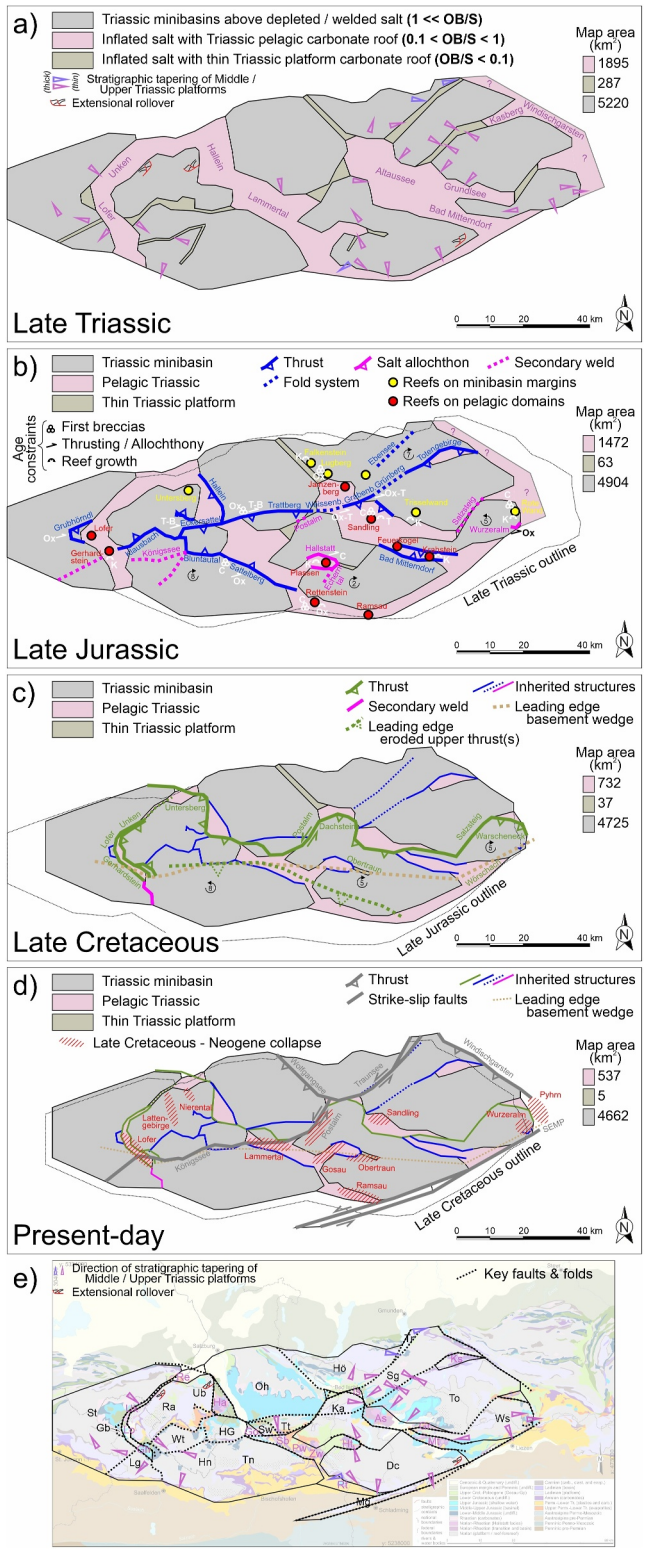

Figure 19.

Figure 19b) are associated to squeezed salt diapirs or ridges. Likewise, reefs that developed on minibasin margins are not associated to any known thrusts, and inflation of salt constitutes the most likely mechanism to have driven uplift. Furthermore, reef growth occurred almost exclusively along NW–SE trending minibasin margins (or their adjoining NW–SE trending pelagic domains), likely indicating this trend was better oriented for salt inflation.

In contrast, the NE–SW trending Grünberg syncline developed as a structure subsiding into salt, where the original stratigraphic roof of a salt ridge was folded (buckled) into a syncline between two relatively undeformed minibasins. The salt that originally filled the salt ridge has been mostly removed (Figures 10e and 10f), most likely due to a combination of lateral evacuation and shortening-driven dissolution, as discussed below. Secondary welds that formed during this time have a similar NE–SW trend as the Grünberg syncline (e.g., Königssee, Echerntal, Salzsteig; Figure 19b) (Fernandez et al., 2021, 2024). Whereas secondary welding under contraction is a frequent feature (e.g., Célini et al., 2021, 2022; Duffy et al., 2018; Oravecz et al., 2023; Rowan & Vendeville, 2006; Vidal-Royo et al., 2021), the squeezing of diapir or ridge roofs into shortening synclines (rather than anticlines or thrusts) is not. Synclinal folding of diapir roofs into pre-existing inflated salt bodies during shortening has been documented by other authors but relates to either rotation of the adjacent minibasin and salt extrusion (Teixell et al., 2024) or the accentuation of synclinal geometries of diapir-collapse or perched minibasins (e.g., Célini et al., 2021; Granado et al., 2019). Neither of these are observed in the Grünberg syncline. A possible alternative explanation could be a pre-contractional sagging (subsidence) of the roof of NE–SW salt bodies that pre-conditioned them into developing into synclines or welds (Figure 20b). If salt evacuated from this trend migrated into NW–SE trending salt bodies, this could have primed the NW–SE trend for uplift. Mild Early Middle Jurassic extension related to the opening of the Alpine Tethys (Böhm et al., 1995; Channell et al., 1992; Krainer et al., 1994) could have driven the pre-shortening redistribution of salt, with local sagging of some salt structures (such as that documented by Kurz et al., 2023 in the Wurzeralm diapir) and inflation of others.

6.2. Role of the Haselgebirge Décollement

The fact that the central NCA remained generally at bathyal depths despite generalized Late Jurassic shortening can be accounted for by the presence of a well-connected and highly efficient basal detachment in the Permo-Triassic salt (Figure 20c). It is known that contractional systems above continuous evaporite décollements develop subdued critical taper geometries and fast propagation of deformation (Célini et al., 2024; Davis & Engelder, 1985; Ford, 2004; Granado et al., 2021; Letouzey et al., 1995; Pla et al., 2019; Santolaria, Granado, Carrera, et al., 2022; Santolaria, Granado, Wilson, et al., 2022).

A thick basal salt can also explain the similar prevalence of north- and south-directed thrusts (e.g., Callot et al., 2007; Koyi & Sans, 2006; Letouzey et al., 1995; Mouthereau et al., 2006) and provides support for the interpreted vertical-axis rotation of the minibasin blocks in the restoration in Figure 19 (e.g., Duffy et al., 2021; Kergaravat et al., 2017; Santolaria, Granado, Carrera, et al., 2022). Likewise, rotation of minibasins around horizontal axes during shortening, such as that experienced by the Loser block (as recorded by the 30° angular unconformity of the Dachsteni Lst below the Oberalm Fm; Figure 8f) is a feature observed in other salt rich basins (e.g., Célini et al., 2022; Kergaravat et al., 2017; Teixell et al., 2024). It is possible, that extensional faults of Late Jurassic age (e.g., those bounding the Loser block, Figure 8f) could result from such rotations.

Figure 19. Palinspastic reconstruction of the central Northern Calcareous Alps (NCA) from Late Triassic to present-day through key time stages: (a) Late Triassic; (b) Late Jurassic; (c) Late Cretaceous; (d) present-day. For the restoration, the structure of the central NCA has been subdivided into domains of thick Upper Triassic carbonate platforms (minibasin domains in the Late Triassic), areas of thin Upper Triassic deposition in shallow water settings (thin Upper Triassic roofs of salt ridges), and areas dominated by Upper Triassic pelagic carbonate deposition (roofs of subsiding diapirs and salt ridges). The map in (b) shows age constraints on deformation including thrusts, breccias and reef growth. Ages for these are abbreviated: C: Callovian; Ox: Oxfordian; K: Kimmeridgian; T: Tithonian; B: Berriasian. The map in panel (c) includes the leading edge of a set of structurally higher thrust sheets emplaced above the southern margin of the NCA whose presence is inferred from Early Cretaceous metamorphism (Fernandez et al., 2024; Frank & Schlager, 2006; Kralik et al., 1987). Likewise, the estimated leading edge of Austroalpine basement transported below the NCA is indicated. The map in (e) shows an overlay of the domains used in the restoration with the present-day geology (cf. Figure 2a). Refer to text and Figure S4 in Supporting Information S1 for details. Platform domain abbreviations (black lettering): Dc: Dachstein; Gb: Grubhörndl; HG: Hoher Göll; Hn: Hagengebirge; Hö: Höllengebirge; Ka: Katrin; Lg: Leoganger Steinberge; Mg: Mandlingzug; Oh: Osterhorngruppe; Ra: Reiteralm; Sg: Singereben; St: Steinplatte; Sw: Schwarzer Berg; Tn: Tennengebirge; To: Totengebirge; Tr: Traunstein; Tt: Trattberg; Ub: Untersberg; Ws: Warscheneck. Pelagic domain abbreviations (purple lettering): As: Altaussee; Gh: Gerhardstein; Go: Golling; Gr: Grundlsee; Ha: Hallein; Ht: Hallstatt; Is: Bad Ischl; Ks: Kasberg; Lo: Lofer; Mt: Bad Mitterndorf; Pw: Pailwand; Re: Bad Reichenhall; Rt: Rettenstein; Sb: Sattelberg; Uk: Unken; Zw: Zwieselalm.

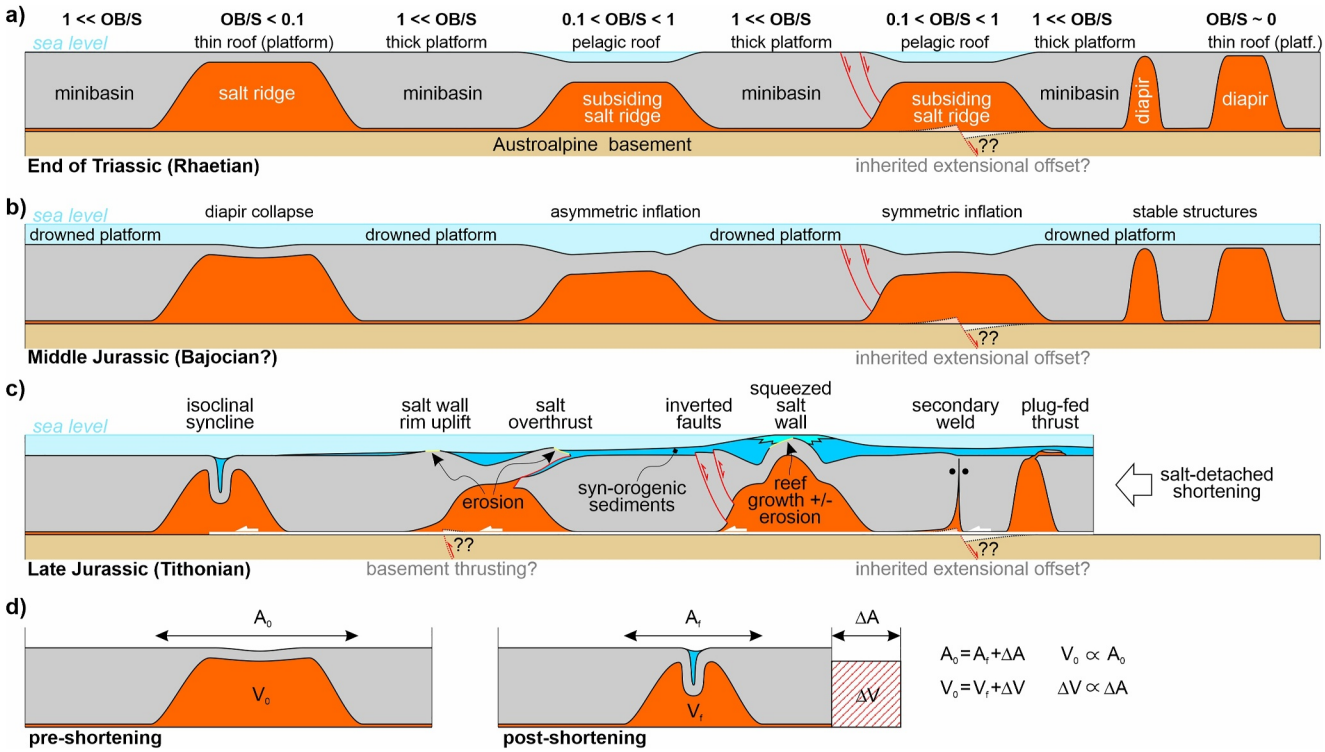

Figure 20. (a) Schematic structure of the central Northern Calcareous Alps (NCA) at the end of the Triassic. The margin was configured in minibasins with thick carbonate platform deposits separated by salt ridges. Some salt ridges were roofed by thin platform carbonates whereas others had subsided and had accumulated pelagic carbonate deposition. Each domain is characterized by a ratio in thickness of the Middle to Upper Triassic carbonates relative to the salt (OB/S). (b) Rapid subsidence of the NCA during the Early Jurassic led to the drowning of the carbonate platforms and overall deepening of the margin to bathyal depths. An inferred phase of redistribution of salt during the Early to Middle Jurassic led to the subsidence of some salt structures (diapir collapse) with salt migrating laterally into others (inflation). (c) Shortening in the Middle to Late Jurassic led to the development of different styles of shortening structures along the salt ridges. The Middle to Late Jurassic basin was partially starved, with the major thickness of sediments relating to the presence of Late Jurassic reefs (Plassen Lst) and their slope equivalents (Oberalm Fm, Tressenstein Lst), and to the erosion and re-deposition of uplifted Triassic carbonates. The presence of inherited or inverted basement structures, or newly formed basement structures during the Late Jurassic is uncertain. (d) 2D representation of the estimation of salt volume loss through deformation. The volume of salt in the undeformed state (left) (V_0) is roughly proportional to the width of the area of inflated salt (map area in 3D: A_0). When the inflated salt body is shortened, the volume of salt is reduced (V_f) to an amount that is roughly proportional to the width of the structure after shortening (map area in 3D: A_f). The change in map area (ΔA) is thus roughly proportional to the loss of volume of salt (ΔV). Whereas in 2D lateral evacuation could be a source for cross-sectional area change, the change in map area (ΔA) implies a net loss of salt (through dissolution, see text).

Finally, but importantly, even though Jurassic shortening re-activated all salt structures, it did not progress to the point of entirely closing the widest domains of inflated salt (Figure 19b). This could be due to either a limited amount of contraction or to the blocking of shortening by some mechanism. The possible presence of basement faults offsetting the Permo-Triassic salt (Figure 20) could have hindered the propagation of deformation (Granado et al., 2021). However, the role of basement structures during inversion is difficult to ascertain due to the present-day decoupling of the NCA from their basement.

6.3. Timing of Middle to Late Jurassic Shortening in the Central NCA

Timing of deformation in the central NCA is constrained by tectonosedimentary relationships and abundant biostratigraphic control on syn-tectonic strata (Figures 19b and 21). Age control is provided in part by breccias and MTDs, re-sedimenting Triassic carbonates. After the Early to Middle Jurassic quiescent stage, the first documented breccias are Early Callovian in the southern half of the study area (Sattelberg, Rettenstein, and Sandlingalm areas) (Auer et al., 2009; Gawlick & Frisch, 2003; Gawlick et al., 2002; Gawlick, Schlagintweit, et al., 2003). In the center (Altaussee) and along the eastern margin of the study area (Wurzeralm and to the east), the earliest breccias are dated to be Mid-Callovian to Oxfordian (Drvoderic et al., 2023; Gawlick et al., 2007; Ottner, 1990). Deformation progressed northwards, with the earliest breccias in the basins along and north of the TTCS being Oxfordian in age (Gawlick & Frisch, 2003; Kügler et al., 2003).

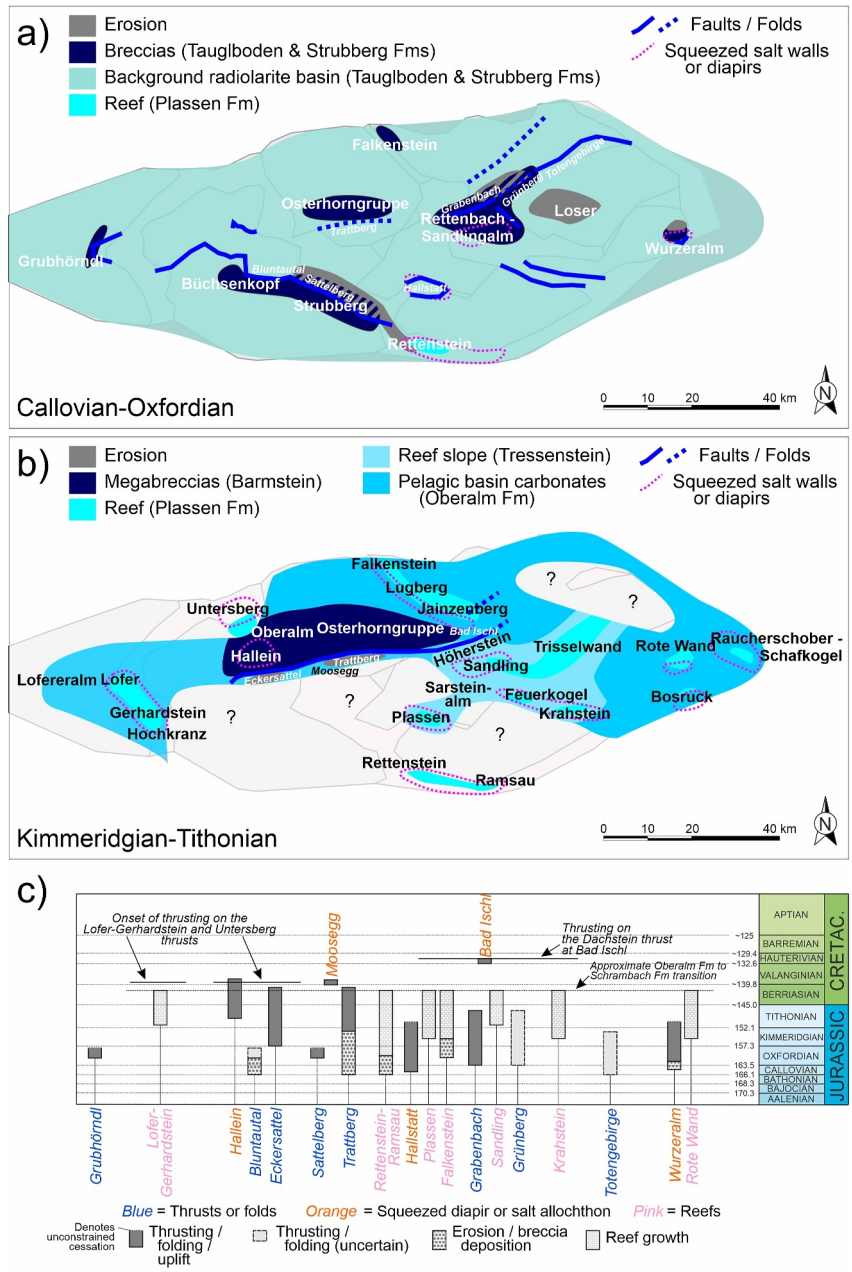

Figure 21. Proposed paleogeography of the central Northern Calcareous Alps at: (a) early Late Jurassic; (b) late Late Jurassic. Names for Jurassic outcrop localities are shown on both maps. The configuration of Triassic minibasins from Figure 19b is shown in the background. Only structures interpreted to be active at each stage are shown. Both maps are based on observations by the authors and on the map of Fenninger and Holzer (1970). (c) Chronologic chart of structure activity and sedimentary record of structure growth (erosion and reef growth). Structures and features are placed in their relative W–E location. Chronostratigraphic ages are from Walker and Geissman (2022).

The youngest strata in the footwall of thrusts and salt allochthons also indicates that deformation on these structures migrated northwards. The salt allochthon of the Hallstatt diapir, where evaporites override Callovian age radiolarites (Suzuki & Gawlick, 2009), is the oldest dated structure in the area. To its west, the Sattelberg and Grubhörndl thrusts override Oxfordian sediments (Gawlick et al., 2002; Ortner et al., 2008), as does the Wurzeralm salt allochthon in the east (Hiebl, 2011; Kurz et al., 2023; Ottner, 1990). Deformation subsequently propagated northwards to the TTCS, of Oxfordian to Berriasian age (Table 4).

Table 4
Characteristics of the Segments of the Totengebirge–Trattberg Contractional System (TTCS)

Segment	Map length (km)	Shortening (km) and source	Pre-shortening OB/S	Syn-tectonic sediment thickness (m)	Type of structure	Age constraints
Totengebirge	19	7–10 (Figure 11, Fernández et al., 2024; Linzer et al., 1995)	0.2–15	0	Plug-fed thrust	Pre-Oxfordian
Grünberg	12	4–5 (Figures 8 and 10)	~0.06	200–800	Synclines-anticlines	Up to Tithonian at Raucherkar, up to Kimmeridgian at Offensee
Grabenbach	7	4 (Figure 6)	0.05–0.3	1,000	Plug-fed thrust	Callovian(?)—Tithonian
Sub-Dachstein (Einberg thrust—Weissenbach anticline)	14	?	~0.3(?)[a]	<1,000	Thrust—anticline	–
Trattberg	21	2–3 (Figure 12)	1.3–3	>1,500	Inverted normal fault	Kimmeridgian—Berriasian (antiform from Callovian or Oxfordian)
Eckersattel	12	3 (Figure 13)	~1	~500	Plug-fed thrust	Kimmeridgian—Berriasian

[a]OB/S based on Jodschwefelbad borehole (Mandl et al., 2012) and comparison with Grabenbach section (Figure 6).

The best constraint on timing on the TTCS is found at the Grabenbach (Figure 6). Here thrusts involving the Oberalm Fm are sealed by almost flat-lying Tithonian Tressenstein Lst. Onset of thrusting is not constrained, but Callovian breccias near Altaussee and onlap of the Oxfordian Tauglboden Fm onto the Dachstein Lst in the footwall of the thrust (Figures 6b and 7c) indicate a relatively early onset of deformation. East of the Grabenbach, Jurassic stratigraphy involved in the TTCS becomes progressively more incomplete eastwards: the youngest sediments in the synclines at the Offensee, are Oxfordian-Kimmeridgian Tauglboden Fm (giving a Kimmeridgian age of the Grünberg syncline at this location). Upper Jurassic sediments are altogether absent under the Totengebirge thrust (indicating a possible pre-Oxfordian age for the Totengebirge thrust).

In the western TTCS, the Eckersattel and the Trattberg were active during deposition of the Oberalm Fm (Figures 12 and 13). The cessation of thrusting on both features has not been constrained, but thrusting involves the youngest Oberalm Fm (Figure 12a). This indicates a Kimmeridgian to (at least) Berriasian age of thrusting, making these the youngest structures in the area. Uplift along the Trattberg prior to the Kimmeridgian is recorded by erosion of Upper Triassic units under the Oxfordian Tauglboden Fm in the footwall of the Trattberg thrust (Figure 12; Ortner, 2017). Initial uplift, possibly as a (salt-cored?) anticline, acted as a paleogeographic threshold, with deposition of the Strubberg Fm mainly to its south, and Tauglboden Fm mostly to its north (Gawlick & Frisch, 2003; Plöchinger, 1953).

North of the TTCS, allochthony in the Hallein diapir was sychronous with deposition of the Oberalm Fm (Plöchinger, 1974) and therefore partly coeval with thrusting on the western TTCS.

Upper Jurassic reefs also becomes younger northwards: the Rettenstein (in the south of the study area), dated as Late Oxfordian (Auer et al., 2008, 2009), is younger than the Kimmeridgian reefs of the Plassen, the Krahstein, the Trisselwand, the Rote Wand, Falkenstein (Gawlick et al., 2009; Gawlick, Schlagintweit, et al., 2003; Hiebl, 2011; Kügler et al., 2003; Schlagintweit & Ebli, 1999; Schlagintweit et al., 2003; Steiner et al., 2021). Reef development in the Mt Sandling and the Lofer-Gerhardstein started in the Tithonian (Gawlick et al., 2007; Sanders et al., 2007) and do not fit the northward migrating trend. These two locations, however, are in the vicinity of the Grabenbach and the Klausbach thrusts, whose emplacement might have altered the rate of uplift on the rising salt structures. Although reef growth likely marks only the culmination of a process of uplift of the Jurassic seafloor to near sea level, rapid rate of salt-related uplift under compression (e.g., Manea et al., 2021; Pérez-Villar et al., 2024) implies this process likely required only hundreds of thousands of years.

Along with the migration of deformation, the inversion of the central NCA led to a transition from a depositional environment starved in carbonates in the Middle to earliest Late Jurassic (Figure 21a) to a setting rich in clastic carbonates during the latest Late Jurassic (Figure 21b). Two carbonate sources appeared during the Middle to Late Jurassic to explain this transition. Initially submarine erosion of uplifted Triassic carbonates along incipient Jurassic structures fed locally-sourced breccia bodies (Gawlick & Missoni, 2015; Gawlick et al., 2002, 2007; Mandl, 2013; Ortner, 2017). Breccias related to uplift and erosion continued to deposit throughout the entire Late Jurassic (Gawlick et al., 2005; Ortner, 2017; Steiger, 1981). Once inversion had progressed sufficiently, reefs developed where the seafloor had reached photic depths and became an additional source of carbonatic material in the basin.

6.4. Architecture of the TTCS

The TTCS is a particularly prominent element of the Jurassic inversion system. This system is a hard-linked system of thrusts and folds that spans 80 km from west to east across the study area, involving multiple Triassic minibasins (Figure 19b), and with contrasting style along strike (Table 4).

The timing of the different segments of the TTCS (Table 4) indicates that the onset of deformation was somewhat coeval along significant portions of TTCS (Figure 21a). Nonetheless, cessation of deformation becomes progressively younger toward the west. This possibly indicates that the TTCS grew initially as a set of isolated features that were posteriorly linked as a pulse of deformation migrated from east to west. This evolution could be the reason the TTCS displays a somewhat anomalous displacement pattern. For one, it lacks the arcuate shape expected for thrusts (Elliot, 1976) and displacement is not maximum at its center, as is expected for linked systems (Kim & Sanderson, 2005). Rather, maximum displacement is at its eastern end, on the Totengebirge thrust (Table 4). This possibly also relates to the fact that the eastern termination of the TTCS was a domain of inflated salt (Eggerth, 2023) (Figure 19a; at present the Windischgarsten fault system, Figure 4). This area may have acted as a "loose-end" for the TTCS during thrusting and could account for the anomalous shortening pattern. This could also explain why the displacement-length ratio on the Totengebirge thrust (only the thrust segment) is in the order of 50%, way above the average value of 7%–10% displacement-length ratio quoted by Kim and Sanderson (2005). Still the displacement-length ratio is in the order of 8%–13% when computed for the total length of the TTCS.

Another feature in the TTCS is the change in structural style along-strike (Table 4), a feature observed in other shortened salt systems (e.g., Célini et al., 2021; Grando & McClay, 2004). Along-strike, the TTCS is formed by low-angle salt overthrusts, syncline–anticline systems, and inverted extensional faults. These changes occur despite the structures having very similar orientations and partly relates to the overburden to salt thickness ratio (e.g., Jordan & Noack, 1992; Santolaria, Harris et al., 2022; and discussed above), which depended on the pre-shortening OB/S and on the evolving contribution of syn-tectonic sediments to the overburden thickness (Table 4) (e.g., Kilian et al., 2021). In the Eckersattel and the Trattberg, thrusting across a thick platform domain was further likely controlled by the presence of pre-existing extensional faults and to the presence of the earlier Bluntautal–Sattelberg thrusts immediately to the south, that possibly significantly exhausted the potential for salt-related deformation in the area.

6.5. Post-Jurassic Deformation

Post-Jurassic deformation is beyond the scope of this article. However, unraveling Cretaceous to Neogene deformation has been a prerequisite to understand the Triassic and Jurassic configuration of the central NCA (Figure 19; Figure S4 in Supporting Information S1). Two key stages of deformation are shown in Figure 19: a phase of Early Cretaceous thrusting, in which the Untersberg–Dachstein–Warscheneck TS was transported over 5–10 km to the NE, partly overriding the TTCS (Fernandez et al., 2024) (Figure 19c); and a phase of Neogene strike-slip that partly offset the pre-existing structures (Linzer et al., 1995; Peresson & Decker, 1997) (Figure 19d).

Thrusting during the Cretaceous, as in the Jurassic, detached along the basal Permo-Triassic salt. This stage of thrusting significantly contracted the salt structures remaining after Jurassic shortening, such that posterior deformation was of smaller magnitude.

From Late Cretaceous through to Neogene times a system of extensional collapse structures developed across the area (Figure 19d) (Fernandez et al., 2022, 2024; Herm, 1962; Kurz et al., 2023; Risch, 1993; Wagreich & Decker, 2001). A possible link between these features and remaining, isolated, salt bodies has been proposed by Fernandez et al. (2022).

Finally, during the Neogene (Figure 19d), pre-existing salt structures were re-activated in thrusting or in strike-slip, with displacements of less than 5 km (Figure S4 in Supporting Information S1).

6.6. Regional Tectonic Transport Directions

Jurassic shortening directions across the central NCA are variable. Thrusting along the Trattberg is N to NE directed (Ortner, 2017) (Figure 12b), whereas thrusting at the eastern end of the Totengebirge thrust is NW directed (Linzer et al., 1995). Folding in turn indicates E–W shortening at the Offensee (Figure 10d), WNW–ESE to N–S shortening at the Grabenbach (Figures 6a, 7b, and 8e) or NE–SW shortening at the Eckersattel (label E, Figure 5). However, the presence of an effective basal décollement and pre-existing salt structures precludes using folds or thrusts as reliable indicators of regional transport directions (e.g., Dooley et al., 2009; Duffy et al., 2018; Muñoz et al., 2013, 2024; Soto et al., 2024).

At a more regional scale, the roughly E–W trend of the two main thrust systems, the TTCS and the Klausbach–Bluntautal–Sattelberg thrusts, could be indicative of dominantly N–S shortening. Nonetheless, the palinspastic reconstruction in Figure 19 indicates that during the Late Jurassic the study area shortened in both N–S and E–W directions.

There is no firm indication in the study area as to the origin of Late Jurassic deformation. The structures in the central NCA are compatible with the currently accepted model of contraction driven by far-field convergence- or subduction-related stress (e.g., Gawlick & Missoni, 2019; Plašienka, 2018; Schmid et al., 2008). An alternative, with gravity-driven gliding on the NCA passive margin in a linked extensional-contractional system, cannot be ruled out with the observations at hand. However, lacking evidence for Late Jurassic extension, far-field stress related to the onset of Alpine orogenesis seems a plausible driver, particularly in view of the abundance of ophiolitic detrita in Upper Jurassic to Cretaceous sediments (Decker et al., 1987; Drvoderic et al., 2023; Krische et al., 2014; Steiner et al., 2021).

6.7. Salt Volume Balance

Shortening from Late Jurassic to present-day led to the major and continued re-activation of salt structures. In the pre-shortening configuration, inflated salt structures were areas with relatively thin Middle-Upper Triassic stratigraphy (OB/S < 1; Figures 19a and 20a). Since the volume of salt below minibasins was very reduced (OB/S >> 1), the map area of domains of thin Triassic stratigraphy can be used as a proxy of the volume of salt in the central NCA. Since no generalized salt-cored structural relief developed during shortening (Figure 20c), reduction in the map area of thin overburden domains (OB/S < 1) have been interpreted to be roughly equivalent to the change in volume of the salt structures (Figure 20d). These map area changes have therefore been used to estimate the progressive loss of salt volume throughout the network of salt structures. In the absence of evidence for major extrusion of salt at the seabed during the Late Jurassic, we assume that salt was most likely removed through pressure-driven dissolution.

The comparison of the map areas of OB/S < 1 domains (Figures 19a–19d) provides a first-order approximation of the loss of Haselgebirge volume through time and indicates a reduction in 70% of salt volume from Late Triassic times to present. This value is consistent with the estimate of Fernandez et al. (2021) for the Hallstatt diapir, and of Santolaria, Granado, & Wilson (2022) for analog models of the eastern NCA. This can furthermore explain why the Haselgebirge is relatively poor in halite (only 50%–65% volume halite; Leitner & Mayr, 2017). If the 70% of volume loss is assumed to have mostly removed halite (the most soluble component in the Haselgebirge), then the original composition can be estimated to have contained 85%–90% of halite (likely including other highly soluble constituents, such as potash salts). This composition would be comparable to that of other salt giants (e.g., Zechstein or South Atlantic salt; Fiduk & Rowan, 2012; Jackson & Stewart, 2017; Szatmari et al., 2021).

7. Conclusions

The central NCA is an outstanding example to study the inversion of salt-dominated margins. Its structural and geomorphologic configuration, with Triassic minibasins preserved in sub-horizontal position, and preserved syntectonic strata, make it feasible to reconstruct the evolution of this province since its passive-margin configuration in Triassic times. This contribution presents the first systematic analysis of the evolution of Late Jurassic inversion of this salt-dominated margin, and sheds new light on the earliest stage of Alpine orogenesis in the Eastern Alps.

An efficient basal salt décollement allowed deformation to propagate across the entire central NCA without the development of major relief, and without a dominant structural vergence. Nonetheless, deformation progressed in a generally coherent manner, from S to N, across the study area. In this process, Triassic-age salt structures strongly controlled the location of the earliest inverted structures during the Late Jurassic. All salt structures that persisted into the Late Triassic were inverted, even if only partially, during the initial Late Jurassic deformation stage.

Deformation during the Late Jurassic did not, however, succeed in completely squeezing all salt structures. The possible interaction of the supra-salt cover with sub-salt basement faults could help explain this pattern.

The same Triassic salt structures continued to play a key role during the later inversion of the margin (Early Cretaceous) and during its partial dismemberment under transpression during the Neogene.

Remarkably, the Late Jurassic Totengebirge–Trattberg contractional system (TTCS), a set of hard-linked folds and thrusts, presents features uncommon for thrust systems; it exhibits outstanding continuity (it is over 80 km in length) with strong along-strike variability in structural style (including low-angle, high-angle faulting, or isoclinal folding) and is postulated to have developed by a combination of linkage and along-strike propagation. The variability in structural style of the TTCS and its peculiarities in growth and displacement patterns can be traced back to the key role exerted by pre-existing salt structures and the supra-diapir stratigraphy.

Conflict of Interest

The authors declare no conflicts of interest relevant to this study.

Data Availability Statement

Field dip data and revised geological mapping compiled by the authors are archived in PANGAEA (Fernandez, 2024; Fernandez & Eggerth, 2024).

Acknowledgments

Research by OF, WM, MM, HO, DS, and BG is supported by FFG and Salinen AG through the FFG-Bridge Project ETAPAS (FO999888049). Research was funded in part by the Austrian Science Fund (FWF) (doi: 10.55776/I5399) and by MCIN/AEI/10.13039/501100011033 (Structure and Deformation of Salt-bearing Rifted Margins (SABREM), PID2020-117598GB-I00). Petex Inc provided academic licenses of Move, that has been used for cross-section construction and restoration. The authors wish to thank J.A. Muñoz, J.-C. Ringenbach, and M. Rowan for enriching discussions. The reviews by A Teixell, J.I. Soto and N. Célini helped us greatly improve the quality of the original manuscript.

References

Auer, M., Gawlick, H.-J., & Schlagintweit, F. (2008). An extensional allochthon at the southern rim of the central Northern Calcareous Alps - The isolated Jurassic occurrence of Mount Rettenstein near Filzmoos. *Journal of Alpine Geology*, *49*, 4–5.

Auer, M., Gawlick, H.-J., Suzuki, H., & Schlagintweit, F. (2009). Spatial and temporal development of siliceous basin and shallow-water carbonate sedimentation in Oxfordian Northern Calcareous Alps. *Facies*, *55*(1), 63–87. https://doi.org/10.1007/s10347-008-0155-3

Bahroudi, A., & Koyi, H. A. (2003). Effect of spatial distribution of Hormuz salt on deformation style in the Zagros fold and thrust belt: An analogue modelling approach. *Journal of the Geological Society, London*, *160*(5), 719–733. https://doi.org/10.1144/0016-764902-135

Beaumont, C., Muñoz, J. A., Hamilton, J., & Fullsack, P. (2000). Factors controlling the Alpine evolution of the central Pyrenees inferred from a comparison of observations and geodynamical models. *Journal of Geophysical Research*, *105*(B4), 8121–8145. https://doi.org/10.1029/1999jb900390

Birkenmajer, K. (1996). Bericht 1993 über geologische Aufnahmen in den Nördlichen Kalkalpen auf Blatt 74 Hohenberg. *Jahrbuch der Geologischen Bundesanstalt*, *139*, 380.

Böhm, F. (1992). Mikrofazies und Ablagerungsmilieu des Lias und Dogger der Nordöstlichen Kalkalpen. *Erlanger Geologische Abhandlungen*, *121*, 57–217.

Böhm, F., Dommergues, J.-L., & Meister, C. (1995). Breccias of the Adnet formation: Indicators of a Mid-Liassic tectonic event in the northern Calcareous Alps (Salzburg/Austria). *Geologische Rundschau*, *84*(2), 272–286. https://doi.org/10.1007/s005310050005

Braun, R. (1998). *Die Geologie des Hohen Gölls*. Nationalpark Berchtesgaden Forschungsbericht 40/1998. Nationalparkverwaltung Berchtesgaden.

Brun, J.-P., & Mauduit, T. P.-O. (2008). Rollovers in salt tectonics: The inadequacy of the listric fault model. *Tectonophysics*, *457*(1–2), 1–11. https://doi.org/10.1016/j.tecto.2007.11.038

Callot, J.-P., Jahani, S., & Letouzey, J. (2007). The role of pre-existing diapirs in fold and thrust belt development. In O. Lacombe, J. Lavé, F. Roure, J. Vergés (Eds.), *Thrust belts and Foreland basins: From fold kinematics to hydrocarbon systems* (pp. 309–325). Springer.

Callot, J.-P., Trocmé, V., Letouzey, J., Albouy, E., Jahani, S., & Sherkati, S. (2012). Pre-existing salt structures and the folding of the Zagros Mountains. In G. I. Alsop, S. G. Archer, A. J. Hartley, N. T. Grant, & R. Hodgkinson (Eds.), *Salt tectonics, sediments and prospectivity* (Vol. 363(1), pp. 545–561). Geological Society, London, Special Publications. https://doi.org/10.1144/SP363.27

Célini, N., Callot, J.-P., Pichat, A., Legeay, E., Graham, R., & Ringenbach, J.-C. (2022). Secondary minibasins in orogens: Examples from the Sivas Basin (Turkey) and the sub-Alpine fold-and-thrust belt (France). *Journal of Structural Geology*, *156*, 104555. https://doi.org/10.1016/j.jsg.2022.104555

Célini, N., Callot, J.-P., Ringenbach, J.-C., & Graham, R. (2020). Jurassic salt tectonics in the SW sub-Alpine fold-and-thrust belt. *Tectonics*, *39*(10), e2020TC006107. https://doi.org/10.1029/2020TC006107

Célini, N., Callot, J.-P., Ringenbach, J.-C., & Graham, R. (2021). Anatomy and evolution of the Astoin diapiric complex, sub-Alpine fold-and-thrust belt (France). *BSGF - Earth Sciences Bulletin*, *192*, 29. https://doi.org/10.1051/bsgf/2021018

Célini, N., Pichat, A., Mouthereau, F., Ringenbach, J.-C., & Callot, J. P. (2024). Along-strike variations of structural style in the external Western Alps (France): Review, insights from analogue models and the role of salt. *Journal of Structural Geology*, *179*, 105048. https://doi.org/10.1016/j.jsg.2023.105048

Channell, J. E. T., Brandner, R., Spieler, A., & Stoner, J. S. (1992). Paleomagnetism and paleogeography of the Northern Calcareous Alps (Austria). *Tectonics*, *11*(4), 792–810. https://doi.org/10.1029/91tc03089

Cornelius, H. P., & Plöchinger, B. (1952). Der Tennengebirgs-N-Rand mit seinen Manganerzen und die Berge im Bereich des Lammertales. *Jahrbuch der Geologischen Bundesanstalt*, *95*, 145–225.

Cotton, J. T., & Koyi, H. A. (2000). Modeling of thrust fronts above ductile and frictional detachments: Application to structures in the Salt Range and Potwar Plateau, Pakistan. *GSA Bulletin*, *112*(3), 351–363. https://doi.org/10.1130/0016-7606(2000)112<351:MOTFAD>2.0.CO;2

Daurer, A., & Schäffer, G. (1983). *Arbeitstagung der Geologischen Bundesanstalt*. Geologische Bundesanstalt.

Davis, D. M., & Engelder, T. (1985). The role of salt in fold-and-thrust belts. *Tectonophysics*, *119*(1–4), 67–88. https://doi.org/10.1016/0040-1951(85)90033-2

Decker, K., Faupl, P., & Müller, A. (1987). Synorogenic sedimentation on the Northern Calcareous Alps during the Early Cretaceous. In H. W. Flügel & P. Faupl (Eds.), *Geodynamics of the Eastern Alps* (pp. 112–125). Deuticke.

Decker, K., Peresson, H., & Faupl, P. (1994). Die miozäne Tektonik der östlichen Kalkalpen: Kinematic, Paläospannungen und Deformationsaufteilung während der "lateralen Extrusion" der Zentralalpen. *Jahrbuch der Geologischen Bundesanstalt*, *137*, 5–18.

De Paor, D. G. (1988). Balanced sections in thrust belts, Part 1: Construction. *AAPG Bulletin*, *72*, 73–90.

Dooley, T. P., Jackson, M. P. A., & Huder, M. R. (2009). Inflation and deflation of deeply buried salt stocks during lateral shortening. *Journal of Structural Geology*, *31*(6), 582–600. https://doi.org/10.1016/j.jsg.2009.03.013

Drvoderic, S. P., Gawlick, H.-J., Suzuki, H., & Schlagintweit, F. (2023). Suprasubduction ophiolite (SSZ) components in a middle to lower upper Jurassic Hallstatt Mélange in the Northern Calcareous Alps (Raucherschober/Schafkogel area). *Geosystems and Geoenvironment*, *2*(3), 100174. https://doi.org/10.1016/j.geogeo.2022.100174

Duffy, O. B., Dooley, T. P., Hudec, M. R., Fernandez, N., Jackson, C. A.-L., & Soto, J. I. (2021). Principles of shortening in salt basins containing isolated minibasins. *Basin Research*, *33*(3), 2089–2117. https://doi.org/10.1111/bre.12550

Duffy, O. B., Dooley, T. P., Hudec, M. R., Jackson, M. P. A., Fernandez, N., Jackson, C. A.-L., & Soto, J. I. (2018). Structural evolution of salt-influenced fold-and-thrust belts: A synthesis and new insights from basins containing isolated salt diapirs. *Journal of Structural Geology*, *114*, 206–221. https://doi.org/10.1016/j.jsg.2018.06.024

Egger, H. (Ed.). (1996). Blatt 66 Gmunden 1:50,000. In *Geologische Karte der Republik Österreich 1:50,000, Nr. 66*. Verlag der Geologischen Bundesanstalt.

Egger, H. (Ed.). (2007). *Erläuterungen zu Blatt 66 Gmunden*. Verlag der Geologischen Bundesanstalt.

Egger, H. & vanHusen, D. (Eds.). (2007). Blatt 67 Grünau 1:50,000. In *Geologische Karte der Republik Österreich 1:50,000, Nr. 67*. Verlag der Geologischen Bundesanstalt.

Eggerth, L. (2023). *3D-structural modelling approach to explore the link between syn-sedimentary deformation of the Lofermauern and salt tectonics (Wurzeralm)* (master's thesis). University of Vienna.

Elliot, D. (1976). The energy balance and deformation mechanisms of thrust sheets. *Philosophical Transactions of the Royal Society of London, Series A*, *283*, 289–312.

Elster, E., Goldbrunner, J., Wessely, G., Niederbacher, P., Schubert, G., Berka, R., et al. (2016). *Erläuterungen zur geologischen Themenkarte 1:500,000 Thermalwässer in Österreich*. Verlag der Geologischen Bundesanstalt.

Faupl, P., & Wagreich, M. (2000). Late Jurassic to Eocene paleogeography and geodynamic evolution of the Eastern Alps. *Mitteilungen der Osterreichischen Geologischen Gesellschaft*, *92*, 79–94.

Faupl, R., & Wagreich, M. (1992). Cretaceous flysch and pelagic sequences of the Eastern Alps: Correlations, heavy minerals, and paleogeographic implications. *Cretaceous Research*, *13*(5–6), 387–403. https://doi.org/10.1016/0195-6671(92)90006-C

Fenninger, A., & Holzer, H.-L. (1970). Fazies und Paläogeographie des oberostalpinen Malm. *Mitteilungen der Geologischen Gesellschaft in Wien*, *63*, 52–141.

Fernández, N., & Kaus, B. J. P. (2014). Influence of pre-existing salt diapirs on 3D folding patterns. *Tectonophysics*, *637*, 354–369. https://doi.org/10.1016/j.tecto.2014.10.021

Fernandez, O. (2024). Geological contacts - Central northern Calcareous Alps (eastern Alps, Austria) [dataset]. *PANGAEA*. Retrieved from https://doi.pangaea.de/10.1594/PANGAEA.968983

Fernandez, O., & Eggerth, L. (2024). Field and dip data - Central Northern Calcareous Alps (Eastern Alps, Austria) [Dataset]. *PANGAEA*. Retrieved from https://doi.pangaea.de/10.1594/PANGAEA.969009

Fernandez, O., Grasemann, B., & Sanders, D. (2022). Deformation of the Dachstein Limestone in the Dachstein thrust sheet (Eastern Alps, Austria). *Austrian Journal of Earth Sciences*, *115*(1), 167–190. https://doi.org/10.17738/ajes.2022.0008

Fernandez, O., Habermüller, M., & Grasemann, B. (2021). Hooked on salt: Rethinking Alpine tectonics in Hallstatt (Eastern Alps, Austria). *Geology*, *49*(3), 325–329. https://doi.org/10.1130/G47981.1

Fernandez, O., Ortner, H., Sanders, D., Grasemann, B., & Leitner, T. (2024). Salt-rich versus salt-poor structural scenarios in the central Northern Calcareous Alps: Implications for the Hallstatt facies and early Alpine tectonic evolution (Eastern Alps, Austria). *International Journal of Earth Sciences*, *113*(2), 245–283. https://doi.org/10.1007/s00531-023-02377-4

Ferrer, O., Carola, E., & McClay, K. (2023). Structural control of inherited salt structures during inversion of a domino basement-fault system from an analogue modelling approach. *Solid Earth*, *14*(5), 517–589. https://doi.org/10.5194/se-14-571-2023

Fiduk, J. C., & Rowan, M. G., (2012). Analysis of folding and deformation within layered evaporites in Blocks BM-S-8 & -9, Santos Basin, Brazil. In G. I. Alsop, S. G. Archer, A. J. Hartley, N. T. Grant, & R. Hodgkinson (Eds.), *Salt tectonics, sediments and prospectivity* (Vol. 363(1), pp. 471–487). Geological Society, London, Special Publications. https://doi.org/10.1144/SP363.22

Fischer, A. G. (1964). The Lofer Cyclothems of the Alpine Triassic. In D. F. Merriam (Ed.), *Symposium on cyclic sedimentation* (Vol. 169, pp. 107–149). Kansas Geological Survey, Bulletin.

Flinch, J., & Soto, J. I. (2022). Structure and Alpine tectonic evolution of a salt canopy in the western Betic Cordillera (Spain). *Marine and Petroleum Geology*, *143*, 105782. https://doi.org/10.1016/j.marpetgeo.2022.105782

Ford, M. (2004). Depositional wedge tops: Interaction between low basal friction external orogenic wedges and flexural foreland basins. *Basin Research*, *16*(3), 361–375. https://doi.org/10.1111/j.1365-2117.2004.00236.x

Frank, W., & Schlager, W. (2006). Jurassic strike slip versus subduction in the Eastern Alps. *International Journal of Earth Sciences*, *95*(3), 431–450. https://doi.org/10.1007/s00531-005-0045-7

Frisch, W., & Gawlick, H.-J. (2003). The nappe structure of the central Northern Calcareous Alps and its disintegration during Miocene tectonic extrusion — A contribution to understanding the orogenic evolution of the Eastern Alps. *International Journal of Earth Sciences*, *92*(1), 712–727. https://doi.org/10.1007/s00531-003-0357-4

Froitzheim, N., & Manatschal, G. (1996). Kinematics of Jurassic rifting, mantle exhumation, and passive-margin formation in the Austroalpine and Penninic nappes (eastern Switzerland). *GSA Bulletin*, *108*(9), 1120–1133. https://doi.org/10.1130/0016-7606(1996)108<1120:kojrme>2.3.co;2

Ganss, O. (1937). Zur Geologie des westlichen Toten Gebirges. *Jahrbuch der Geologischen Bundesanstalt*, *87*, 331–374.

Garrison, R. E. (1967). Pelagic limestones of the Oberalm beds (Upper Jurassic – Lower Cretaceous), Austrian Alps. *Bulletin of Canadian Petroleum Geology*, *15*, 21–49.

Garrison, R. E., & Fischer, A. (1969). Deep-water limestones and radiolarites of the Alpine Jurassic. In G. M. Friedman (Ed.), *Depositional environments in carbonate rocks* (Vol. 14, pp. 20–56). SEPM Special Publication.

Gawlick, H. J. (1998). Obertriassische Brekzienbildung und Schollengleitung im Zlambachfaziesraum (Pötschenschichten) – Stratigraphie, Paläogeographie und diagenetische Überprägung des Lammeregg-Schollenkomplexes (Nördliche Kalkalpen, Salzburg). *Jahrbuch der Geologischen Bundesanstalt*, *141*, 147–165.

Gawlick, H.-J., & Frisch, W. (2003). The Middle to Late Jurassic carbonate clastic radiolaritic flysch sediments in the Northern Calcareous Alps: Sedimentology, basin evolution, and tectonics - An overview. *Neues Jahrbuch für Geologie und Paläontolgie – Abhandlungen*, *230*(2–3), 163–213. https://doi.org/10.1127/njgpa/230/2003/163

Gawlick, H.-J., Frisch, W., Missoni, S., & Suzuki, H. (2002). Middle to Late Jurassic radiolarite basins in the central part of the Northern Calcareous Alps as a key for the reconstruction of their early tectonic history – An overview. *Memorie della Societa Geologica Italiana*, *57*, 123–132.

Gawlick, H.-J., Frisch, W., Vecsei, A., Steiger, T., & Böhm, F. (1999). The change from rifting to thrusting in the Northern Calcareous Alps as recorded in Jurassic sediments. *Geologische Rundschau*, *87*(4), 644–657. https://doi.org/10.1007/s005310050237

Gawlick, H. J., Janauscheck, W., Missoni, S., Diersche, V., & Zankl, H. (2003). Fazies, Alter und Komponentenbestand der jurassischen Kieselsedimente mit polymikten Brekzien (Callovium-Oxfordium) des Büchsenkopfes im Nationalpark Berchtesgaden und deren Bedeutung für die tektonische und paläogeographische Interpretation der Berchtesgadener Kalkalpen (Deutschland). *Neues Jahrbuch für Geologie und Paläontologie - Abhandlungen*, *228*, 275–304.

Gawlick, H.-J., & Lein, R. (1997). Neue stratigraphische und fazielle Daten aus dem Jakobberg-und Wolfdietrichstollen des Hallein-Bad Dürrnberger Salzberges und ihre Bedeutung für die Interpretation der geologischen Verhältnisse im Bereich der Hallein - Berchtesgadener Schollenregion. *Geologisch - Palaontologische Mitteilungen Innsbruck*, *22*, 199–225.

Gawlick, H.-J., & Missoni, S. (2015). Middle Triassic radiolarite pebbles in the Middle Jurassic Hallstatt Mélange of the Eastern Alps: Implications for Triassic–Jurassic geodynamic and paleogeographic reconstructions of the western Tethyan realm. *Facies*, *61*(3), 13. https://doi.org/10.1007/s10347-015-0439-3

Gawlick, H.-J., & Missoni, S. (2019). Middle-Late Jurassic sedimentary mélange formation related to ophiolite obduction in the Alpine-Carpathian-Dinaridic Mountain Range. *Gondwana Research*, *74*, 144–172. https://doi.org/10.1016/j.gr.2019.03.003

Gawlick, H.-J., Missoni, S., Schlagintweit, F., Suzuki, H., Frisch, W., Krystyn, L., et al. (2009). Jurassic tectonostratigraphy of the Austroalpine domain. *Journal of Alpine Geology*, *50*, 1–152.

Gawlick, H.-J., & Schlagintweit, F. (2006). Berriasian drowning of the Plassen carbonate platform at the type-locality and its bearing on the early Eoalpine orogenic dynamics in the Northern Calcareous Alps (Austria). *International Journal of Earth Sciences*, *95*(3), 451–462. https://doi.org/10.1007/s00531-005-0048-4

Gawlick, H.-J., Schlagintweit, F., Ebli, O., & Suzuki, H. (2003). Die Plassen-Formation (Kimmeridgium) des Krahstein (Steirisches Salzkammergut, Österreich) und ihre Unterlagerung: Neue Daten zur Fazies, Biostratigraphie und Sedimentologie. *Zentralblatt für Geologie und Paläontologie – Teil*, *I*(3–4), 295–334.

Gawlick, H.-J., Schlagintweit, F., & Missoni, S. (2005). Die Barmsteinkalke der Typlokalität nordwestlich Hallein (hohes Tithonium bis tieferes Berriasium; Salzburger Kalkalpen) – Sedimentologie, Mikrofazies, Stratigraphie und Mikropaläontologie: Neue Aspekte zur Interpretation der Entwicklungsgeschichte der Ober-Jura-Karbonatplattform und der tektonischen Interpretation der Hallstätter Zone von Hallein – Bad Dürrnberg. *Neues Jahrbuch für Geologie und Paläontologie - Abhandlungen*, *236*(3), 351–421. https://doi.org/10.1127/njgpa/236/2005/351

Gawlick, H.-J., Schlagintweit, F., & Suzuki, H. (2007). Die Ober-Jura bis Unter-Kreide Schichtfolge des Gebiets Höherstein-Sandling (Salzkammergut, Österreich) – Implikationen zur Rekonstruktion des Block-Puzzles der zentralen Nördlichen Kalkalpen, der Gliederung der Radiolaritflyschbecken und der Plassen-Karbonatplattform. *Neues Jahrbuch für Geologie und Paläontologie - Abhandlungen*, *243*, 1–70. https://doi.org/10.1127/0077-7749/2007/0243-0001

Gawlick, H. J., Suzuki, H., & Missoni, S. (2011). Neue Radiolarienfaunen aus der Ruhpolding-Formation im Liegenden der Rofan-Brekzie des Rofan-/Sonnwendgebirges: Implikationen zur Deckenneugliederung der westlichen Nördlichen Kalkalpen. *Arbeitstagung der Geologischen Bundesanstalt*, *2011*, 39–50.

Geutebrück, E., Klammer, W., Schimunek, K., Steiger, E., Ströbl, E., Winkler, G., et al. (1984). Oberflächengeophysikalische Verfahren im Rahmen der KW-exploration der ÖMV. *Erdöl Und Erdgas*, *100*, 296–304.

Graham, R., Jackson, M., Pilcher, R., & Kilsdonk, B. (2012). Allochthonous salt in the sub-Alpine fold–thrust belt of Haute Provence, France. In G. I. Alsop, S. G. Archer, A. J. Hartley, N. T. Grant, & R. Hodgkinson (Eds.), *Salt tectonics, sediments and prospectivity* (Vol. 363(1), pp. 595–615). Geological Society, London, Special Publications. https://doi.org/10.1144/SP363.30

Granado, P., Roca, E., Strauss, P., Pelz, K., & Muñoz, J. A. (2019). Structural styles in fold-and-thrust belts involving early salt structures: The Northern Calcareous Alps (Austria). *Geology*, *47*(1), 51–54. https://doi.org/10.1130/G45281.1

Granado, P., Ruh, J. B., Santolaria, P., Strauss, P., & Muñoz, J. A. (2021). Stretching and contraction of extensional basins with pre-rift salt: A numerical modeling approach. *Frontiers in Earth Science*, *9*, 648937. https://doi.org/10.3389/feart.2021.648937

Grando, G., & McClay, K. (2004). Structural evolution of the Frampton growth fold system, Atwater Valley-Southern Green Canyon area, deep water Gulf of Mexico. *Marine and Petroleum Geology*, *21*(7), 889–910. https://doi.org/10.1016/j.marpetgeo.2003.12.005

Griesmeier, G. E. U. & Hornung, T. (Eds.). (2023). Blatt 68 Kirchdorf a.d. Krems 1:50,000. In *Zusammenstellung ausgewählter Archivunterlagen der GeoSphere Austria GEOFAST 1:50,000, Nr. 68*. Verlag der Geologischen Bundesanstalt.

Griffiths, P., Jones, S., Salter, N., Schaefer, F., Osfield, R., & Reiser, H. (2002). A new technique for 3-D flexural slip restoration. *Journal of Structural Geology*, *24*(4), 773–782. https://doi.org/10.1016/s0191-8141(01)00124-9

Groshong, R. H. (2006). *3-D structural geology* (p. 400). Springer.

Hahn, F. F. (1913a). Grundzüge des Baues der nördlichen Kalkalpen zwischen Inn und Enns. I Teil. *Mitteilungen der Osterreichischen Geologischen Gesellschaft*, *9*, 238–357.

Hahn, F. F. (1913b). Grundzüge des Baues der nördlichen Kalkalpen zwischen Inn und Enns. II Teil. *Mitteilungen der Osterreichischen Geologischen Gesellschaft*, *9*, 374–500.

Hamilton, W. (1989). Geologische Ergebnisse von Tiefbohrungen im Flysch und Kalkalpin zwischen Wien und Salzburg. In *Exkursionsführer der Österreichischen Geologischen Gesellschaft Nr 12* (p. 55). Österreichische Geologische Gesellschaft.

Haq, B. U., & Al-Qahtani, A. M. (2005). Phanerozoic cycles of sea-level change on the Arabian Platform. *GeoArabi*, *10*(2), 127–160. https://doi.org/10.2113/geoarabia1002127

Häusler, H. (1979). Zur Geologie und Tektonik der Hallstätter Zone im Bereich des Lammertales zwischen Golling und Abtenau (Sbg.). *Jahrbuch der Geologischen Bundesanstalt*, *122*(1), 75–141.

Herm, D. (1962). Stratigraphische und mikropaläontologische Untersuchungen der Oberkreide im Lattengebirge und im Nierental. *Bayerische Akademie der Wissenschaften: Mathematisch-Naturwissenschaftliche Klasse, Abhandlungen Neue Folge*, *10*, 9–119.

Hiebl, R. (2011). *Mikrofazies, Stratigraphie und Bewertung von Massenbewegungen der Mittel-bis Ober-Jura – Sedimente im Gebiet Wurzerkampl – Rote Wand – Mitterberg (Oberösterreich, Österreich)* (master's thesis). Montanuniversität Leoben.

Howlett, D. M., Gawthorpe, R. L., Ge, Z., Rotevatn, A., & Jackson, C. A.-L. (2020). Turbidites, topography and tectonics: Evolution of submarine channel-lobe systems in the salt-influenced Kwanza Basin, offshore Angola. *Basin Research*, *33*(2), 1076–1110. https://doi.org/10.1111/bre.12506

Jackson, C. A. L., & Stewart, S. (2017). Composition, tectonics, and hydrocarbon significance of Zechstein Supergroup salt on the United Kingdom and Norwegian continental shelves: A review. In J. I. Soto, J. F. Flinch, & G. Tari (Eds.), *Permo-triassic salt provinces of Europe, north Africa and the Atlantic margins* (pp. 175–201). Elsevier. https://doi.org/10.1016/B978-0-12-809417-4.00009-4

Jackson, M. P. A., & Hudec, M. R. (2017). *Salt tectonics: Principles and Practice*. Cambridge University Press.

Jordan, P., & Noack, T. (1992). Hangingwall geometry of overthrusts emanating from ductile decollements. In K. R. McClay (Ed.), *Thrust tectonics* (pp. 311–318). Chapman-Hall.

Jourdon, A., Mouthereau, F., Le Pourhiet, L., & Callot, J.-P. (2020). Topographic and tectonic evolution of mountain belts controlled by salt thickness and rift architecture. *Tectonics*, *39*(1), e2019TC005903. https://doi.org/10.1029/2019TC005903

Kellerbauer, S. (1996). Geologie und Geomechanik der Salzlagerstätte Berchtesgaden. *Munchner Geologische Hefte. Reihe B, Angewandte Geologie*, *2*, 1–101.

Kenter, J. A. M., & Schalger, W. (2009). Slope angle and basin depth of the Triassic platform-basin transition at the Gosaukamm, Austria. *Austrian Journal of Earth Sciences*, *102*, 15–22.

Kergaravat, C., Ribes, C., Callot, J.-P., & Ringenbach, J.-C. (2017). Tectono-stratigraphic evolution of salt-controlled minibasins in a fold and thrust belt, the Oligo-Miocene central Sivas Basin. *Journal of Structural Geology*, *102*, 75–97. https://doi.org/10.1016/j.jsg.2017.07.007

Kilian, S., & Ortner, H. (2019). Structural evidence of in-sequence and out-of-sequence thrusting in the Karwendel mountains and the tectonic subdivision of the western Northern Calcareous Alps. *Austrian Journal of Earth Sciences*, *112*(1), 62–83. https://doi.org/10.17738/ajes.2019.0005

Kilian, S., Ortner, H., & Schneider-Muntau, B. (2021). Buckle folding in the Northern Calcareous Alps - Field observations and numeric experiments. *Journal of Structural Geology*, *150*, 104416. https://doi.org/10.1016/j.jsg.2021.104416

Kim, Y.-S., & Sanderson, D. J. (2005). The relationship between displacement and length of faults: A review. *Earth-Science Reviews*, *68*(3–4), 317–334. https://doi.org/10.1016/j.earscirev.2004.06.003

Klaus, W. (1965). Zur Einstufung alpiner Salztone mittels Sporen. *Verhandlung der Geologischen Bundesanstalt*, *116*, 288–292.

Koyi, H. A., Ghasemi, A., Hessami, K., & Dietl, C. (2008). The mechanical relationship between strike-slip faults and salt diapirs in the Zagros fold–thrust belt. *Journal of the Geological Society, London*, *165*(6), 1031–1044. https://doi.org/10.1144/0016-76492007-142

Koyi, H. A., & Sans, M., (2006). Deformation transfer in viscous detachments: Comparison of sandbox models to the South Pyrenean Triangle Zone. In S. J. H. Butler & G. Schreurs (Eds.), *Analogue and numerical modelling of crustal-scale processes* (Vol. 253(1), pp. 117–134). Geological Society, London, Special Publication. https://doi.org/10.1144/gsl.sp.2006.253.01.06

Krainer, K., Mostler, H., & Haditsch, J. G. (1994). Jurassische Beckenbildung in den Nördlichen Kalkalpen bei Lofer (Salzburg) unter besonderer Berücksichtigung der Manganerz-Genese. *Abhandlungen der Geologischen Bundesanstalt*, *50*, 257–293.

Kralik, M., Krumm, H., & Schramm, J. M. (1987). Low grade and very low grade metamorphism in the Northern Calcareous Alps and in the Greywacke Zone: Illite-crystallinity data and isotopic ages. In H. W. Flügel & P. Faupl (Eds.), *Geodynamics of the Eastern Alps* (pp. 164–178). Franz Deuticke.

Kramer, H., & Kröll, A. (1979). Die Untersuchungsbohrung Vigaun U 1 bei Hallein in den Salzburger Kalkalpen. *Mitteilungen der Osterreichischen Geologischen Gesellschaft*, *70*, 1–10.

Krenmayr, H. G. (2005). *Geologische Karte von Salzburg 1:200,000*. Geologische Bundesanstalt.

Krenmayr, H. G., & Schnabel, H.-J. (2006). *Geologische Karte von Oberösterreich 1:200,000*. Geologische Bundesanstalt.

Krische, O., Goričan, Š., & Gawlick, H.-J. (2014). Erosion of a Jurassic ophiolitic nappe-stack as indicated by exotic components in the Lower Cretaceous Rossfeld Formation of the Northern Calcareous Alps (Austria). *Geologica Carpathica*, *65*(1), 3–24. https://doi.org/10.2478/geoca-2014-0001

Krystyn, L. (1971). Stratigraphie, Fauna und Fazies der Klaus-Schichten (Aalenium-Oxford) in den östlichen Nordalpen. *Verhandlungen der Geologischen Bundesanstalt*, *1971*, 486–509.

Krystyn, L. (1975). Die *Tirolites*-Fauna (Ammonoidea) der untertriassischen Werfener Schichten Europas und ihre stratigraphische Bedeutung. *Sitzungsberichte der Akademie der Wissenschaften mathematischnaturwissenschaftliche Klasse*, *183*, 29–50.

Krzywiec, P., & Vergés, J. (2007). Role of the foredeep evaporites in wedge tectonics and formation of triangle zones: Comparison of the Carpathian and Pyrenean thrust fronts. In O. Lacombe, J. Lavé, F. Roure, & J. Vergés (Eds.), *Thrust belts and Foreland basins: From fold kinematics to hydrocarbon systems* (pp. 385–396). Springer.

Kügler, U., Schlagintweit, F., Suzuki, H., & Gawlick, H.-J. (2003). Stratigraphie und Fazies des Höheren Mittel-bis Ober-Jura im Bereich des Falkensteinzuges am Wolfgangsee, Salzkammergut (Österreich) mit besonderer Berücksichtigung der Plassen-Formation (Kimmeridgium). *Gmundner Geo-Studien*, *2*, 97–106.

Kurz, M., Fernandez, O., Eggerth, L., Grasemann, B., & Strauss, P. (2023). Emplacement and associated sedimentary record of the Jurassic submarine salt allochthon of the Wurzeralm (Eastern Alps, Austria). *Terra Nova*, *35*(6), 524–532. https://doi.org/10.1111/ter.12675

Lein, R. (1987). Zur Verbreitung der Hallstätter Zone beiderseits der Pyhrn-Passes. *OÖ Geonachrichten*, *2*, 21–37.

Lein, R., Suzuki, H., & Gawlick, H. J. (2009). Die Obersee-Brekzie bei Lunz (Niederösterreich): Revision der Stratigraphie und des Komponentenbestandes. *Arbeitstagung Geologische Bundesanstalt*, *2009*, 204–210.

Leitner, C., & Neubauer, F. (2011). Tectonic significance of structures within the salt deposits Altaussee and Berchtesgaden–Bad Dürrnberg, Northern Calcareous Alps. *Austrian Journal of Earth Sciences*, *104*, 2–21.

Leitner, C., & Spötl, C. (2017). The Eastern Alps: Multistage development of extremely deformed evaporites. In J. I. Soto, J. F. Flinch, & G. Tari (Eds.), *Permo-triassic salt provinces of Europe, North Africa and the Atlantic margins* (pp. 467–482). Elsevier. https://doi.org/10.1016/B978-0-12-809417-4.00022-7

Leitner, C., Wiesmayer, S., Köster, M. H., Gilg, H. A., Finger, F., & Neubauer, F. (2017). Alpine halite-mudstone-polyhalite tectonite: Sedimentology and early diagenesis of evaporites in an ancient rift setting (Haselgebirge Formation, eastern Alps). *GSA Bulletin*, *129*, 1537–1553. https://doi.org/10.1130/B31747.1

Leitner, T., & Mayr, M. (2017). Die Salinen Austria AG und die Geologie ihrer Salzlagerstätten im Salzkammergut. In I. Wimmer-Frey, A. Römer, & C. Janda (Eds.), *Arbeitstagung 2017 Bad Ischl, Hallstatt, Gmunden* (pp. 80–85). Geologische Bundesanstalt.

Letouzey, J., Colletta, B., Vially, R., & Chermette, J. C. (1995). Evolution of salt related structures in compressional settings. In M. P. A. Jackson, D. G. Roberts, & S. Snelson (Eds.), *Salt tectonics: A global perspective* (Vol. 65, pp. 41–60). AAPG, AAPG Memoir. https://doi.org/10.1306/m65604c3

Levi, N. (2023). Polyphase tectonics in the central Salzkammergut (Northern Calcareous Alps, Austria): An updated interpretation. *Journal of Geodynamics*, *156*, 101793. https://doi.org/10.1016/j.jog.2023.101973

Linzer, H.-G., Decker, K., Peresson, H., Dell'Mour, R., & Frisch, W. (2002). Balancing lateral orogenic float of the Eastern Alps. *Tectonophysics*, *354*(3–4), 211–237. https://doi.org/10.1016/s0040-1951(02)00337-2

Linzer, H.-G., Ratschbacher, L., & Frisch, W. (1995). Transpressional collision structures in the upper crust: The fold-thrust belt of the Northern Calcareous Alps. *Tectonophysics*, *242*(1–2), 41–61. https://doi.org/10.1016/0040-1951(94)00152-Y

Lopez-Mir, B. (2019). Cross-section construction and balancing: Examples from the Spanish Pyrenees. In A. Billi & Å. Fagereng (Eds.), *Problems and solutions in structural geology and tectonics* (pp. 3–23). Elsevier. https://doi.org/10.1016/b978-0-12-814048-2.00001-6

López-Mir, B., Muñoz, J. A., & García-Senz, J. (2015). Extensional salt tectonics in the partially inverted Cotiella post rift basin (south central Pyrenees): Structure and evolution. *International Journal of Earth Sciences*, *104*(2), 419–434. https://doi.org/10.1007/s00531-014-1091-9

Mandl, G. W. (1982). Jurassische Gleittektonik im Bereich der Hallstätter Zone zwischen Bad Ischl und Bad Aussee (Salzkammergut, Österreich). *Mitteilungen der Gesellschaft der Geologie- und Bergbaustudenten in Österreich*, *28*, 55–76.

Mandl, G. W. (1996). Zur Geologie des Ödenhof-Fensters (Nördliche Kalkalpen, Österreich). *Jahrbuch der Geologischen Bundesanstalt*, *139*, 459–473.

Mandl, G. W. (2000). The Alpine sector of the Tethyan shelf — Examples of Triassic to Jurassic sedimentation and deformation from the North Calcareous Alps. *Mitteilungen der Osterreichischen Geologischen Gesellschaft*, *92*, 61–77.

Mandl, G. W. (2013). Zur Geologie des Raumes Hütteneckalm–Sandlingalm–Blaa-Alm (Salzkammergut, Österreich) mit kritischen Anmerkungen zur Sandlingalm-Formation. *Jahrbuch der Geologischen Bundesanstalt*, *153*, 33–74.

Mandl, G. W., Hejl, E., & van Husen, D. (2014). *Erläuterungen zu Blatt 127 Schladming*. Geologische Bundesanstalt.

Mandl, G. W., & Matura, A. (Eds.). (1995). Blatt 127 Schladming 1:50,000. In *Geologische Karte der Republik Österreich 1:50,000, Nr. 127*. Verlag der Geologischen Bundesanstalt.

Mandl, G. W., vanHusen, D., & Lobitzer, H. (Eds.). (2012). *Erläuterung zu Blatt 96 Bad Ischl*. Geologische Bundesanstalt.

Manea, V. C., Armaş, I., Manea, M., & Gheorghe, M. (2021). InSAR surface deformation and numeric modeling unravel an active salt diapir in southern Romania. *Scientific Reports*, *11*(1), 12091. https://doi.org/10.1038/s41598-021-91517-4

Medwenitsch, W. (1960). Zur Geologie des Halleiner Salzberges. Die Profile des Jakobberg-und Wolfdietrichstollens. *Mitteilungen der Geologischen Gesellschaft in Wien*, *51*, 197–218.

Miladinova, I., Froitzheim, N., Nagel, T. J., Janák, M., Fonseca, R. O. C., Sprung, P., & Münker, C. (2022). Constraining the process of intracontinental subduction in the Austroalpine Nappes: Implications from petrology and Lu-Hf geochronology of eclogites. *Journal of Metamorphic Geology*, *40*(3), 423–456. https://doi.org/10.1111/jmg.12634

Missoni, S., & Gawlick, H.-J. (2011). Evidence for Jurassic subduction from the Northern Calcareous Alps (Berchtesgaden; Austroalpine, Germany). *International Journal of Earth Sciences*, *100*(7), 1605–1631. https://doi.org/10.1007/s00531-010-0552-z

Moser, M. (2003). Bericht 2002 über geologische Aufnahmen im Gebiet zwischen Salzatal und Gamsforst auf Blatt 101 Eisenerz. *Jahrbuch der Geologischen Bundesanstalt*, *143*, 471–475.

Moser, M. (Ed.). (2014). Blatt 97 Bad Mitternndorf 1:50,000. In *Provisorische Geologische Karte der Republik Österreich GEOFAST 1:50,000, Nr. 97*. Verlag der Geologischen Bundesanstalt.

Moser, M., & Moshammer, B. (2018). Die Mitteltrias-Schichtfolge des Kasberg-Gebietes in Oberösterreich (Totengebirgsdecke) und deren Bedeutung für die Mitteltrias Stratigrafie der Nördlichen Kalkalpen. *Geo Australasia*, *15*, 37–59.

Moser, M., & Pavlik, W. (Eds.). (2013). Blatt 98 Liezen 1:50,000. In *Provisorische Geologische Karte der Republik Österreich GEOFAST 1: 50,000, Nr. 98*. Verlag der Geologischen Bundesanstalt.

Mosna, D. (2010). *Die Lärchberg-Schichten im Gebiet des Gerhardsteins nahe Lofer* (master's thesis). University of Innsbruck.

Mostler, H. (1972). Zur Gliederung der Permoskyth-Schichtfolge im Räume zwischen Wörgl und Hochfilzen (Tirol). *Verhandlungen der Geologischen Bundeanstalt*, *1972*, 155–162.

Mostler, H., & Roßner, R. (1977). Stratigraphisch-fazielle und tektonische Betrachtungen zu Aufschlüssen in skyth-anisischen Grenzschichten im Bereich der Annaberger Senke (Salzburg, Österreich). *Geologisch - Palaontologische Mitteilungen Innsbruck*, *6*, 1–44.

Mouthereau, F., Lacombe, O., & Meyer, B. (2006). The Zagros fold belt (Fars, Iran): Constraints from topography and critical wedge modelling. *Geophysical Journal International*, *165*(1), 336–356. https://doi.org/10.1111/j.1365-246X.2006.02855.x

Muñoz, J. A., Beamud, E., Fernandez, O., Arbués, P., Dinarès-Turell, J., & Poblet, J. (2013). The Ainsa Fold and thrust oblique zone of the central Pyrenees: Kinematics of a curved contractional system from paleomagnetic and structural data. *Tectonics*, *32*(5), 1142–1175. https://doi.org/10.1002/tect.20070

Muñoz, J. A., Ferrer, O., Gratacós, O., & Roca, E. (2024). The influence of the geometry of salt detachments on thrust salient development: An analogue modelling approach based on the South-Central Pyrenean thrust salient. *Journal of Structural Geology*, *180*, 105078. https://doi.org/10.1016/j.jsg.2024.105078

Neubauer, F., & Genser, J. (2018). Field Trip Post-EX-1 – Transect across the Eastern Alps. *Berichte der Geologischen Bundesanstalt*, *126*, 137–222.

Neubauer, F., & Moser, M. (Eds.). (2022). Blatt 126 Radstadt 1:50,000. In *Zusammenstellung ausgewählter Archivunterlagen der GeoSphere Austria GEOFAST 1:50,000, Nr. 126*. Verlag der Geologischen Bundesanstalt.

Nittel, P. (2006). Beitrage zur Stratigraphie und Mikropaläontologie der Mitteltrias der Innsbrucker Nordkette (Nömittelrdliche Kalkalpen, Austria). *Geo Australasia*, *3*, 93–145.
Oravecz, E., Héja, G., & Fodor, L. (2023). Salt tectonics versus shortening: Recognizing pre-orogenic evaporite deformation in salt-bearing fold-and-thrust belts on the example of the Silica Nappe (Inner Western Carpathians). *Tectonics*, *42*(8), e2023TC007842. https://doi.org/10.1029/2023TC007842
Ortner, H. (2001). Growing folds and sedimentation of the Gosau Group, Muttekopf, Northern Calcareous Alps, Austria. *International Journal of Earth Sciences*, *90*(3), 727–739. https://doi.org/10.1007/s005310000182
Ortner, H. (2003). Cretaceous thrusting in the western part of the Northern Calcareous Alps (Austria) - Evidences from synorogenic sedimentation and structural data. *Mitteilungen der Osterreichischen Geologischen Gesellschaft*, *94*, 63–77.
Ortner, H. (2017). Geometry of growth strata in wrench-dominated transpression: 3D-model of the Upper Jurassic Trattberg rise, Northern Calcareous Alps, Austria. *Geophysical Research Abstracts*, *19*, EGU2017–9222.
Ortner, H., & Kilian, S. (2022). Thrust tectonics in the Wetterstein and Mieming mountains, and a new tectonic subdivision of the Northern Calcareous Alps of Western Austria and Southern Germany. *International Journal of Earth Sciences*, *11*(2), 543–571. https://doi.org/10.1007/s00531-021-02128-3
Ortner, H., Kositz, A., Willingshofer, E., & Sokoutis, D. (2016). Geometry of growth strata in a transpressive fold belt in field and analogue model: Gosau Group at Muttekopf, Northern Calcareous Alps, Austria. *Basin Research*, *28*(6), 731–751. https://doi.org/10.1111/bre.12129
Ortner, H., Ustaszewski, M., & Rittner, M. (2008). Late Jurassic tectonics and sedimentation: Breccias in the Unken syncline, central Northern Calcareous Alps. *Swiss Journal of Geosciences*, *101*(S1), S55–S71. https://doi.org/10.1007/s00015-008-1282-0
Ottner, F. (1990). Zur Geologie der Wurzer Deckenscholle und deren Rahmen im Bereich des Warschenecks (OÖ). *Mitteilungen der Gesellschaft der Geologie- und Bergbaustudenten Österreichs*, *36*, 101–145.
Pak, E., & Schauberger, O. (1981). Die geologische Datierung der ostalpinen Salzlagerstätten mittels Schwefelisotopenuntersuchungen. *Verhandlungen der Geologischen Bundesanstalt*, *1981*, 185–192.
Pavlik, W. (Ed.). (2006). Blatt 92 Lofer 1:50,000. In *Provisorische Geologische Karte der Republik Österreich GEOFAST 1:50,000, Nr. 92*. Verlag der Geologischen Bundesanstalt.
Pavlik, W. (Ed.). (2007). Blatt 93 Bad Reichenall 1:50,000. In *Zusammenstellung ausgewählter Archivsunterlagen der Geologischen Bundesanstalt GEOFAST 1:50,000, Nr. 93*. Verlag der Geologischen Bundesanstalt.
Peresson, H., & Decker, K. (1997). The Tertiary dynamics of the northeastern Eastern Alps (Austria): Changing paleostresses in a collisional plate boundary. *Tectonophysics*, *272*(2–4), 125–157. https://doi.org/10.1016/S0040-1951(96)00255-7
Pérez-Villar, G., Gutiérrez, F., Zarroca, M., Roqué, C., Benito-Calvo, A., & Menció, A. (2024). Late Quaternary morpho-stratigraphic record of diapir rise in the Cardona salt extrusion, NE Spain. Halokinetic sequences, raised terraces and uplift rates. *Quaternary Science Reviews*, *324*, 108462. https://doi.org/10.1016/j.quascirev.2023.108462
Piller, W. E., Egger, H., Erhart, C. W., Gross, M., Harzhauser, M., Hubmann, B., et al. (2004). *Die stratigraphische Tabelle von Österreich 2004 (sedimentäre Schichtfolgen)*. Österreichische Stratigraphische Kommission.
Pla, O., Roca, E., Xie, H., Izquierdo-Lavall, E., Muñoz, J. A., Rowan, M. G., et al. (2019). Influence of syntectonic sedimentation and décollement rheology on the geometry and evolution of orogenic wedges: Analog modeling of the Kuqa fold-and-thrust belt (NW China). *Tectonics*, *38*(8), 2727–2755. https://doi.org/10.1029/2018TC005386
Plašienka, D. (2018). Continuity and episodicity in the early Alpine tectonic evolution of the Western Carpathians: How large-scale processes are expressed by the orogenic architecture and rock record data. *Tectonics*, *37*(7), 2029–2079. https://doi.org/10.1029/2017TC004779
Platt, L. B. (1998). Interpretation of geologic maps. In S. Marshak & G. Mitra (Eds.), *Basic methods of structural geology, Part I: Elementary techniques* (pp. 177–192). Prentice Hall.
Plöchinger, B. (1953). Der Bau der südlichen Osterhorngruppe und die Thiton-Neokomtransgression. *Jahrbuch der Geologischen Bundesanstalt*, *96*, 257–273.
Plöchinger, B. (1974). Gravitativ transportiertes permisches Haselgebirge in den Oberalmer Schichten (Tithonium, Salzburg). *Verhandlungen der Geologischen Bundesanstalt*, *1974*, 71–88.
Plöchinger, B. (1977). Die Untersuchungsbohrung Gutrathsberg BI südlich St. Leonhard im Salzachtal (Salzburg). *Verhandlungen der Geologischen Bundesanstalt*, *1977*, 3–11.
Plöchinger, B. (1979). Argumente für die intramalmische Eingleitung von Hallstätter Schollen bei Golling (Salzburg). *Verhandlungen der Geologischen Bundesanstalt*, *1979*, 181–194.
Plöchinger, B. (Ed.). (1982). Blatt 95 Sankt Wolfgang 1:50,000. In *Geologische Karte der Republik Österreich 1:50,000, Nr. 95*. Verlag der Geologischen Bundesanstalt.
Plöchinger, B. (1984). Zum Nachweis jurassisch-kretazischer Eingleitungen von Hallstätter Gesteinsmassen beiderseits des Salzach-Quertales (Salzburg). *Geologische Rundschau*, *73*, 293–306.
Plöchinger, B. (Ed.). (1987). Blatt 94 Hallein 1:50,000. In *Geologische Karte der Republik Österreich 1:50,000, Nr. 94*. Verlag der Geologischen Bundesanstalt.
Plöchinger, B. (Ed.). (1990). *Erläuterungen zu Blatt 94 Hallein*. Verlag der Geologischen Bundesanstalt.
Pueyo, E. L., Mauritsch, H. J., Gawlick, H.-J., Scholger, R., & Frisch, W. (2007). New evidence for block and thrust sheet rotations in the central northern Calcareous Alps deduced from two pervasive remagnetization events. *Tectonics*, *26*(5), TC5011. https://doi.org/10.1029/2006TC001965
Rasser, M. W., Vasicek, Z., Skupien, P., Lobitzer, H., & Boorova, D. (2003). Die Schrambach-Formation an ihrer Typuslokalität (Unter-Kreide, Nördliche Kalkalpen, Salzburg): Lithostratigraphische Formalisierung und "historische" Irrtümer. In W. E. Piller (Ed.), Stratigraphia Austriaca*, 193–216. Schriftenreihe der Erdwissenschaftlichen Kommission Österreichische Akademie der Wissenschaften*. ÖAK.
Riba, O. (1976). Syntectonic unconformities of the Alto Cardener, Spanish Pyrenees: A genetic interpretation. *Sedimentary Geology*, *15*(3), 213–233. https://doi.org/10.1016/0037-0738(76)90017-8
Ribes, C., Lopez, M., Kergaravat, C., Crumeyrolle, P., Poisson, A., Callot, J.-P., et al. (2018). Facies partitioning and stratal pattern in salt-controlled marine to continental mini-basins: Examples from the Late Oligocene to Early Miocene of the Sivas Basin, Turkey. *Marine and Petroleum Geology*, *93*, 468–496. https://doi.org/10.1016/j.marpetgeo.2018.03.018
Risch, H. (Ed.). (1993). *Erläuterungen zum Blatt Nr. 8343 Berchtesgaden West*. Bayerisches Geologisches Landesamt.
Rowan, M. G., & Ratliff, R. A. (2012). Cross-section restoration of salt-related deformation: Best practices and potential pitfalls. *Journal of Structural Geology*, *41*, 24–37. https://doi.org/10.1016/j.jsg.2011.12.012
Rowan, M. G., Tilton, J., Lebit, H., & Fiduk, C. J. (2022). Thin-skinned extensional salt tectonics, counterregional faults, and the Albian Gap of Brazil. *Marine and Petroleum Geology*, *137*, 105478. https://doi.org/10.1016/j.marpetgeo.2021.105478

Rowan, M. G., & Vendeville, B. C. (2006). Foldbelts with early salt withdrawal and diapirism: Physical model and examples from the northern Gulf of Mexico and the Flinders Ranges, Australia. *Marine and Petroleum Geology*, *23*(9–10), 871–891. https://doi.org/10.1016/j.marpetgeo.2006.08.003

Roßner, R. (1972). Die Geologie des nordwestlichen St. Martiner Schuppenlandes am Südostrand des Tennengebirges (Oberostalpin). *Erlanger Geologische Abhandlungen*, *89*, 1–57.

Sanders, D. (1998). Tectonically controlled Late Cretaceous terrestrial to neritic deposition (Northern Calcareous Alps, Tyrol, Austria). *Facies*, *39*(1), 139–177. https://doi.org/10.1007/BF02537015

Sanders, D., Lukesch, M., Rasser, M., & Skelton, P. (2007). Shell beds of diceratid rudists ahead of a low-energy gravelly beach (Tithonian, Northern Calcareous Alps, Austria): Palaeoecology and Taphonomy. *Austrian Journal of Earth Sciences*, *100*, 186–199.

Santolaria, P., Ferrer, O., Rowan, M. G., Snidero, M., Carrera, N., Granado, P., et al. (2021). Influence of preexisting salt diapirs during thrust wedge evolution and secondary welding: Insights from analog modeling. *Journal of Structural Geology*, *149*, 104374. https://doi.org/10.1016/j.jsg.2021.104374

Santolaria, P., Granado, P., Carrera, N., Schneider, C. L., Ferrer, O., Snidero, M., et al. (2022). From downbuilding to contractional reactivation of salt-sediment systems: Insights from analog modeling. *Tectonophysics*, *819*, 229078. https://doi.org/10.1016/j.tecto.2021.229078

Santolaria, P., Granado, P., Wilson, E., de Matteis, M., Ferrer, O., Strauss, P., et al. (2022). From salt-bearing rifted margins to fold-and-thrust belts. Insights from analog modeling and Northern Calcareous Alps case study. *Tectonics*, *41*(11), e2022TC007503. https://doi.org/10.1029/2022TC007503

Santolaria, P., Harris, L. B., Casas, A. M., & Soto, R. (2022). Influence of *décollement*-cover thickness variations in fold-and-thrust belts: Insights from centrifuge analog modeling. *Journal of Structural Geology*, *163*, 104704. https://doi.org/10.1016/j.jsg.2022.104704

Schäffer, G. (Ed.). (1982). Blatt 96 Bad Ischl 1:50,000. In *Geologische Karte der Republik Österreich 1:50,000, Nr. 96*. Verlag der Geologischen Bundesanstalt.

Schauberger, O. (1972). *Längsprofil durch den Salzstock von Hallein-Dürrenberg in der Achse der Wolfdietrichstollens* (internal report). Österreichische Salinen AG.

Schlager, W., & Schöllnberger, W. (1974). Das Prinzip stratigraphischer Wende in der Schichtfolge der Nördlichen Kalkalpen. *Mitteilungen der Geologischen Gesellschaft in Wien*, *66/67*, 165–193.

Schlagintweit, F., & Ebli, O. (1999). New results on microfacies, biostratigraphy and sedimentology of Late Jurassic - Early Cretaceous platform carbonates of the Northern Calcareous Alps – Part I: Tressenstein limestone, Plassen formation. *Abhandlungen der Geologischen Bundesanstalt*, *56*, 379–418.

Schlagintweit, F., & Gawlick, H.-J. (2008). The occurrence and role of microencruster frameworks in Late Jurassic to Early Cretaceous platform margin deposits of the Northern Calcareous Alps (Austria). *Facies*, *54*(2), 207–231. https://doi.org/10.1007/s10347-007-0131-3

Schlagintweit, F., Gawlick, H.-J., & Lein, R. (2003). Die Plassen-Formation der Typlokalität (Salzkammergut, Österreich) – Neue Daten zu Fazies, Sedimentologie und Stratigraphie. *Mitteilungen der Gesellschaft Geologie- und Bergbaustudenten Österreichs*, *46*, 1–34.

Schmid, S. M., Bernoulli, D., Fügenschuh, B., Matenco, L., Schefer, S., Schuster, R., et al. (2008). The Alpine-Carpathian-Dinaridic orogenic system: Correlation and evolution of tectonic units. *Swiss Journal of Geosciences*, *101*(1), 139–183. https://doi.org/10.1007/s00015-008-1247-3

Schmid, S. M., Fügenschuh, B., Kissling, E., & Schuster, R. (2004). Tectonic map and overall architecture of the Alpine orogen. *Ecologae geologicae Helvetiae*, *97*(1), 93–117. https://doi.org/10.1007/s00015-004-1113-x

Schuster, R., Egger, H., Krenmayr, H.-G., Linner, M., Mandl, G. W., Matura, A., et al. (2013). Geologische Übersichtskarte der Republik Österreich 1:1 500 000 (ohne Quartär). In R. Schuster, A. Daurer, H.-G. Krenmayr, M. Linner, G. W. Mandl, G. Pestal, et al. (Eds.), *Rocky Austria – Geologie von Österreich – kurz und bunt*. Geologische Bundesanstalt.

Soto, J. I., Tranos, M. D., Bega, Z., Dooley, T. P., Hernández, P., Hudec, M. R., et al. (2024). Contrasting styles of salt-tectonic processes in the Ionian Zone (Greece and Albania): Integrating surface geology, subsurface data, and experimental models. *Tectonics*, *43*(1), e2023TC008104. https://doi.org/10.1029/2023TC008104

Spengler, E. (1924). Zur Frage des "Almenfensters" in der Grünauer Voralpen. *Verhandlungen der Geologischen Bundesanstalt*, *9*, 157–164.

Steiger, T. (1981). Kalkturbidite im Oberjura der Nördlichen Kalkalpen (Barmsteinkalke, Salzburg, Österreich). *Facies*, *4*(1), 215–347. https://doi.org/10.1007/BF02536589

Steiner, T. M. C., Gawlick, H.-J., Melcher, F., & Schlagintweit, F. (2021). Ophiolite derived material as parent rocks for Late Jurassic bauxite: Evidence for Tithonian unroofing in the Northern Calcareous Alps (Eastern Alps, Austria). *International Journal of Earth Sciences*, *110*(5), 1847–1862. https://doi.org/10.1007/s00531-021-02044-6

Storti, F., Soto Marín, R., Rosetti, F., & Casas, A. M. (2007). Evolution of experimental thrust wedges accreted from along-strike tapered, silicone-floored multilayers. *Journal of the Geological Society*, *164*(1), 73–85. https://doi.org/10.1144/0016-76492005-186

Strauss, P., Granado, P., & Muñoz, J. A. (2021). Subsidence analysis of salt tectonics-driven carbonate minibasins (Northern Calcareous Alps, Austria). *Basin Research*, *33*(2), 968–990. https://doi.org/10.1111/bre.12500

Strauss, P., Granado, P., Muñoz, J. A., Böhm, K., & Schuster, R. (2023). The Northern Calcareous Alps revisited: Formation of a hyperextended margin and mantle exhumation in the Northern Calcareous Alps sector of the Neo-Tethys (Eastern Alps, Austria). *Earth-Science Reviews*, *243*, 104488. https://doi.org/10.1016/j.earscirev.2023.104488

Suzuki, H., & Gawlick, H.-J. (2009). Jurassic radiolarians from cherty limestones below the Hallstatt salt mine (Northern Calcareous Alps, Austria). *Neues Jahrbuch für Geologie und Paläontologie - Abhandlungen*, *251*(2), 155–197. https://doi.org/10.1127/0077-7749/2009/0251-0155

Szatmari, P., Moré de Lima, C., Fontaneta, G., de Melo Lima, M., Zambonato, E., Menezes, M. R., et al. (2021). Petrography, geochemistry and origin of South Atlantic evaporites: The Brazilian side. *Marine and Petroleum Geology*, *127*, 104805. https://doi.org/10.1016/j.marpetgeo.2020.104805

Teixell, A., Hudec, M. R., Arboleya, M.-L., & Fernandez, N. (2024). 3D variation of shortened salt walls from the Moroccan Atlas: Influence of salt inclusions and suprasalt sedimentary wedges. *Journal of Structural Geology*, *183*, 105125. https://doi.org/10.1016/j.jsg.2024.105125

Tollmann, A. (1975). Zur Frage der Parautochthonie der Lammereinheit in der Salzburger Hallstätter Zone. *Sitzungsberichte der Akademie der Wissenschaften, mathematisch-naturwissenschaftliche Klasse, Abteilung*, *1*(184), 237–257.

Tollmann, A. (1976a). *Analyse des klassischen nordalpinen Mesozoikums: Stratigraphie, Fauna und Fazies der Nördlichen Kalkalpen*. Franz Deuticke.

Tollmann, A. (1976b). *Der Bau der Nördlichen Kalkalpen: Orogene Stellung und regionale Tektonik*. Franz Deuticke.

Tollmann, A. (1985). *Geologie von Österreich, Band II: Außerzentralalpiner Anteil*. Franz Deuticke.

Tollmann, A. (1987). Late Jurassic/Neocomian gravitational tectonics in the Northern Calcareous Alps in Austria. In H. W. Flügel & P. Faupl (Eds.), *Geodynamics of the eastern Alps* (pp. 112–125). Deuticke.

Vendeville, B. C., & Jackson, M. P. A. (1992). The fall of diapirs during thin-skinned extension. *Marine and Petroleum Geology*, *9*(4), 354–371. https://doi.org/10.1016/0264-8172(92)90048-j

Vergés, J., Marzo, M., & Muñoz, J. A. (2002). Growth strata in foreland basins. *Sedimentary Geology*, *146*(1–2), 1–9. https://doi.org/10.1016/s0037-0738(01)00162-2

Vidal-Royo, O., Rowan, M. G., Ferrer, O., Fischer, M. P., Fiduk, C. J., Canova, D. P., et al. (2021). The transition from salt diapir to weld and thrust: Examples from the Northern Flinders Ranges in South Australia. *Basin Research*, *33*(5), 2675–2705. https://doi.org/10.1111/bre.12579

Wagreich, M., & Decker, K. (2001). Sedimentary tectonics and subsidence modelling of the type Upper Cretaceous Gosau basin (Northern Calcareous Alps, Austria). *International Journal of Earth Sciences*, *90*(3), 714–726. https://doi.org/10.1007/s005310000181

Wagreich, M., & Faupl, P. (1994). Palaeogeography and geodynamic evolution of the Gosau Group of the Northern Calcareous Alps (Late Cretaceous, Eastern Alps, Austria). *Palaeogeography, Palaeoclimatology, Palaeoecology*, *110*(3–4), 235–254. https://doi.org/10.1016/0031-0182(94)90086-8

Walker, J. D., & Geissman, J. W. (Eds.). (2022). *Geologic time scale v. 6.0*. Geological Society of America. https://doi.org/10.1130/2022.CTS006C

Weber, F. (1958). Zur Geologie der Kalkalpen zwischen Traunsee und Almtal. *Mitteilungen der Geologischen Gesellschaft in Wien*, *51*, 295–352.

Wojtal, S. (1988). Objective methods for constructing profiles and block diagrams of folds. In S. Marshak & G. Mitra (Eds.), *Basic methods of structural geology, Part I: Elementary techniques* (pp. 269–302). Prentice Hall.

Woodcock, N. H. (1979). Sizes of submarine slides and their significance. *Journal of Structural Geology*, *1*(2), 137–142. https://doi.org/10.1016/0191-8141(79)90050-6